Thesis for the Degree of Master of Engineering

Refined Construction of Universal Asymptotic Model for Composite Sandwich Plates and Shells

by

YuRim Noh

Department of Mechanical Engineering

The Graduate School

Pukyong National University

February 2021

Refined Construction of Universal Asymptotic Model for Composite Sandwich Plates and Shells (복합재 샌드위치 플레이트 및 셸에 대한 통합형 점근적 모델의 개선된 구성)

Advisor: Prof. Chang-Yong Lee

by

YuRim Noh

A thesis submitted in partial fulfillment of the requirements
for the degree of

Master of Engineering

in Department of Mechanical Engineering, The Graduate School,
Pukyong National University

February 2021

Refined Construction of Universal Asymptotic Model for Composite Sandwich Plates and Shells

A dissertation
by
YuRim Noh

Approved by:

(Chairman) Oh-Boong Kwon

(Member) Jeong Park

(Member) Chang-Yong Lee

February 19, 2021

Contents

List of tables ····· iii

List of figures ····· iv

Abstract ····· vi

1. Introduction ····· 1

2. Equivalent 2D shell model from the ESL perspective ····· 8

2.1 3D shell kinematics and 3D energy formulation ····· 8

2.1.1 Shell kinematics ····· 9

2.1.2 Energy formulation in intrinsic form ····· 17

2.2 Dimensional reduction under VAM ····· 22

2.2.1 Order analysis ····· 23

2.2.2 Zeroth-order approximation (00EE) ····· 23

2.2.3 First-order approximation (11EE and 22CS) ····· 25

3. Universal 2D shell model from the LW perspective ····· 31

3.1 PA(00EE) ····· 31

3.2 PA(11EE) ····· 38

3.3 PA(22CS) ····· 43

4. Recovery relations from 2D to 3D ····· 47

4.1 Second-order approximation(22CS) ····· 47

4.2 3D refined recovery relations (22CS) ····· 51

4.3 3D recovery relations with stress recovery (00EE&11EE) ····· 52

5. Validation Examples ····· 56

5.1 Effect of different orders of 2D generalized transverse motion measures into two universal theories ····· 59

5.2 Bending analysis of composite sandwich plates/shells related to different values of LTR and RTR for a fixed FCSR ····· 61

5.2.1 Symmetric sandwich plate proposed by Pagano [4] and Carrera and Demasi [6] ····· 63

5.2.2 Bending analysis of sandwich spherical shells ····· 65

5.3 Bending analysis of composite sandwich plates/shells related to different values of LTR, RTR and FCSR ····· 66

5.3.1 Symmetric sandwich plate proposed by Carrera and Brischetto [7] and Demasi and Yu [8] ····· 67

5.3.2 Single curved shells proposed by Carrera and Brishchetto [9] ·· 70

6. Conclusions ····· 74

REFERENCES ····· 101

List of tables

Table 1. Comparison of $\overline{U}_3(L/2,L/2,0)$ from different plate theories ····· 76

Table 2. Comparison of $\overline{\sigma}_{11}(L/2,L/2,h/2)$ from different plate theories 76

Table 3. Comparison of $\overline{\sigma}_{13}(0,L/2,0)$ from different plate theories ····· 76

Table 4. Comparison of $\overline{U}_3(L/2,L/2,0)$ from different plate theories ····· 77

Table 5. Comparison of $\overline{\sigma}_{11}(L/2,L/2,h/2)$ from different plate theories 78

Table 6. Comparison of $\overline{\sigma}_{13}(0,L/2,0)$ from different plate theories ····· 79

Table 7. Ren shell. Comparison of $\overline{U}_3(L_1/2,L_2/2,0)$ from different shell theories ····· 80

Table 8. Ren shell. Comparison of $\overline{\sigma}_{11}(L_1/2,L_2/2,h/2)$ from different shell theories ····· 81

Table 9. Ren shell. Comparison of $\overline{\sigma}_{13}(0,L_2/2,0)$ from different shell theories ····· 82

Table 10. Varadan-Baskar shell. Comparison of $\overline{U}_3(L_1/2,L_2/2,0)$ from different shell theories ····· 83

Table 11. Varadan-Baskar shell. Comparison of $\overline{\sigma}_{11}(L_1/2,L_2/2,h/2)$ from different shell theories ····· 84

Table 12. Varadan-Baskar shell. Comparison of $\overline{\sigma}_{13}(0,L_2/2,0)$ from different shell theories ····· 85

List of figures

Fig. 1 Schematic of shell deformation ····· 9

Fig. 2 Undeformed configuration for the shell ····· 10

Fig. 3 Antisymmetric sandwich plate configuration of the bending problem 59

Fig. 4 Symmetric sandwich plate and spherical sandwich shell configuration of the bending problem ····· 62

Fig. 5 Geometry of Ren(left) and Varadan and Baskar(right) shells ····· 70

Fig. 6 Distribution of ($\overline{U}_3$(a), $\overline{\sigma}_{11}$(b), $\overline{\sigma}_{13}$(c), $\overline{\sigma}_{33}$(d)) vs. the through-thickness coordinate for FCSR=10^1 ····· 86

Fig. 7 Distribution of ($\overline{U}_3$(a), $\overline{\sigma}_{11}$(b), $\overline{\sigma}_{13}$(c), $\overline{\sigma}_{33}$(d)) vs. the through-thickness coordinate for FCSR=10^3 ····· 87

Fig. 8 Distribution of ($\overline{U}_3$(a), $\overline{\sigma}_{11}$(b), $\overline{\sigma}_{13}$(c), $\overline{\sigma}_{33}$(d)) vs. the through-thickness coordinate for FCSR=10^5 ····· 88

Fig. 9 Distribution of ($\overline{U}_3$(a), $\overline{\sigma}_{11}$(b), $\overline{\sigma}_{13}$(c), $\overline{\sigma}_{33}$(d)) vs. the through-thickness coordinate ····· 89

Fig. 10 Distribution of ($\overline{U}_3$(a), $\overline{\sigma}_{11}$(b), $\overline{\sigma}_{13}$(c), $\overline{\sigma}_{33}$(d)) vs. the through-thickness coordinate for $R/L=10$ ····· 90

Fig. 11 Distribution of ($\overline{U}_3$(a), $\overline{\sigma}_{11}$(b), $\overline{\sigma}_{13}$(c), $\overline{\sigma}_{33}$(d)) vs. the through-thickness coordinate for $R/L=1$ ····· 91

Fig. 12 Distribution of ($\overline{U}_3$(a), $\overline{\sigma}_{11}$(b), $\overline{\sigma}_{13}$(c), $\overline{\sigma}_{33}$(d)) vs. the through-thickness coordinate for $FCSR_L=7.3\times10^4$ and $FCSR_z=9.624$ ····· 92

Fig. 13 Distribution of ($\overline{U}_3$(a), $\overline{\sigma}_{11}$(b), $\overline{\sigma}_{13}$(c), $\overline{\sigma}_{33}$(d)) vs. the through-thickness coordinate for $FCSR_L=7.3\times10^6$ and $FCSR_z=9.624\times10^2$ ··· 93

Fig. 14 Distribution of ($\overline{U}_3$(a), $\overline{\sigma}_{11}$(b), $\overline{\sigma}_{13}$(c), $\overline{\sigma}_{33}$(d)) vs. the through-thickness coordinate for $FCSR_L=7.3\times10^8$ and $FCSR_z=9.624\times10^4$ ··· 94

Fig. 15 Ren shell. Distribution of ($\overline{U}_3$(a), $\overline{\sigma}_{11}$(b), $\overline{\sigma}_{13}$(c), $\overline{\sigma}_{33}$(d)) vs. the through-thickness coordinate for $FCSR_L=7.3\times10^4$ and $FCSR_z=9.624$ ····· 95

Fig. 16 Ren shell. Distribution of ($\overline{U}_3$(a), $\overline{\sigma}_{11}$(b), $\overline{\sigma}_{13}$(c), $\overline{\sigma}_{33}$(d)) vs. the through-thickness coordinate for $FCSR_L=7.3\times10^6$ and $FCSR_z=9.624\times10^2$ ····· 96

Fig. 17 Ren shell. Distribution of ($\overline{U}_3$(a), $\overline{\sigma}_{11}$(b), $\overline{\sigma}_{13}$(c), $\overline{\sigma}_{33}$(d)) vs. the through-thickness coordinate for $FCSR_L=7.3\times10^6$ and $FCSR_z=9.624\times10^2$ ····· 97

Fig. 18 Varadan-Baskar shell. Distribution of ($\overline{U}_3$(a), $\overline{\sigma}_{11}$(b), $\overline{\sigma}_{13}$(c), $\overline{\sigma}_{33}$(d)) vs. the through-thickness coordinate for $FCSR_L=7.3\times10^4$ and $FCSR_z=9.624$ ····· 98

Fig. 19 Varadan-Baskar shell. Distribution of ($\overline{U}_3$(a), $\overline{\sigma}_{11}$(b), $\overline{\sigma}_{13}$(c), $\overline{\sigma}_{33}$(d)) vs. the through-thickness coordinate for $FCSR_L=7.3\times10^6$ and $FCSR_z=9.624\times10^2$ ····· 99

Fig. 20 Varadan-Baskar shell. Distribution of ($\overline{U}_3$(a), $\overline{\sigma}_{11}$(b), $\overline{\sigma}_{13}$(c), $\overline{\sigma}_{33}$(d)) vs. the through-thickness coordinate for $FCSR_L=7.3\times10^8$ and $FCSR_z=9.624\times10^4$ ····· 100

복합재 샌드위치 플레이트 및 셸에 대한 통합형 점근적 모델의 개선된 구성

노 유 림

부 경 대 학 교　대 학 원　기 계 공 학 과

요　　약

효율성과 정확성의 우수한 타협을 얻기 위해 등가단층 이론과 층별 이론을 합성하여 복합재 샌드위치 플레이트 및 셸에 대한 통합형 점근적 모델을 변분점근법을 사용하여 구성한다. 다양한 길이 대 두께 비와 반경 대 두께 비에 대한 셸 모델은 횡전단응력과 횡단수직응력 효과를 포함한 점근적으로 정확한 에너지 범함수로서 유도되어 진다. 점근 셸 모델을 구성할 때, 플레이트 모델에서 추가된 작은 변수로서 반경 대 두께 비가 고려되어진다. 이때, 점근적 개선된 모델에서 포함하는 차수가 달라지는데, 반경(R)의 차수에 따라서 변하는 효과를 비교하기 위해서 $l \sim R$로 보는 접근 방식인 PA(11EE)를 구성하고, $l \sim \sqrt{hR}$로 보는 접근 방식 PA(22CS)를 구성하여 비교한다. 샌드위치 구조물의 각 층을 탄성 셸로 고려되어지면, 셸들의 모든 물질 상수는 똑같은 차수로 볼 수 있고, 등가 셸 모델은 등가단층 관점으로 구성되어 질 수 있다. 그런 다음, 샌드위치 셸은 층별 관점으로 볼 때 3개의 층의 조합으로서 고려 될 수 있고 층마다 서로 다른 물질의 특성으로 인해 횡방향 변형의 차수 변화가 이루어진다. 어떠한 스킨 대 코어 강성, 길이 대 두께 그리고 반경 대 두께 비를 가지는 경우의 복합재 샌드위치 셸의 기계적 거동을 예측하기 위한 통합형 모델이 유도되어진다. 층간 변위와 횡방향 응력의 연속 조건아래, 코어 층의 셸 변수들과 그 변수들의 편도함수로 표현되는 점근적으로 정확한 에너지 범함수를 가진다. 샌드위치 구조물에서 일반적으로 스킨은 코어와 비교했을 때 상대적으로 얇고 딱딱한데, 이러한 서로 다른 물질의 특성으로 인해 경계층 효과가 발생하게 된다. 이로 인해 횡방향 응력을 예측하는 것은 어렵고, 추가적인 복원 관계가 필요한데 본 논문에서는 다음에 제시할 2가지 방식을 적용하고 비교 할 것이다. 첫째로, PA(22CS)에서의 에너지 식과 차수가 같은 개선된 복원 관계는 추가 와핑과 그에 상응하는 층간 연속 조건이 요구되어지고, 점근적으로 2번째 차수까지 계산되어 진다. 두 번째로, PA(11EE)와 PA(00EE)에서는 3차원 횡방향 응력은 3차원 탄성의 평형 방정식을 셸의 두께로 적분함으로서 계산된다. 끝으로 본 논문에서 제시한 방식들과 3차원 완전해 그리고 다른 논문에서 제시하는 다른 방식들을 비교하고, 본 논문에서 제시한 방식들의 다양한 스킨 대 코어 강성 비, 길이 대 두께 비 그리고 반경 대 두께 비로 구성된 복합재

샌드위치 구조의 기계적 거동을 해석하기 위한 유효성과 정확성을 검증할 것이다.

1. Introduction

The use of composite sandwich shells continues to increase in many engineering applications. This is associated with their high strength and low weight, superior noise and energy absorption, and/or high thermal resistance under a variety of extreme environments. These structures consist of two stiff metallic or composite thin face sheets separated by a soft honeycomb or a thick foam core by utilizing mismatched constituent material and geometric properties to achieve the ever-increasing structural performance and stability requirements. Usually, the core of sandwich structures is modelled as a medium with low transverse shear modulli and therefore, transverse shear has an important role for most of sandwich theories. To estimate and predict unique mechanical behaviors of composite sandwich structures, research involving the accurate and general modeling has consistently remained as a very active field in the last several decades; see Sayyad and Ghugal [1] and Birman and Kardomateas [2]. Although a formulation based on three-dimensional elasticity can be used for direct modeling to study the detailed behavior of such structures and to accurately calculate their mechanical characteristics to any degree of generality, to do so is inordinately complex and constly. Even in the linear elasticity case, the number of relevant papers is very limited to Pagano [3, 4] and Brischetto [5]. Thus, a clear need exists for an alternative, less costly and more convenient approach than 3D elasticity.

From a dimensional reduction perspective, these structures can be effectively modeled as two-dimensional shells by taking advantage of the smallness of thickness to in-plane wavelength of deformations (h/l) and thickness to minimum curvature radius of the reference surface (h/R). As a result, theoretical researchers have striven to construct accurate and general 2D shell models under various *ad hoc* kinematic assumptions, which are convenient to eliminate the thickness coordinate from the independent mechanical variables of the governing partial differential equations. By referring to the existing literature by Carrera and Demasi [6], Carrera and Brischetto [7, 9] and Demasi and Yu [8], one can easily observe that there has been a tremendous amount of work done to construct plate/shell models extendable to sandwich plate/shell ones, most of which differ from each other only by how to introduce *ad hoc* kinematic assumptions into their models collectively or individually. In particular, these models are mainly based on two competing theories: equivalent single-layer (ESL) theories and layer-wise (LW) theories. In ESL theories, it is easy to affordably implement theoretical and computational procedures because *ad hoc* kinematic assumptions are only relied upon in the mid-surface of the shell, regardless of how many layers the shell is comprised of. However, as pointed out by Carrera and Brischetto [7, 9] and Demasi and Yu [8], most ESL models fail to predict accurate 3D displacement/stress fields for the sandwich plate/shell problems in high face-to-core-stiffness-ratio (FCSR), small length-to-thickness-ratio (LTR) and small radius-to-thickness-ratio (RTR) cases. On the other hand, since the sandwich structure in LW

theories is modeled as an assembly of three individual shells with interlaminar displacement and transverse stress continuity conditions, their own specific kinematic assumptions for each layer must be used to capture interlaminar discontinuity phenomena of the displacement and stress fields. However, attempts to utilize this directly will meet with the same difficulties as using a 3D elasticity approach. Therefore, such models based on these theories have always suffered from an unbalanced compromise between accuracy and efficiency, or between simplicity and generality, for predicting mechanical characteristics of composite sandwich shells.

To resolve the above unbalanced compromise, a universal asymptotic theory as the synthesis of ESL and LW theories based on 3D elasticity formulation and the zeroth-order approximation was recently proposed by Berdichevsky [10] for sandwich plates and Berdichevsky [11] for hard-skin plates and shells. For simplicity, we will henceforth refer to these two papers as “Berdichevsky’s papers” or “Berdichevsky’s works”. At first, when all constituent material constants of a sandwich structure are assumed to have the same order, such structure can be described by an elastic plate/shell from the ESL perspective. And then, under the variational asymptotic method (VAM) introduced by Berdichevsky [12] an equivalent 2D plate/shell model is formulated in a manner similar to that introduced for laminated composite plate/shell models by Yu [13, 14] and is based on an asymptotically correct energy functional capable of capturing the transverse deformations. On the other hand, when the sandwich structure can be regarded as the assembly of three individual layers with mismatched

constituent material and geometric properties, a new 2D plate/shell model different from the ESL theories is introduced. By considering the smallness of a new coupled parameter ($\mu^s h^s/\mu^c h^c$), called "the ratio of effective extensional rigidities of the core and the skin", and by performing kinematic identity procedures via the interlaminar continuity of the 3D displacement components, a universal theory from the LW perspective is asymptotically established for geometrically linear/nonlinear problem of sandwich plates/shells. Here μ^s and μ^c denote characteristic elastic moduli of the skin and the core, while h^s and h^c thickness of the skin and the core, respectively. Nevertheless, Berdichevsky's papers are not only restricted to predict the mechanical characteristics of symmetric sandwich plates/shells made of isotropic materials, but two important shortcomings inherent in the theoretical derivation procedure are also found: (1) no clear mathematical and physical explanations to exclude the usage of interlaminar transverse stress continuity conditions, and (2) no a general procedure for 3D recovery relations (i.e., expressions for 3D displacement, strain and stress fields of the original 3D sandwich structures). Later, Berdichevsky's works was theoretically extended by Lee et al. [15] to resolve these two deficiencies. In the intrinsic form suitable for composite structure analysis, it involves constructing the universal asymptotic theory of composite sandwich plates by utilizing both interlaminar displacement/transverse stress continuity conditions and recovering the 3D displacement, strain and in-plane stress fields by using the original 3D constitutive relations and the 3D transverse stress components by integration of the equilibrium equations from the 3D

elasticity theory through the plate thickness under the traction boundary conditions on top and bottom surfaces and the transverse stress continuity conditions at skin-core interfaces. However, from various validation examples performed by Lee et al. [15], one can observe that the universal asymptotic theory based on the zeroth-order approximation did not provide satisfactory results for a thick plate with very and extremely hard skin, even though it can do a good job in predicting the mechanical behaviors for thin and moderately thick structures for a wide range of face-to-core-stiffness-ratio (FCSR). And also the theory is just a special case of a shell. Therefore, this can be directly explained that a higher-order universal shell theory in the asymptotic sense should be required for such an extreme case and complex shell geometry.

Usually, the faces of the sandwich structures are built of stiff and strong materials and they are much thinner than the light and relatively soft core. Therefore, due to the mismatch in the material properties between constituent materials, high transverse stresses can be created at the vicinity of the edges, which is known as boundary layer phenomena. It has been shown that this phenomena is not captured accurately by the zeroth-order approximation found in Lee et al. [15]. To capture boundary layer effect, we need to use a post processing step. As a post processing step, additional integration procedure for 3D stress recovery has been used widely in many cases and leads to accurate results. For example, from Pagano [4], interlaminar stresses calculated by integrating equilibrium equation over the plate thickness with the assumption of linear in-plane stresses. The

interlaminar stresses calculated agreed well with three-dimensional elasticity solution. And, as mentioned in Cho and Parmerter [16], integrating equilibrium equations of three-dimensional elasitcity produce better transverse shear stresses when comparing a way directly from the constitutive equation. In addition, crossply parabolic and hyperbolic caps subjected to uniform external pressure and a simply supported cylindrical shell subjected to an internal sinusoidal pressure were considered in the paper Ramalingeswara and Ganesan [17]. This paper also following conclusion were drawn: interlaminar stresses evaluated using material law directly are not corect. In recent years, many researchers have published papers using integrating equilibrium equations; see Shah and Batra [18], Tornabene and Brischetto [19] and Sayyad and Naik [20]. In addition, as another processing step, 3D refined recovery relations introduced by Yu [13, 14] for derive the asymptotically correct energy functional capable of capturing the small LTR and RTR effects and based on the first-order approximation.

For accurately predicting 3D displacement and stress components of composite sandwich shells for various FCSR, LTR and RTR cases, the main objective of this paper is to construct a universal shell model which is based on the energy functional and interlaminar displacement/transverse stress continuity conditions asymptotically correct up to the second order. At first, when all constituent material constants of the sandwich structure are assumed to be of the same order, the equivalent 2D shell theory from the ESL perspective is systematically formulated in an intrinsic form by Hodges et al. [21] suitable for composite structure analysis. And then, from the LW

perspective, both interlaminar displacement/transverse stress continuity conditions asymptotically correct to the first order are established and introduced into the present approach to construct the universal asymptotic theory of composite sandwich shells when the sandwich shell model can be regarded as the assembly of three individual shell models.

Morever, when constructing the refined theory denoting by PA(11EE), we follow the additional integration procedure for 3D recovery relations as a post processing step. On the other hand, for 3D refined recovery relations of PA(22CS) without additional integration procedure, 3D displacement, strain and stress fields can be directly recovered under refined interlaminar displacement/transverse stress continuity conditions valid to the same order as the energy formulation. As a preliminary validation, a set of bending problems for various FCSR, LTR and RTR cases illustrated by Carrera and Demasi [6], Carrera and Brischetto [7, 9], Demasi and Yu [8] and Lee et al. [15] are finally presented to demonstrate the capability and accuracy of this present approach together with critical comparisons of the 3D exact solutions found in Pagano [4] and Brischetto [5].

2. Equivalent 2D shell model from the ESL perspective

When all constituent material constant of a sandwich structure are assumed to be of the same order, such structure can be modeled as a shell from the ESL-based perspective. From the 3D elasticity problem under the variational asymptotic procedure, an equivalent 2D refined shell model for any LTRs and RTRs is derived in terms of the asymptotically correct energy functional taking account of transverse shear/normal deformations and incorporating the additional energy contributions due to the small ratios (h/l, h/R).

2.1 3D shell kinematics and 3D energy formulation

In a three-dimensional shell, Consider the surface Ω_b and, at each point on the surface, erect a segment of length h directed along the normal to the surface; the centers of the segments are on Ω_b. An arbitrarily curved shell can be considered as a solid medium geometrically defined by a surface Ω_b immersed in three-dimensional physical space and a constant thickness h of the medium around the surface Ω_b

2.1.1 Shell kinematics

Let Ω_b be called the reference surface of the 3-D body, bounded by a smooth closed curve $\partial\Omega_b$ and mathematically represented by a set of arbitrary curvilinear coordinates, x_α. However, without loss of generality, one may choose the lines of curvature to be the curvilinear coordinates to simplify the formulation. In addition, for representing the 3-D medium uniquely and following a very natural choice generally, the third coordinate is selected as the coordinate normal to the reference surface specified by x_3. (Here and throughout the rest of the development, Greek indices assume values 1 and 2, while Latin indices assume values 1, 2, and 3. Repeated indices are summed over their range except where explicitly mentioned.) Note that a plate is a special case of a shell whose middle surface is planar. As sketched in Fig. 2.1, letting $\boldsymbol{b}_3(x_1,x_2)$ denote the unit vector nor-

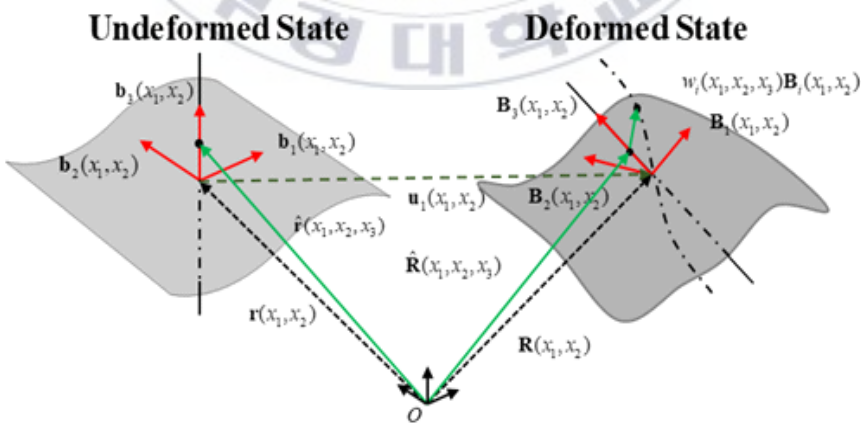

Fig. 1 Schematic of shell deformation

mal to the reference surface, one can then describe the position of any material point in the stress-free, undeformed configuration by its position vector $\hat{\boldsymbol{r}}$ relative to an inertially fixed point O, such that

$$\hat{\boldsymbol{r}}(x_1,x_2,x_3)=\boldsymbol{r}(x_1,x_2)+x_3\boldsymbol{b}_3(x_1,x_2) \tag{1}$$

where $\boldsymbol{r}$ is the position vector from O to the point located by x_α on the reference surface. Following Berdichevsky's papers, the 2D position vector is naturally defined as

$$\boldsymbol{r}(x_1,x_2)=\frac{1}{2}\left[\hat{\boldsymbol{r}}^{+}(x_1,x_2)+\hat{\boldsymbol{r}}^{-}(x_1,x_2)\right] \tag{2}$$

When the reference surface of the undeformed shell is coincided with its middle surface Ω_b and the position vectors on the top and bottom surfaces (Ω_b^+ and Ω_b^-) (See Fig. 2) are given by $\hat{\boldsymbol{r}}^{+}$ and $\hat{\boldsymbol{r}}^{-}$, respectively. Here $(\bullet)^+=(\bullet)\big|_{x_3=h/2}$ and $(\bullet)^-=(\bullet)\big|_{x_3=-h/2}$ denote the values prescribed at

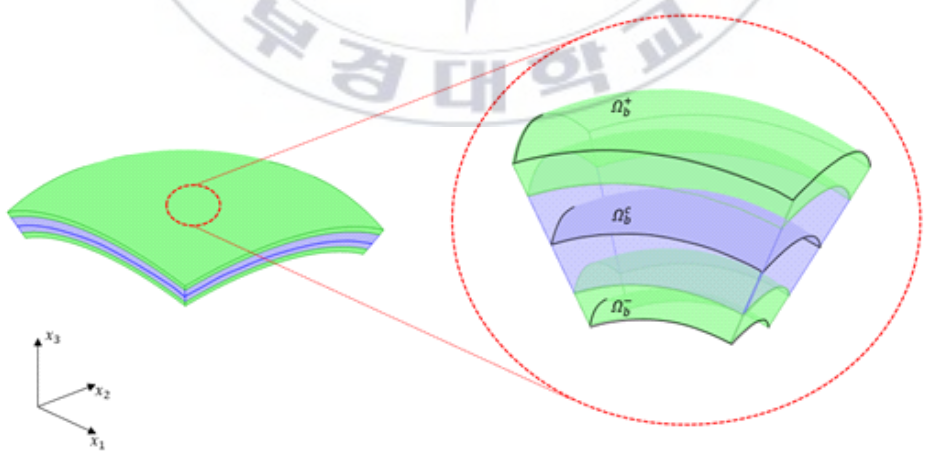

Fig. 2 Undeformed configuration for the shell

the top and bottom thickness coordinates $x_3 = \pm h/2$, respectively, and will be used throughout this paper.

Typically, let 2-D base vectors $\mathbf{a}_\alpha$ associated with x_α be defined as:

$$\mathbf{a}_\alpha(x_1, x_2) = \boldsymbol{r}_{,\alpha} \tag{3}$$

From henceforth, for simplicity, we will avoid including the independent variables on which a function depends unless it is not obvious for the reader to determine what they are. From Eq. (3) one can define the so-called Lame parameters as:

$$A_\alpha(x_1, x_2) = \sqrt{\mathbf{a}_\alpha \cdot \mathbf{a}_\alpha} \tag{4}$$

Let us mention that in Eq. (4), the summation convention is not applied because α is not a dummy index. The same rule will apply to the rest of development without repeating the same statement. Then, for the computational procedures used later, the 2D unit base vectors $\boldsymbol{b}_i$ constitute an orthogonal triad system such that

$$\begin{aligned} \boldsymbol{b}_\alpha(x_1, x_2) &= \frac{\mathbf{a}_\alpha}{A_\alpha} \\ \boldsymbol{b}_3 = \boldsymbol{b}_1 \times \boldsymbol{b}_2 &= \frac{\mathbf{a}_1 \times \mathbf{a}_2}{|\mathbf{a}_1 \times \mathbf{a}_2|} \end{aligned} \tag{5}$$

Now by taking the partial derivatives of Eq. (1) with respect to x_α, it is easy to see that the covariant 3D base vectors $\mathbf{g}_i$ associated with the chosen coordinate system are given by:

$$\begin{aligned}\mathbf{g}_1 &= \mathbf{a}_1 + x_3 \boldsymbol{b}_{3,1} \\ \mathbf{g}_2 &= \mathbf{a}_2 + x_3 \boldsymbol{b}_{3,2} \\ \mathbf{g}_3 &= \boldsymbol{b}_3\end{aligned} \tag{6}$$

From the differential geometry of the surface and with the help of Ref. [21, 22] one can express the derivative of 2D unit base vectors $\boldsymbol{b}_{i,\alpha}$ as follows:

$$\boldsymbol{b}_{i,\alpha} = A_\alpha \mathbf{k}_\alpha \times \boldsymbol{b}_i \tag{7}$$

with

$$\mathbf{k}_\alpha = (-k_{\alpha 2}\boldsymbol{b}_1 + k_{\alpha 1}\boldsymbol{b}_2 + k_{\alpha 3}\boldsymbol{b}_3) \tag{8}$$

where $\mathbf{k}_\alpha$ is the curvature vector measured in $\boldsymbol{b}_i$ in which $k_{\alpha\beta}$ refers to out-of-plane curvatures. We note that $k_{12} = k_{21} = 0$ because the coordinates are defined to be the lines of curvatures. However, the geodesic curvatures $k_{\alpha 3}$ do not necessarily vanish for the chosen coordinate system, and they can be expressed in terms of Lame parameters as:

$$k_{13} = -\frac{A_{1,2}}{A_1 A_2}, \qquad k_{23} = \frac{A_{2,1}}{A_1 A_2} \tag{9}$$

As we are interested in the interior solution with geometrical and shear refinements for regular shells, we assume that the initial curvatures k_{ij} and Lame parameters A_α are slowly varying or constant. This assumption will result in the neglect of all the derivatives of these quantities with respect to in-plane coordinates x_α in the formulation.

Using Eqs. (7) and (8) one can rewrite the expression for the covariant 3D base vectors from Eq. (6) as:

$$\begin{aligned}\mathbf{g}_1 &= A_1(1+x_3k_{11})\boldsymbol{b}_1\\ \mathbf{g}_2 &= A_2(1+x_3k_{22})\boldsymbol{b}_2\\ \mathbf{g}_3 &= \boldsymbol{b}_3\end{aligned} \tag{10}$$

By the standard definition [21], the contravariant base vectors are given by

$$\mathbf{g}^i = \frac{1}{2\sqrt{\mathrm{g}}} e_{ijk}\mathbf{g}_j \times \mathbf{g}_k \tag{11}$$

Where $\mathrm{g} = \det(\mathbf{g}_i \cdot \mathbf{g}_j)$ is the determinant of the metric tensor for the undeformed configuration, and e_{ijk} are the components of the permutation tensor in a Cartesian coordinate system. Thus, one can define the contravariant 3D base vectors $\mathbf{g}^i$ as

$$\begin{aligned}\mathbf{g}^1 &= \frac{\mathbf{g}_2 \times \mathbf{g}_3}{\sqrt{\mathrm{g}}} = \frac{A_2(1+x_3k_{22})}{\sqrt{\mathrm{g}}}\boldsymbol{b}_1\\ \mathbf{g}^2 &= \frac{\mathbf{g}_3 \times \mathbf{g}_1}{\sqrt{\mathrm{g}}} = \frac{A_1(1+x_3k_{11})}{\sqrt{\mathrm{g}}}\boldsymbol{b}_2\\ \mathbf{g}^3 &= \frac{\mathbf{g}_1 \times \mathbf{g}_2}{\sqrt{\mathrm{g}}} = \boldsymbol{b}_3\end{aligned} \tag{12}$$

When the shell is deformed, the particle that had position vector in the undeformed state now has the position vector $\hat{\mathrm{R}}$ in the deformed configuration. The latter can be uniquely determined by the deformation of the 3-D body. A new triad B_i unit vectors are just tools to enable one to express vectors and tensors in their component form during the derivation. They are not necessarily tangent to the coordinates of the deformed shell. The relation between B_i and $\boldsymbol{b}_i$ can be specified by an arbitrarily large rotation specified in terms of the matrix of direction cosines $\hat{C}(x_1, x_2)$, so that

$$\mathrm{B}_i = \hat{C}_{ij}\boldsymbol{b}_j$$
$$\hat{C}_{ij} = \mathrm{B}_i \cdot \boldsymbol{b}_j \tag{13}$$

subject to the requirement that B_i is coincident with $\boldsymbol{b}_i$ when the structure is undeformed. Without loss of generality, the position vector $\hat{\mathrm{R}}$ can be defined as:

$$\hat{\mathrm{R}}(x_1, x_2, x_3) = \mathrm{R}(x_1, x_2) + x_3\mathrm{B}_3(x_1, x_2) + w_i(x_1, x_2, x_3)\mathrm{B}_i(x_1, x_2) \tag{14}$$

where $\mathrm{R} = \mathrm{r} + \mathrm{u}$ describes the position vector from the point O to the point on the reference surface of the deformed shell, $\mathrm{u} = u_i\boldsymbol{b}_i$ the 2D displacement vector from the undeformed configuration, and the unknown 3D functions w_i represent the general warping displacement of an arbitrary point on the normal line of the deformed shell, consisting of both in- and out-of-plane components so that all possible deformations are considered. Here, six constraints are required to ensure a one-to-one mapping between $\hat{\mathrm{R}}$ and (R, B_i, w_i) in Eq. (14). At first, three redundancies can be removed by choosing appropriate definitions of B_i. One of them can be selected by taking B_3 as the normal to the reference surface Ω_B of the deformed shell in such a way

$$\mathrm{B}_3 \cdot \mathrm{R}_{,\alpha} = 0 \quad \text{with} \quad (\bullet)_{,\alpha} = \partial(\bullet)/\partial x_\alpha \tag{15}$$

It is pointed out that this choice is only for convenience in the derivation and has nothing to do with the Kirchhoff assumption. In addition, the second constraint introduced in most 2D shell models, can be specified by the rotation of B_α around B_3 such that

$$\frac{\mathbf{B}_1 \cdot \mathbf{R}_{,2}}{A_2} = \frac{\mathbf{B}_2 \cdot \mathbf{R}_{,1}}{A_1} \tag{16}$$

which can serve as another constraint to specify the global rotation of the triad $\mathbf{B}_i$ and make the formulation in (14) unique. For the last constraints, it can be obtained from a proper definition of $\mathbf{R}$. Similar to the way $\mathbf{r}$ is defined in Eq. (2), $\mathbf{R}$ can be defined as the average of two position vectors $\hat{\mathbf{R}}^+$ and $\hat{\mathbf{R}}^-$ on the top and bottom surfaces (Ω_b^+ and Ω_b^-):

$$\mathbf{R}(x_1, x_2) = \frac{1}{2}\left[\hat{\mathbf{R}}^+(x_1, x_2) + \hat{\mathbf{R}}^-(x_1, x_2)\right] \tag{17}$$

Therefore, if Eq. (14) is substituted into Eq. (17), then the warping functions must satisfy the following three constraints as the last constraints:

$$w_i^+(x_1, x_2) = -w_i^-(x_1, x_2) \tag{18}$$

It means that the warping functions do not contribute to the rigid-body displacement of the 2D shell model. So far, a total of six constraints have been introduced, and then Eq. (14) designates a unique point in the 2D shell model.

Before closing this subsection, definitions of the 2-D generalized LK strain measures ($\varepsilon_{\alpha\beta}$ and κ_{ij}) can be first defined from the partial derivatives of $\mathbf{R}$ and $\mathbf{B}_i$ with respect to x_α as follows:

$$\begin{aligned} \mathbf{R}_{,\alpha} &= A_\alpha(\mathbf{B}_\alpha + \varepsilon_{\alpha\beta}\mathbf{B}_\beta) \\ \mathbf{B}_{i,\alpha} &= A_\alpha(-K_{\alpha 2}\mathbf{B}_1 + K_{\alpha 1}\mathbf{B}_2 + K_{\alpha 3}\mathbf{B}_3) \times \mathbf{B}_i \end{aligned} \tag{19}$$

where $\varepsilon_{\alpha\beta}$ are the 2D in-plane strains, and K_{ij} are the curvatures of the deformed surface, which are the summation of curvatures of undeformed geometry k_{ij} and curvatures introduced by the deformation κ_{ij}. Here, using

Eq. (19), it can be shown that the second constraint, the one in Eq. (16), actually implies symmetry of 2D in-plane strains, such that $\varepsilon_{12} = \varepsilon_{21}$. Second, as pointed out in Berdichevsky's papers, three additional degrees of freedom (DOFs) associated with transverse deformations should be introduced into Eq. (14) because shell models taking account of such deformations are required to accurate estimate and predict mechanical behaviors of hard-skin sandwich structures. For development of the universal asymptotic model introduced later, let us first replace w_i^+ and w_i^- by $h\varphi_i(x_1,x_2)/2$ and $-h\varphi_i(x_1,x_2)/2$, respectively, due to Eq. (18) and then implement the following change of variables into the original 3D warping functions:

$$w_i(x_1,x_2,x_3) = x_3\varphi_i(x_1,x_2) + y_i(x_1,x_2,x_3) \tag{20}$$

where φ_1 and φ_2 denote the rotations of a transverse normal about the x_2 and x_1 axes, respectively, and φ_3 represents the elongation of a transverse normal along the x_3 axis. Here to differentiate from the 2D generalized LK strain measures, φ_i are referred to the 2D generalized transverse motion measures throughout the rest of the development. Therefore, instead of Eq. (18), the following six constraints are used to ensure a one-to-one mapping between w_i and (φ_i, y_i) in Eq. (20):

$$y_i^+(x_1,x_2) = 0 \quad y_i^-(x_1,x_2) = 0 \tag{21}$$

Finally, substituting Eq. (21) into Eq. (14), we can redefine the deformed position vectors considering the transverse shear and normal effects, such that

$$\begin{aligned}\hat{\mathbf{R}}(x_1,x_2,x_3) = \mathbf{R}(x_1,x_2) + x_3\varphi_\alpha(x_1,x_2)\mathbf{B}_\alpha + x_3[1+\varphi_3(x_{1,}x_2)]\mathbf{B}_3 \\ + y_i(x_1,x_2,x_3)\mathbf{B}_i\end{aligned} \tag{22}$$

2.1.2 Energy formulation in intrinsic form

Based on the decomposition concept of rotation tensor introduced by Danielson and Hodges [23], the Jauman-Biot-Cauchy strain components for small local rotation are given by

$$\Gamma_{ij} = \frac{1}{2}(F_{ij} + F_{ji}) - \delta_{ij} \tag{23}$$

where δ_{ij} is the Kronecker symbol, and F_{ij} the mixed-basis component of the deformation gradient tensor such that

$$F_{ij} = \mathbf{B}_i \cdot \mathbf{G}_k \mathbf{g}^k . \boldsymbol{b}_j \tag{24}$$

Here $\mathbf{G}_i = \partial \hat{\mathbf{R}} / \partial x_i$ denotes the 3D covariant basis vectors of the deformed configuration and $\mathbf{g}^i$ are the 3D contravariant base vectors of the undeformed configuration. In the plate case, it is obvious that $\mathbf{g}^i = \boldsymbol{b}_i$.

Until now, we have been trying to keep the analysis both general and simple. However, to make the problem more manageable, we have to make some inevitable approximations that published shell theories have almost universally used. There are several small parameters inherent in engineering structures, and the existence of small parameters brings about a great variety of possibilities for application of asymptotic methods. In the shell problem considered, three possible small parameters exist: the maximum strain $\hat{\varepsilon}$, the physical parameter h/l, and the geometric parameter h/R, where R is the characteristic radius of curvature of the shell reference surface, l a characteristic length in the in-plane directions (determined by the loads applied for static behavior). Having made the above approximations, the 2D generalized LK strain and transverse motion measures are considered to be small compared to unity and the 3D warping functions are of the order of

those measures or smaller, and then we can safely neglect all the terms that are products of the 3D warping functions and both 2D generalized LK strain measures and 2D generalized transverse motion measures. With the help of Eqs. (19), (23) and (24), one can obtain the 3D strain field as:

$$\begin{aligned}
\Gamma_{11} &= \frac{\varepsilon_{11}+x_3\kappa_{11}+x_3\varphi_{1;1}+x_3k_{11}\varphi_3+w_{1;1}+k_{11}w_3}{1+x_3k_{11}} \\
2\Gamma_{12} &= \frac{\varepsilon_{21}+x_3\kappa_{21}+x_3\varphi_{1;2}+w_{1;2}}{1+x_3k_{22}}+\frac{\varepsilon_{12}+x_3\kappa_{12}+x_3\varphi_{2;1}+w_{2;1}}{1+x_3k_{11}} \\
\Gamma_{22} &= \frac{\varepsilon_{22}+x_3\kappa_{22}+x_3\varphi_{2;2}+x_3k_{22}\varphi_3+w_{2;2}+k_{22}w_3}{1+x_3k_{22}} \\
2\Gamma_{13} &= \varphi_1+w_1{}'+\frac{x_3\varphi_{3;1}-x_3k_{11}\varphi_1+w_{3;1}-k_{11}w_1}{1+x_3k_{11}} \\
2\Gamma_{23} &= \varphi_2+w_2{}'+\frac{x_3\varphi_{3;2}-x_3k_{22}\varphi_2+w_{3;2}-k_{22}w_2}{1+x_3k_{22}} \\
\Gamma_{33} &= \varphi_3+w_3{}'
\end{aligned} \tag{25}$$

where $(\bullet)_{;\alpha}=\partial(\bullet)/A_\alpha\partial x_\alpha$, $(\bullet)'=\partial(\bullet)/\partial x_3$.

By definition, the 3D strain energy stored in the shell can be then expressed as:

$$\begin{aligned}
2U &= \int_{x_1}\int_{x_2}\left\langle \begin{bmatrix}\Gamma_e\\ 2\Gamma_s\\ \Gamma_t\end{bmatrix}^T\begin{bmatrix}D_e & D_{es} & D_{et}\\ D_{es}^T & D_s & D_{st}\\ D_{et}^T & D_{st}^T & D_t\end{bmatrix}\begin{bmatrix}\Gamma_e\\ 2\Gamma_s\\ \Gamma_t\end{bmatrix}\chi\right\rangle dx_1dx_2 \\
&= \int_\Omega \langle \Gamma^T D\Gamma\chi\rangle d\Omega = \int_\Omega 2\overline{U}d\Omega
\end{aligned} \tag{26}$$

where $\Gamma_e = \lfloor\, \Gamma_{11}\ \ 2\Gamma_{12}\ \ \Gamma_{22}\,\rfloor^T$, $\Gamma_s = \lfloor\, 2\Gamma_{13}\ \ 2\Gamma_{23}\,\rfloor^T$, $\Gamma_t=\Gamma_{33}$ and

$$\chi = \frac{\mathbf{g}_1\times\mathbf{g}_2\cdot\mathbf{g}_3}{|\mathbf{a}_1\times\mathbf{a}_2|} = 1+2x_3H+x_3^2K \tag{27}$$

Here $H=(k_{11}+k_{22})/2$ and $K=k_{11}k_{22}$ are called the mean and the Gaussian

curvatures of the surface, respectively. And angle-brackets $\langle \bullet \rangle$ represents the definite integral through the shell thickness, $\overline{\mathrm{U}}$ denotes the 3D strain energy density per unit area, and $D(x_3)$ is the 6×6 material matrix, which comes from the fourth-order elasticity tensor expressed in the $\boldsymbol{b}_i$ basis. This matrix is in general fully populated. However, if it is desired to model laminated composite shells in which each lamina exhibits a monoclinic symmetry about its own mid-surface (for which the material matrix is determined by 13 constraints instead of 21) and rotated about the local normal to be a layer in the composite laminated shell, then D_{es} and D_{st} will always vanish no matter what the layup angle is. To make this problem tractable and procedure simpler, the nonzero components of the material matrix are also assumed to be constants along the shell thickness. Considering these, we can simplify the strain energy expression to the following form:

$$\begin{aligned} 2\overline{\mathrm{U}} &= \left\langle \left[\Gamma_e^T D_e \Gamma_e + 2\Gamma_e^T D_{et} \Gamma_t + (2\Gamma_s)^T D_s (2\Gamma_s) + \Gamma_t^T D_t \Gamma_t \right] \chi \right\rangle \\ &= \left\langle \left[\Gamma_e^T D_{\parallel} \Gamma_e + (2\Gamma_s)^T D_s (2\Gamma_s) + (\Gamma_t + D_{\perp}^T \Gamma_e)^T D_t (\Gamma_t + D_{\perp}^T \Gamma_e) \right] \chi \right\rangle \end{aligned} \tag{28}$$

with $D_{\parallel} = D_e - D_{\perp} D_{et}^T$ and $D_{\perp} = D_{et} D_t^{-1}$.

To deal with the 3D virtual work done by applied loads, we follow the similar methodology introduced by Yu et al. [24] and Yu [25]. When the 3D virtual work done is developed, at first leaving the existence of a potential energy open, the 3D virtual work of the applied loads through a virtual displacement of the 3D shell structure can be generally represented as

$$\overline{\delta W} = \int_{\Omega} \left(\langle \mathrm{P} \cdot \delta \hat{\mathrm{R}} \rangle + \tau \cdot \delta \hat{\mathrm{R}}^{+} + \beta \cdot \delta \hat{\mathrm{R}}^{-} \right) d\Omega + \int_{\partial\Omega} \langle \mathrm{Q} \cdot \delta \hat{\mathrm{R}} \rangle d(\partial\Omega) \tag{29}$$

where $\mathrm{P} = P_i \mathrm{B}_i$ is the applied body force, $\tau = \tau_i \mathrm{B}_i$ and $\beta = \beta_i \mathrm{B}_i$ are the applied surface tractions on the top and bottom surfaces, respectively, and

$\mathbf{Q}_i = Q_i \mathbf{B}_i$ denotes the applied traction on the lateral surfaces (i.e., the vertical surface on the boundaries). Taking the variation of Eq. (22)

$$\begin{aligned}\delta\hat{\mathbf{R}} = \overline{\delta q_i}\mathbf{B}_i + x_3\delta\varphi_\alpha\mathbf{B}_\alpha + x_3\varphi_\alpha\delta\mathbf{B}_\alpha + x_3\delta\varphi_3\mathbf{B}_3 + x_3[1+\varphi_3]\delta\mathbf{B}_3 \\ + \delta y_i\mathbf{B}_i + y_i\delta\mathbf{B}_i\end{aligned} \tag{30}$$

the 2D virtual displacement and rotation of the reference surface and 2D virtual transverse motions are given in the $\mathbf{B}_i$ system by

$$\begin{aligned}\overline{\delta q_i} &= \delta\mathbf{u}\cdot\mathbf{B}_i \\ \delta\mathbf{B}_i &= (-\overline{\delta\psi_2}\mathbf{B}_1 + \overline{\delta\psi_1}\mathbf{B}_2 + \overline{\delta\psi_3}\mathbf{B}_3)\times\mathbf{B}_i \\ \overline{\delta\varphi_i} &= \delta\varphi_i\cdot\mathbf{B}_i\end{aligned} \tag{31}$$

However, unlike Yu et al. [24] and Yu [25]., it is possible to write the 2D virtual rotations in terms of the partial derivatives of the 2D virtual displacements with respect to x_α because $\mathbf{B}_3$ is taken as the normal to the reference surface of the deformed shell. This means that the present shell model can be determined in terms of six independent 2D shell quantities, not nine.

In a manner similar to the procedure to obtain the 3D strain field under the small strain assumption, we can safely ignore products of the warping functions and the loading in the virtual rotation term. Then, the virtual work done by the applied loads is

$$\overline{\delta W} = \overline{\delta W}_{2D} + \overline{\delta W}^* \tag{32}$$

where

$$\begin{aligned}\overline{\delta W}_{2D} &= \int_{\Omega}\left[f_{\alpha}\overline{\delta q}_{\alpha}+(f_3+e_{3ij}m_{i,j})\overline{\delta q}_3+m_i\overline{\delta\varphi_i}\right]d\Omega \\ &+\int_{\partial\Omega}\left[\langle Q_{\alpha}\rangle\overline{\delta q}_{\alpha}+\langle Q_3+x_3e_{3ij}Q_{i,j}\rangle\overline{\delta q}_3+\langle x_3Q_i\rangle\overline{\delta\varphi_i}\right]d(\partial\Omega) \qquad (33)\\ \overline{\delta W}^{*} &= \int_{\Omega}\left(\langle P_i\delta y_i\rangle+\tau_i\delta y_i^{+}+\beta_i\delta y_i^{-}\right)d\Omega+\int_{\partial\Omega}\langle Q_i\delta y_i\rangle d(\partial\Omega)\end{aligned}$$

with e_{ijk} denoted by the 3D permutation symbol and the generalized forces f_i and moments m_i defined as

$$f_i=\langle P_i\rangle+\tau_i+\beta_i \qquad m_i=\langle x_3P_i\rangle+\frac{h}{2}(\tau_i-\beta_i) \qquad (34)$$

Here the second integral part of $\overline{\delta W}^{*}$ in Eq. (33) accounts for the virtual work done through the warping functions along the lateral boundaries of the shell. This term is only necessary for the edge-zone problem, which is beyond the scope of the present paper. Therefore, we will drop this term hereafter.

Now, the complete statement of the problem can be presented in terms of the principle of virtual work, such that

$$\delta U-\overline{\delta W}^{*}=0 \qquad (35)$$

In spite of the possibility of taking nonconservative forces into account in Eq. (35), the problem governed by the 3D unknown warping functions is conservative. Thus, one can pose the problem that governs the warping functions as a minimum total potential energy:

$$\Pi=U-W^{*} \qquad (36)$$

so that

$$\delta\Pi = 0 \tag{36}$$

where W^* contains the load-related terms such that

$$W^* = \int_\Omega \mathbb{W}^* d\Omega \tag{38}$$

with

$$\mathbb{W}^* = \langle P^T y \rangle + \tau^T y^+ + \beta^T y^- = \langle P^T y \rangle \tag{39}$$

Here Eq. (21) is used the above. Up to this point, this is simply an alternative formulation of the original 3D elasticity problem. Attempts to solve this problem directly will meet with the same difficulties as solving any full 3D elasticity problem. Fortunately, as shown below, the VAM can be used to calculate the 3D unknown warping functions asymptotically up to the desired order.

2.2 Dimensional reduction under VAM

To rigorously and efficiently reduce the original 3D problem to that of an equivalent 2D shell, the VAM will be first used to reproduce the 3D total potential energy functional stored in the structure into the intrinsic formulation in terms of 2D generalized LK strain and transverse motion measures. Then, asymptotically correct solutions will be estimated up to the desired order taking advantage of the small parameters inherent in the structure.

2.2.1 Order analysis

Following Sutyrin [26] and Berdichevsky [27], the quantities of interest assess and keep track of the following determined orders in the formulation:

$$\begin{aligned} &\overline{\delta q}_\alpha \sim h(l/h)\hat{\varepsilon} \quad \overline{\delta q}_3 \sim h(l/h)^2\hat{\varepsilon} \\ &\varepsilon_{\alpha\beta} \sim h\kappa_{\alpha\beta} \sim h\varphi_i \sim \hat{\varepsilon} \quad k_{\alpha\alpha} \sim 1/R \\ &hP_\alpha \sim \tau_\alpha \sim \beta_\alpha \sim \mu(h/l)\hat{\varepsilon} \quad Q_\alpha \sim \mu\hat{\varepsilon} \\ &hP_3 \sim \tau_3 \sim \beta_3 \sim \mu(h/l)^2\hat{\varepsilon} \quad Q_3 \sim \mu(h/l)\hat{\varepsilon} \end{aligned} \tag{40}$$

where μ is the order of the material constants (all of which are assumed to be of the same order). For most engineering structures, ε is a small parameter in the order of $10^{-5} \sim 10^{-3}$ and it is not necessary to keep terms in the order of ε in comparison with unity. And also, in the shell problem, two more small parameters (h/R, h/l) need to be considered. The existence of three small parameters brings about a great variety of asymptotics. Therefore, to compare the approximation theories, the approach denoting by 00EE, 11EE deals with the case of $l \sim R$ while the approach denoting by 22CS deals with the case of $l \sim \sqrt{hR}$.

2.2.2 Zeroth-order approximation (00EE)

Let us now construct a shell model up to the zeroth-order approximation under the VAM. Following the methodology introduced by Berdichevsky [12], the VAM requires one to find the leading terms of the energy functional according to the different orders. For the zeroth-order approximation, at first, the 3D virtual work per unit area in Eq. (38) can be negligible because the applied loads are of higher order according to the order analysis based on Eq. (40). On the other hand, the 3D strain energy per unit area in Eq. (28) can be systematically obtained by dropping the

derivatives with respective to x_α and the terms related to initial curvature, resulting in

$$2\overline{\mathrm{U}}_0 = \left\langle \begin{array}{l} (\varepsilon + x_3\kappa)^T D_{\|} (\varepsilon + x_3\kappa) + (\varphi_{\|} + y_{\|}{}')^T D_s (\varphi_{\|} + y_{\|}{}') \\ + [\varphi_3 + y_3{}' + D_{\perp}^T (\varepsilon + x_3\kappa)]^T D_t [\varphi_3 + y_3{}' + D_{\perp}^T (\varepsilon + x_3\kappa)] \end{array} \right\rangle \tag{41}$$

where $\varepsilon = [\varepsilon_{11} \;\; 2\varepsilon_{12} \;\; \varepsilon_{22}]^T, \kappa = [\kappa_{11} \;\; \kappa_{12} + \kappa_{21} \;\; \kappa_{22}]^T, (\bullet)_{\|} = [(\bullet)_1 \;\; (\bullet)_2 \;\; 0]^T$. Therefore, the 3D total potential functional in Eq. (35) can be simply expressed as:

$$\delta \Pi_0 = 0 \;\text{ with }\; \delta \overline{\mathrm{U}}_0 = 0 \tag{42}$$

along with the constraints in Eq. (21).

By applying the usual procedure of the calculus of variations, this variational principle has the following Euler-Lagrange equations for $y_{\|}$ and y_3:

$$\begin{array}{l} [D_s (\varphi_{\|} + y_{\|}{}')]' = 0 \\ \left\{ D_t [\varphi_3 + y_3{}' + D_{\perp}^T (\varepsilon + x_3\kappa)] \right\}' = 0 \end{array} \tag{43}$$

with the associated in-plane and normal constraints in Eq. (21), respectively, Solving the equations in Eq. (43) along with Eq. (21), one obtains the following warping functions:

$$y_{\|} = 0 \qquad y_3 = -\frac{1}{2}\left[x_3^2 - \left(\frac{h}{2} \right)^2 \right] D_{\perp}^T \kappa \tag{44}$$

By substituting Eq. (44) back into Eq. (41), the asymptotically correct energy functional capable of capturing the transverse shear/normal deformations and based on the zeroth-order approximation can be finally obtained as:

$$2\Pi_0 = \mathcal{E}^T A^0 \mathcal{E} \quad \text{where} \quad A^0 = \begin{bmatrix} A_{11}^0 & 0 & 0 & A_{14}^0 \\ 0 & A_{22}^0 & 0 & 0 \\ 0 & 0 & A_{33}^0 & 0 \\ A_{41}^0 & 0 & 0 & A_{44}^0 \end{bmatrix} \tag{45}$$

with $\mathcal{E} = \left[\varepsilon \ \kappa \ \varphi_{\|} \ \varphi_3\right]^T$ and

$$\begin{aligned} A_{11}^0 &= hD_e \quad A_{14}^0 = hD_{et} \quad A_{22}^0 = \frac{h^3}{12} D_{\|} \\ A_{33}^0 &= hD_s \quad A_{41}^0 = (A_{14}^0)^T \quad A_{44}^0 = hD_t \end{aligned} \tag{46}$$

It is obvious that the total potential energy functional of this approximation coincides with 2D shell model, which is the same as that restricted by the shell composed of an isotropic material found in the Berdichevsky's works.

2.2.3 First-order approximation (11EE and 22CS)

As pointed out in Berdichevsky [12, 27], refined theories taking advantage of small parameters h/R and h/l are required for both moderately thick and thick shells to give a better prediction of global deformation, in-plane quantities and especially out-of-plane stresses and strains, even though the classical shell theory based on the zeroth-order approximation can do a good job in predicting the global deformation and in-plane quantities for thin structures. Therefore, to accurate obtain the energy contributions for shells, another more approximation under the VAM is carried out in the asymptotic sense.

Before proceeding to the derivation of the refined shell model, let us check that if all terms containing $\kappa_{12} - \kappa_{21}$ can be neglected as higher-order terms according to the 2D compatibility equation or not. As pointed out in Yu and Hodges [28], from the $\mathbf{B}_3$ components of the equality $\mathbf{R}_{;12} = \mathbf{R}_{;21}$,

the difference between κ_{21} and κ_{12} can be obtained as

$$\frac{\kappa_{12}-\kappa_{21}}{2}=\frac{\varepsilon_{12}(K_{22}-K_{11})+\dfrac{\kappa_{12}+\kappa_{21}}{2}(\varepsilon_{11}-\varepsilon_{22})}{2+\varepsilon_{11}+\varepsilon_{22}}=\frac{k_{22}-k_{11}}{2}\varepsilon_{12}+O(\hat{\varepsilon}^2) \tag{47}$$

The difference is clearly $O\left(\dfrac{\hat{\varepsilon}h}{l^2}\right)$ or $O\left(\dfrac{\hat{\varepsilon}}{R}\right)$, and one can show that it contributes terms that are $O\left(\dfrac{\mu\hat{\varepsilon}^3h^2}{l^2}\right)$ or $O\left(\dfrac{\mu\hat{\varepsilon}^2h^2}{R^2}\right)$. Therefore, as mentioned in Yu and Hodges [28], $\kappa_{12}-\kappa_{21}$ is neglected as higher-order terms in the first-order approximation for the case $l\sim\sqrt{hR}$. However, if $l\sim R$, such terms should be considered. Hence, in the approach 11EE, $\kappa_{12}-\kappa_{21}$ is included in the 3-D strain field, where the difference will be used as a result obtained from the compatibility equation instead of using it directly.

At first, let us consider the case of $l\sim R$. Having made the approximation ($l\sim R$), one can express the 3-D strain field including the terms of order h/R, $(h/R)^2$, h/l and $(h/l)^2$, such as

$$\begin{aligned}
\Gamma_e &= \varepsilon+x_3\kappa-I_{Re}x_3(\varepsilon+x_3\kappa)+I_{RRe}x_3^2(\varepsilon+x_3\kappa)+I_\alpha(x_3\varphi_{\|;\alpha}+y_{\|;\alpha})\\
&\quad -I_\alpha e_{R\alpha}x_3^2\varphi_{|}+I_R(x_3\varphi_3+y_3)-I_{Re}I_Rx_3(x_3\varphi_3+y_3)+x_3^2I_{RR\omega}\varepsilon\\
2\Gamma_s &= \varphi_\|+y_\|'+e_\alpha(x_3\varphi_{3;\alpha}+y_{3;\alpha})-e_R(x_3\varphi_\|+y_\|)\\
&\quad -x_3e_Re_\alpha(x_3\varphi_{3;\alpha}+y_{3;\alpha})+x_3^2e_Re_R\varphi_\|\\
\Gamma_t &= \varphi_3+y_3'
\end{aligned} \tag{48}$$

with

$$I_1=\begin{bmatrix}1&0\\0&1\\0&0\end{bmatrix}\quad I_2=\begin{bmatrix}0&0\\1&0\\0&1\end{bmatrix}\quad e_1=\begin{bmatrix}1\\0\end{bmatrix}\quad e_2=\begin{bmatrix}0\\1\end{bmatrix}\quad I_R=\begin{bmatrix}k_{11}\\0\\k_{22}\end{bmatrix}\quad e_R=\begin{bmatrix}k_{11}&0\\0&k_{22}\end{bmatrix}$$

$$I_{Re}=\begin{bmatrix}k_{11}&0&0\\0&\dfrac{k_{11}+k_{22}}{2}&0\\0&0&k_{22}\end{bmatrix}\quad I_{RRe}=\begin{bmatrix}k_{11}^2&0&0\\0&\dfrac{k_{11}^2+k_{22}^2}{2}&0\\0&0&k_{22}^2\end{bmatrix}\quad e_{R1}=\begin{bmatrix}k_{11}&0\\0&k_{11}\end{bmatrix}\qquad (49)$$

$$e_{R2}=\begin{bmatrix}k_{22}&0\\0&k_{22}\end{bmatrix}\quad I_{RRw}=\begin{bmatrix}0&0&0\\0&\left(\dfrac{k_{11}-k_{22}}{2}\right)^2&0\\0&0&0\end{bmatrix}$$

Then the zeroth-order result is perturbed to find the 3D refined warping fields of order h/l, h/R, resulting in the following form:

$$y_{\|}=v_{\|}\ \text{ and }\ y_3=\bar{y}_3+v_3\ \text{ with }\ \bar{y}_3=-\frac{1}{2}\left[x_3^2-\left(\frac{h}{2}\right)^2\right]D_{\perp}^{T}\kappa \qquad (50)$$

In a manner similar to the procedure used to obtain the warping functions for the zeroth-order approximation, one obtains the following warping functions. For $v_{\|}$:

$$v_{\|}=-\frac{1}{2}\left[x_3^2-\left(\frac{h}{2}\right)^2\right]\left\{D_s^{-1}I_{\alpha}^{T}D_e^{T}\varepsilon_{;\alpha}+\frac{x_3}{3}D_{\|\alpha}\kappa_{,\alpha}+D_{s\alpha}\varphi_{3;\alpha}+D_{R\varphi}\varphi_{\|}\right\} \qquad (51)$$

where $D_{\|\alpha}=D_s^{-1}I_{\alpha}^{T}D_{\|}^{T}-e_{\alpha}D_{\perp}^{T}$, $D_{s\alpha}=D_s^{-1}I_{\alpha}^{T}D_{et}+e_{\alpha}$ and $D_{R\varphi}=D_s^{-1}e_R^{T}D_s^{T}+k_{11}+k_{22}-e_R$, and for v_3:

$$v_3=\frac{1}{2}\left[x_3^2-\left(\frac{h}{2}\right)^2\right]\left\{D_{R\varepsilon}\varepsilon+\frac{x_3}{3}D_{R\kappa}\kappa-D_{t\alpha}\varphi_{\|;\alpha}-(k_{11}+k_{22})\varphi_3\right\} \qquad (52)$$

where $D_{R\varepsilon}=D_t^{-1}I_R^{T}D_e+D_{\perp}^{T}I_{Re}-(k_{11}+k_{22})D_{\perp}^{T}$, $D_{R\kappa}=D_t^{-1}I_R^{T}D_e+2D_{\perp}^{T}I_{Re}$ and $D_{t\alpha}=D_t^{-1}e_{\alpha}^{T}D_s^{T}+D_{\perp}^{T}I_{\alpha}$.

Now, all the information needed to obtain a total energy functional that is asymptotically correct up to the order of $\mu(h/l)^2\hat{\varepsilon}^2$ and $\mu(h/R)^2\hat{\varepsilon}^2$ has been found, viz.,

$$2\Pi_1 = \mathcal{E}^T(A^0 + A^0_{R1} + A^0_{R2})\mathcal{E} + 2\mathcal{E}^T(A^{01}_{\alpha}\mathcal{E}_{;\alpha} + A^{01}_{R\alpha}\mathcal{E}_{;\alpha} + A^{02}_{\alpha\beta}\mathcal{E}_{;\alpha\beta}) + \mathcal{E}^T_{;\alpha}A^{11}_{\alpha\beta}\mathcal{E}_{;\beta} \tag{53}$$

Where

$$A^{01}_{\alpha} = \begin{bmatrix} 0 & 0 & 0 & 0 \\ 0 & 0 & A^{01}_{23\alpha} & 0 \\ 0 & A^{01}_{32\alpha} & 0 & 0 \\ 0 & 0 & 0 & 0 \end{bmatrix} \quad A^{02}_{\alpha\beta} = \begin{bmatrix} A^{02}_{11\alpha\beta} & 0 & 0 & 0 \\ 0 & A^{02}_{22\alpha\beta} & 0 & A^{02}_{24\alpha\beta} \\ 0 & 0 & A^{02}_{33\alpha\beta} & 0 \\ 0 & A^{02}_{42\alpha\beta} & 0 & A^{02}_{44\alpha\beta} \end{bmatrix}$$

$$A^{11}_{\alpha\beta} = \begin{bmatrix} A^{11}_{11\alpha\beta} & 0 & 0 & A^{11}_{14\alpha\beta} \\ 0 & A^{11}_{22\alpha\beta} & 0 & 0 \\ 0 & 0 & A^{11}_{33\alpha\beta} & 0 \\ A^{11}_{41\alpha\beta} & 0 & 0 & A^{11}_{44\alpha\beta} \end{bmatrix} \quad A^{0}_{R1} = \begin{bmatrix} 0 & A^{0}_{12R1} & 0 & 0 \\ A^{0}_{21R1} & 0 & 0 & A^{0}_{24R1} \\ 0 & 0 & 0 & 0 \\ 0 & A^{0}_{42R1} & 0 & 0 \end{bmatrix} \tag{54}$$

$$A^{0}_{R2} = \begin{bmatrix} A^{0}_{11R2} & 0 & 0 & A^{0}_{14R2} \\ 0 & A^{0}_{22R2} & 0 & 0 \\ 0 & 0 & A^{0}_{33R2} & 0 \\ A^{0}_{41R2} & 0 & 0 & A^{0}_{44R2} \end{bmatrix} \quad A^{01}_{R\alpha} = \begin{bmatrix} 0 & 0 & A^{01}_{13R\alpha} & 0 \\ 0 & 0 & 0 & 0 \\ A^{01}_{31R\alpha} & 0 & 0 & A^{01}_{34R\alpha} \\ 0 & 0 & A^{01}_{43R\alpha} & 0 \end{bmatrix}$$

with

$$A^{01}_{23\alpha} = \frac{h^3}{12}(D_s^{-1}I_\alpha^T D_\parallel)^T D_s \quad A^{01}_{32\alpha} = \frac{h^3}{12}D_s e_\alpha D_\perp^T \quad A^{02}_{11\alpha\beta} = \frac{h^3}{12}(D_s^{-1}I_\alpha^T D_e)^T I_\beta^T D_e$$

$$A^{02}_{22\alpha\beta} = \frac{h^5}{720}(D_s^{-1}I_\alpha^T D_\parallel)^T D_s D_{\parallel\beta} \quad A^{02}_{24\alpha\beta} = \frac{h^3}{12}(D_s^{-1}I_\beta^T D_e)^T I_\alpha^T D_{et} \quad A^{02}_{42\alpha\beta} = (A^{02}_{24\alpha\beta})^T$$

$$A^{11}_{14\alpha\beta} = \frac{h^3}{12}(D_s^{-1}I_\alpha^T D_e)^T I_\beta^T D_{et} \quad A^{11}_{33\alpha\beta} = \frac{h^3}{12}[I_\alpha^T D_\parallel I_\beta + (D_t^{-1}e_\alpha^T D_s)^T I_\beta^T D_{et}]$$

$$A^{11}_{22\alpha\beta} = \frac{h^5}{720}[(D_s^{-1}I_\alpha^T D_\parallel)^T I_\beta^T D_\parallel + 5(e_\alpha D_\perp^T)^T D_s (e_\beta D_\perp^T)] \quad A^{11}_{41\alpha\beta} = (A^{11}_{14\alpha\beta})^T$$

$$A^{02}_{33\alpha\beta}=\frac{h^3}{12}(e^T_\alpha D_s)^T D_{t\beta}\;A^{02}_{44\alpha\beta}=\frac{h^3}{12}(D_s^{-1}I^T_\alpha D_{et})^T D_s D_{s\beta}\;\;A^0_{21R1}=(A^0_{12R1})^T$$

$$A^{11}_{44\alpha\beta}=\frac{h^3}{12}(D_s^{-1}I^T_\alpha D_{et})^T I^T_\beta D_{et}\;\;A^0_{12R1}=\frac{h^3}{12}[-2D_eI_{Re}+(k_{11}+k_{22})D_\parallel+D_eI_RD^T_\perp]$$

$$A^0_{11R2}=\frac{h^3}{12}[\,2D_e(I_{RRe}+I_{RR\omega})+I^T_{Re}D_eI_{Re}-2(k_{11}+k_{22})D_eI_{Re}$$
$$+k_{11}k_{22}D_e-D_t^{-1}D^T_{R\varepsilon}D_{R\varepsilon}]$$

$$A^0_{14R2}=\frac{h^3}{12}\begin{bmatrix}-D_eI_{Re}I_R-I^T_{Re}D_eI_R+2(k_{11}+k_{22})D_eI_R\\-(k^2_{11}+k_{11}k_{22}+k^2_{22})D_{et}+(I_{RRe}+I_{RR\omega})D_{et}\end{bmatrix}\;\;A^0_{41R2}=(A^0_{14R2})^T$$

$$A^0_{22R2}=\frac{h^5}{720}\begin{bmatrix}18D_\parallel I_{RRe}+9(I^T_{Re}D_e-2(k_{11}+k_{22})D_\parallel)I_{Re}+9k_{11}k_{22}D_\parallel\\-D_tD^T_{R\kappa}D_{R\kappa}+6(-2D_eI_{Re}+(k_{11}+k_{22})D_e\\+D_\perp(I^T_RD_e+D^T_{et}I_{Re}-(k_{11}+k_{22})D^T_{et}))I_RD^T_\perp\end{bmatrix}$$

$$A^0_{24R1}=\frac{h^3}{12}(D_eI_R-I^T_{Re}D_{et})\;\;A^0_{42R1}=(A^0_{24R1})^T$$

$$A^0_{33R2}=\frac{h^3}{12}[2D_se_Re_R+e^T_RD_se_R-2(k_{11}+k_{22})D_se_R-(k_{11}-k_{11}k_{22}+k_{22})D_s]$$

$$A^0_{44R2}=\frac{h^3}{12}\begin{bmatrix}-2D^T_{et}I_{Re}I_R+I^T_RD_eI_R+2(k_{11}+k_{22})D^T_{et}I_R\\-(k^2_{11}+k_{11}k_{22}+k^2_{22})D_t\end{bmatrix}$$

$$A^{01}_{13R\alpha}=\frac{h^3}{12}\begin{bmatrix}-D_eI_\alpha e_{R\alpha}-I^T_{Re}D_eI_\alpha+(k_{11}+k_{22})D_eI_\alpha+D_eI_\alpha D_{R\varphi}\\+(I^T_{Re}D_{et}-(k_{11}+k_{22})D_{et}+D_eI_R)D_{t\alpha}-D^T_{R\varepsilon}e^T_\alpha D_s\end{bmatrix}$$

$$A^{01}_{31R\alpha}=-\frac{h^3}{12}\left[D_se_\alpha D_{R\varepsilon}+(k_{11}+k_{22})I^T_\alpha D^T_e-D^T_{R\varphi}D_s^TD_s^{-1}I^T_\alpha D^T_e\right]$$

$$A^{01}_{34R\alpha}=\frac{h^3}{12}\begin{bmatrix}-D_se_Re_\alpha-(k_{11}+k_{22})I^T_\alpha D_{et}+(k_{11}+k_{22})D_se_\alpha\\-e^T_RD^T_se_\alpha+D^T_{R\varphi}I^T_\alpha D_{et}\end{bmatrix}$$

$$A^{01}_{43R\alpha}=\frac{h^3}{12}\left[-D^T_{et}I_\alpha e_{R\alpha}+I^T_RD_eI_\alpha+D^T_{et}I_\alpha D_{R\varphi}\right]\qquad(55)$$

If $l\sim\sqrt{hR}$, we are only interested in obtaining an energy functional asymptotically correct up to the order of h/R, it is unnecessary to calculate the refined warping functions with respect to h/R because they make no contribution to the energy up to the order of h/R. Therefore, one needs only to find the 3D refined warping fields of the order of h/l and simply

perturb the zeroth-order result. Then, the 3D refined warping field can be constructed by discarding all the terms of initial curvatures, which leads to

$$\begin{aligned} v_{\|} &= -\frac{1}{2}\left[x_3^2-\left(\frac{h}{2}\right)^2\right]\left\{D_s^{-1}I_\alpha^T D_e^T \varepsilon_{;\alpha}+\frac{x_3}{3}D_{\|\alpha}\kappa_{;\alpha}+D_{s\alpha}\varphi_{3;\alpha}\right\} \\ v_3 &= -\frac{1}{2}\left[x_3^2-\left(\frac{h}{2}\right)^2\right]D_{t\alpha}\varphi_{\|;\alpha} \end{aligned} \tag{56}$$

All the information needed to obtain a total energy functional that is asymptotically correct up to the order of $\mu(h/l)^2\hat{\varepsilon}^2$ and $\mu(h/R)\hat{\varepsilon}^2$ has been found, viz.,

$$2\Pi_1 = \mathcal{E}^T(A^0+A_{R1}^0)\mathcal{E}+2\mathcal{E}^T(A_\alpha^{01}\mathcal{E}_{;\alpha}+A_{\alpha\beta}^{02}\mathcal{E}_{;\alpha\beta})+\mathcal{E}_{;\alpha}^T A_{\alpha\beta}^{11}\mathcal{E}_{;\beta} \tag{57}$$

Before closing this subsection, it is noted that in order to obtain the asymptotically correct energy functional, integration of parts with respect to was naturally introduced into Yu [13, 14] for no apparent reason. However, according to Lee and Hodges [29] and Lee [30], one can observe that it causes a violation of the positive definiteness of derived stiffness coefficients, so it was not applied in Eqs. (53) and (57).

3. Universal 2D shell model from the LW perspective

Carrera and Brischetto [9] and Demasi and Yu [8] provided an excellent review of various ESL- and LW-based shell models that had been applied to the analysis of multilayered and sandwich structures by comparing 3D exact solutions as well as the results from these models. In particular, they have shown that since most of ESL-based models have significant problems to accurate predict mechanical characteristics of sandwich shells with very high FCSRs, LW-based shell ones should be used instead. Moreover, as pointed out the Berdichevsky's works, to accurate predict the mechanical behaviors of the sandwich shell, the 2D generalized transverse motion measures, "in the worst case scenario", is chosen to be on the order of $(l/h)\hat{\varepsilon}$ due to mismatch between constituent materials.

For this reason, from the LW-based perspective, let us first regard the sandwich shell as an assembly of three individual layers with mismatched constituent material and geometric properties and describe each layer of which as an equivalent 2D shell model composed of material and geometry having different orders.

3.1 PA(00EE)

The energy functional storing in the composite sandwich shell and based on asymptotically correct through the zeroth-order can be obtained by utilizing Eq. (45) for two skin-layers and one core-layer, resulting in

$$2\Pi = (\mathcal{E}^{\lambda})^{T} A^{0\lambda} (\mathcal{E}^{\lambda}) + (\mathcal{E}^{c})^{T} A^{0c} (\mathcal{E}^{c}) \tag{58}$$

where the superscripts $\lambda(=t,b)$ and c identify the quantities at the "top-skin", "bottom-skin" and "core" layers of the composite sandwich shell, respectively. However, because the numbers of required DOF of Eq. (58) are much higher than ones of Eq. (45), attempt to utilize this directly will meet with the same difficulties as the 3D elasticity-based approach. Therefore, to maximize the simplicity and enhance the efficiency of the present approach, another expression of the energy functional for composite sandwich shells is inevitably required.

Similar to the analytic framework proposed by the Berdichevsky's works, twelve continuity conditions at each skin-core interfaces are first introduced into Eq. (58) to reduce the numbers of DOF up to six and then to develop the energy functional in terms of the only core-layer's 2D generalized LK strain, transverse motion measures and initial curvatures of undeformed geometry. (ε^{c}, κ^{c}, φ_{i}^{c} and $k_{\alpha\alpha}^{c}$). First of all, eight of them can be specified by defining the interlaminar 3D displacement continuity conditions with $\mathrm{U} = \hat{\mathrm{R}} - \hat{\mathrm{r}}$ such that

$$\mathrm{U}^{t}\big|_{x_3^t = -h^t/2} = \mathrm{U}^{c}\big|_{x_3^c = h^c/2} \qquad \mathrm{U}^{b}\big|_{x_3^b = h^b/2} = \mathrm{U}^{c}\big|_{x_3^c = -h^c/2} \tag{59}$$

Alternatively, by substituting the following kinematic identities with $\boldsymbol{b}_3^t = \boldsymbol{b}_3^b = \boldsymbol{b}_3^c$

$$\mathrm{r}^{t} = \mathrm{r}^{c} + \frac{h^c}{2}\mathrm{b}_3^c + \frac{h^t}{2}\mathrm{b}_3^t \qquad \mathrm{r}^{b} = \mathrm{r}^{c} - \frac{h^c}{2}\mathrm{b}_3^c - \frac{h^b}{2}\mathrm{b}_3^b \tag{60}$$

into Eq. (59), it is straightforward to be replaced with the continuity conditions of undeformed and deformed position vectors at the interfaces between the core-layer and two skin-layers, such as

$$\hat{\mathbf{r}}^{\mathrm{t}}\big|_{x_3^t=-h^t/2}=\hat{\mathbf{r}}^{\mathrm{c}}\big|_{x_3^c=h^c/2}\qquad \hat{\mathbf{r}}^{\mathrm{b}}\big|_{x_3^b=h^b/2}=\hat{\mathbf{r}}^{\mathrm{c}}\big|_{x_3^c=-h^c/2} \tag{61}$$

and

$$\hat{\mathbf{R}}^{\mathrm{t}}\big|_{x_3^t=-h^t/2}=\hat{\mathbf{R}}^{\mathrm{c}}\big|_{x_3^c=h^c/2}\qquad \hat{\mathbf{R}}^{\mathrm{b}}\big|_{x_3^b=h^b/2}=\hat{\mathbf{R}}^{\mathrm{c}}\big|_{x_3^c=-h^c/2} \tag{62}$$

Although the universal model developed by the Berdichevsky's works satisfies the interlaminar displacement continuity, it does not mention about the aspects related to transverse stress continuity as other six constraints. By definition, the interlaminar continuity conditions of the transverse shear and normal stress fields can be obtained by

$$\begin{aligned}
&\sigma_s^t\big|_{x_3^t=-h^t/2}=\sigma_s^c\big|_{x_3^c=h^c/2} \qquad \sigma_t^t\big|_{x_3^t=-h^t/2}=\sigma_t^c\big|_{x_3^c=h^c/2}\\
&\sigma_s^b\big|_{x_3^b=h^b/2}=\sigma_s^c\big|_{x_3^c=-h^c/2} \qquad \sigma_t^b\big|_{x_3^b=h^b/2}=\sigma_b^c\big|_{x_3^c=-h^c/2}
\end{aligned} \tag{63}$$

where

$$\begin{aligned}
\sigma_s &= D_s(2\Gamma_s)=D_s\varphi_{\|}\\
\sigma_t &= D_{et}^T\Gamma_e+D_t\Gamma_t=D_t^{-1}(\varphi_3+D_{\perp}^T\varepsilon)
\end{aligned} \tag{64}$$

Before imposing Eqs. (62) and (63) on Eq. (58) to reduce the numbers of DOF up to six, the continuity conditions of undeformed position vectors can be first mentioned. Firstly, let us try to establish the relationship between $\boldsymbol{b}_i^t$ for the top skin-layer and $\boldsymbol{b}_i^c$ for the core-layer. By differentiating both side of Eq. (61) with respect to x_α and then introducing Eqs. (3) and (4) into the obtained result, the relationships between Lame parameters for the upper skin-layer and Lame parameters for the core are given by

$$A_\alpha^t=A_\alpha^c S_\alpha^t \tag{65}$$

with $S_1^t = 1 + \frac{h^c}{2}\left[1 + \frac{h^t}{h^c}\right]k_{11}^c$ and $S_2^t = 1 + \frac{h^c}{2}\left[1 + \frac{h^t}{h^c}\right]k_{22}^c$.

And then, to find the relationship between initial curvatures, differentiate both side of the following kinematic identity $\boldsymbol{b}_3^t = \boldsymbol{b}_3^c$ with respect to x_α. Initial curvatures of top-skin layer can be specified in terms of the initial curvatures of core-layer, such as

$$S_\alpha^t k_{\alpha\alpha}^t = k_{\alpha\alpha}^c \tag{66}$$

Analogously, one can also obtain the relationship between $k_{\alpha\alpha}^b$ and $k_{\alpha\alpha}^c$ such as

$$S_\alpha^b k_{\alpha\alpha}^b = k_{\alpha\alpha}^c \tag{67}$$

with $S_1^b = 1 - \frac{h^c}{2}\left[1 + \frac{h^b}{h^c}\right]k_{11}^c$ and $S_2^b = 1 - \frac{h^c}{2}\left[1 + \frac{h^b}{h^c}\right]k_{22}^c$.

And, let us try to establish the relationship between B_i^t and B_i^b for two skin-layers and B_i^c for the core-layer. By differentiating both sides of the first equation of Eq. (62) with respect to x_α and then introducing Eqs. (19) and (44) into the obtained results, the first-order derivative of $\hat{\mathrm{R}}$ on the interface is given by

$$\begin{aligned} &A_1^t[(1+\varepsilon_{11}^t - \frac{h^t}{2}K_{11}^t - \frac{h^t}{2}\varphi_{1|1}^t - \frac{h^t}{2}k_{11}^t\varphi_3^t)\mathrm{B}_1^t + (\varepsilon_{12}^t - \frac{h^t}{2}\kappa_{12}^t - \frac{h^t}{2}\varphi_{2|1}^t)\mathrm{B}_2^t \\ &+ (-\frac{h^t}{2}\varphi_{3|1}^t + \frac{h^t}{2}k_{11}^t\varphi_1^t)\mathrm{B}_3^t] = A_1^c[(1+\varepsilon_{11}^c + \frac{h^c}{2}K_{11}^c + \frac{h^c}{2}\varphi_{1;1}^c + \frac{h^c}{2}k_{11}^c\varphi_3^c)\mathrm{B}_1^c \\ &+ (\varepsilon_{12}^c + \frac{h^c}{2}\kappa_{12}^c + \frac{h^c}{2}\varphi_{2;1}^c)\mathrm{B}_2^c + (\frac{\mathrm{h}^c}{2}\varphi_{3;1}^c - \frac{\mathrm{h}^c}{2}\mathrm{k}_{11}^c\varphi_1^c)\mathrm{B}_3^c] \end{aligned} \tag{68}$$

and

$$A_2^t[(\varepsilon_{21}^t-\frac{h^t}{2}\kappa_{21}^t-\frac{h^t}{2}\varphi_{1|2}^t)\mathbf{B}_1^t+(1+\varepsilon_{22}^t-\frac{h^t}{2}K_{22}^t-\frac{h^t}{2}\varphi_{2|2}^t-\frac{h^t}{2}k_{22}^t\varphi_3^t)\mathbf{B}_2^t$$
$$+(-\frac{h^t}{2}\varphi_{3|2}^t+\frac{h^t}{2}k_{22}^t\varphi_2^t)\mathbf{B}_3^t]=A_2^c[(\varepsilon_{21}^c+\frac{h^c}{2}\kappa_{21}^c+\frac{h^c}{2}\varphi_{1;2}^c)\mathbf{B}_1^c$$
$$+(1+\varepsilon_{22}^c+\frac{h^c}{2}K_{22}^c+\frac{h^c}{2}\varphi_{2;2}^c+\frac{h^c}{2}k_{22}^c\varphi_3^c)\mathbf{B}_2^c+(\frac{h^c}{2}\varphi_{3;2}^c-\frac{h^c}{2}k_{22}^c\varphi_2^c)\mathbf{B}_3^c] \tag{69}$$

Similar to the kinematic identity suggested by Yu [13] under the small strain assumption, the relationship between these two sets of basis vectors can be specified by a direction cosine matrix which will be expressed in terms of the partial derivatives of φ_3^c with respect to x_α

$$\begin{bmatrix}\mathbf{B}_1^c\\ \mathbf{B}_2^c\\ \mathbf{B}_3^c\end{bmatrix}=C^{\mathbf{B}^c\mathbf{B}^t}\begin{bmatrix}\mathbf{B}_1^t\\ \mathbf{B}_2^t\\ \mathbf{B}_3^t\end{bmatrix}=\begin{bmatrix}C_{11}^t & C_{12}^t & C_{13}^t\\ C_{21}^t & C_{22}^t & C_{23}^t\\ C_{31}^t & C_{32}^t & C_{33}^t\end{bmatrix}\begin{bmatrix}\mathbf{B}_1^t\\ \mathbf{B}_2^t\\ \mathbf{B}_3^t\end{bmatrix} \tag{70}$$

Multiplying both sides of Eqs. (68) and (69) by $\mathbf{B}_3^c$, one obtains

$$\begin{aligned}&S_1^t[(1+\varepsilon_{11}^t-\frac{h^t}{2}K_{11}^t-\frac{h^t}{2}\varphi_{1|1}^t-\frac{h^t}{2}k_{11}^t\varphi_3^t)\mathbf{B}_1^t.+(\varepsilon_{12}^t-\frac{h^t}{2}\kappa_{12}^t-\frac{h^t}{2}\varphi_{2|1}^t)\mathbf{B}_2^t\\ &+(-\frac{h^t}{2}\varphi_{3|1}^t+\frac{h^t}{2}k_{11}^t\varphi_1^t)\mathbf{B}_3^t].\mathbf{B}_3^c=\frac{h^c}{2}\varphi_{3;1}^c-\frac{h^c}{2}k_{11}^c\varphi_1^c\\ &S_2^t[(\varepsilon_{21}^t-\frac{h^t}{2}\kappa_{21}^t-\frac{h^t}{2}\varphi_{1|2}^t)\mathbf{B}_1^t+(1+\varepsilon_{22}^t-\frac{h^t}{2}K_{22}^t-\frac{h^t}{2}\varphi_{2|2}^t-\frac{h^t}{2}k_{22}^t\varphi_3^t)\mathbf{B}_2^t\\ &+(-\frac{h^t}{2}\varphi_{3|2}^t+\frac{h^t}{2}k_{22}^t\varphi_2^t)\mathbf{B}_3^t].\mathbf{B}_3^c=\frac{h^c}{2}\varphi_{3;2}^c-\frac{h^c}{2}k_{22}^c\varphi_2^c\end{aligned} \tag{71}$$

Considering the fact that we assume the strains to be small, one can easily inspect that

$$C_{31}^t=\frac{h^c}{2}(\varphi_{3;1}^c-k_{11}^c\varphi_1^c),\quad C_{32}^t=\frac{h^c}{2}(\varphi_{3;2}^c-k_{22}^c\varphi_2^c) \tag{72}$$

When the following identity for the third row of the direction cosine matrix

in Eq. (71) is also restricted

$$(C_{31}^t)^2+(C_{32}^t)^2+(C_{33}^t)^2=1 \tag{73}$$

one can deduce that $C_{33}^t=1$. Having known the third row of the direction cosine matrix, one can obtain all the other components in this matrix according to Hodges [23]. Using the fact that the direction cosine matrices $C^{\mathbf{B}^c\mathbf{B}^t}$ and $C^{\mathbf{B}^t\mathbf{B}^c}$ are transposed and inverted of each other, one can finally obtain the following relationship between $\mathbf{B}_i^t$ and $\mathbf{B}_i^c$:

$$\mathbf{B}_\alpha^t=\mathbf{B}_\alpha^c+\frac{h^c}{2}(\varphi_{3;\alpha}^c-k_{\alpha\alpha}^c\varphi_\alpha^c)\mathbf{B}_3^c \qquad \mathbf{B}_3^t=-\frac{h^c}{2}(\varphi_{3;\alpha}^c-k_{\alpha\alpha}^c\varphi_\alpha^c)\mathbf{B}_\alpha^c+\mathbf{B}_3^c \tag{74}$$

Analogously, one can also obtain the relationship between $\mathbf{B}_i^b$ and $\mathbf{B}_i^c$ such as

$$\mathbf{B}_\alpha^b=\mathbf{B}_\alpha^c-\frac{h^c}{2}(\varphi_{3;\alpha}^c-k_{\alpha\alpha}^c\varphi_\alpha^c)\mathbf{B}_3^c \qquad \mathbf{B}_3^b=\frac{h^c}{2}(\varphi_{3;\alpha}^c-k_{\alpha\alpha}^c\varphi_\alpha^c)\mathbf{B}_\alpha^c+\mathbf{B}_3^c \tag{75}$$

From Eqs. (62) with Eqs. (74) and (75), we can then derive the following kinematic identities of the generalized LK strain and transverse motion measures of two skin-layers in terms of the corresponding ones of the core-layer,

$$\varepsilon^\lambda=\varepsilon^c+\Gamma_\kappa^{\lambda c}\kappa^c+\Gamma_{\|\alpha}^{\lambda c}\varphi_{\|;\alpha}^c+\Gamma_{\perp R}^{\lambda c}\varphi_3^c+\Gamma_{\|\alpha}^{\lambda}\varphi_{\|;\alpha}^\lambda+\Gamma_{\perp R}^{\lambda}\varphi_3^\lambda \tag{76}$$

where $\delta^t=-\delta^b=1$ and

$$\begin{aligned}&\Gamma_\kappa^{\lambda c}=\delta^\lambda\frac{h^c}{2}\left[1+\frac{h^\lambda}{h^c}\right] \quad \Gamma_{\|\alpha}^{\lambda c}=\delta^\lambda\frac{h^c}{2}I_\alpha \quad \Gamma_{\perp R}^{\lambda c}=\delta^\lambda\frac{h^c}{2}I_R^c\\ &\Gamma_{\|\alpha}^{\lambda}=\delta^\lambda\frac{h^\lambda}{2}I_\alpha \quad \Gamma_{\perp R}^{\lambda}=\delta^\lambda\frac{h^\lambda}{2}I_R^c\end{aligned} \tag{77}$$

Similar to Lee et al. [1], plugging Eq. (64) into Eq. (63) with Eqs. (74) and (75) we obtain φ^t and φ^b in terms of φ^c and ε^t, ε^b and ε^c

$$\begin{aligned}\varphi_{\|}^{\lambda} &= \Phi_{\|}^{\lambda c}\varphi_{\|}^{c} \\ \varphi_{3}^{\lambda} &= \Psi_{\varepsilon}^{\lambda c}\varepsilon^{c} + \Psi_{\perp}^{\lambda c}\varphi_{3}^{c} + \Psi_{\varepsilon}^{\lambda}\varepsilon^{\lambda}\end{aligned} \tag{78}$$

where

$$\begin{aligned}&\Phi_{\|}^{\lambda c} = (D_s^{\lambda})^{-1} D_s^{c} \\ &\Psi_{\varepsilon}^{\lambda c} = [(D_t^{\lambda})^{-1} D_t^{c}](D_{\perp}^{c})^{T} \quad \Psi_{\perp}^{\lambda c} = (D_t^{\lambda})^{-1} D_t^{c} \quad \Psi_{\varepsilon}^{\lambda} = -(D_{\perp}^{\lambda})^{T}\end{aligned} \tag{79}$$

By using Eqs. (76) and (78), the kinematic identities of the generalized LK strain and transverse motion measures ($\mathcal{E}^t$ and $\mathcal{E}^b$) of two skin-layers for PA(00EE) can be derived in terms of the corresponding ones ($\mathcal{E}^c$) and their partial derivatives ($\mathcal{E}_{;\alpha}^{c}$) of the core-layer through the zeroth-order approximation. viz.,

$$\mathcal{E}^{\lambda} = \Gamma^{\lambda}\mathcal{E}^{c} + \Gamma_{R}^{\lambda 0}\mathcal{E}^{c} + \Gamma_{\alpha}^{\lambda 0}\mathcal{E}_{;\alpha}^{c} \tag{80}$$

Where the associated operators used in Eq. (80) are also defined as

$$\Gamma^{\lambda} = \begin{bmatrix} \Gamma_{11}^{\lambda} & \Gamma_{12}^{\lambda} & 0 & 0 \\ 0 & \Gamma_{22}^{\lambda} & 0 & 0 \\ 0 & 0 & \Gamma_{33}^{\lambda} & 0 \\ \Gamma_{41}^{\lambda} & \Gamma_{42}^{\lambda} & 0 & \Gamma_{44}^{\lambda} \end{bmatrix} \quad \Gamma_{R}^{\lambda 0} = \begin{bmatrix} 0 & 0 & 0 & \Gamma_{14R}^{\lambda} \\ 0 & 0 & 0 & 0 \\ 0 & 0 & 0 & 0 \\ 0 & 0 & 0 & \Gamma_{44R}^{\lambda} \end{bmatrix} \quad \Gamma_{\alpha}^{\lambda 0} = \begin{bmatrix} 0 & 0 & \Gamma_{13\alpha}^{\lambda} & 0 \\ 0 & 0 & 0 & 0 \\ 0 & 0 & 0 & 0 \\ 0 & 0 & \Gamma_{43\alpha}^{\lambda} & 0 \end{bmatrix} \tag{81}$$

with

$$
\begin{aligned}
&\Gamma_{11}^{\lambda}=\Gamma_{22}^{\lambda}=\triangle_3\ \ \Gamma_{12}^{\lambda}=\Gamma_{\kappa}^{\lambda c}\ \ \Gamma_{33}^{\lambda}=\Phi_{\|}^{\lambda c}\ \ \Gamma_{41}^{\lambda}=\Psi_{\varepsilon}^{\lambda c}\ \ \Gamma_{42}^{\lambda}=\Psi_{\varepsilon}^{\lambda}\Gamma_{\kappa}^{\lambda c}\\
&\Gamma_{44}^{\lambda}=\Psi_{\perp}^{\lambda c}\ \ \Gamma_{14R}^{\lambda}=\Gamma_{\perp R}^{\lambda}\Psi_{\perp}^{\lambda c}\ \ \Gamma_{44R}^{\lambda 0}=\Psi_{\varepsilon}^{\lambda}(\Gamma_{\perp R}^{\lambda c}+\Gamma_{\perp R}^{\lambda}\Psi_{\perp}^{\lambda c})\\
&\Gamma_{13\alpha}^{\lambda}=\Gamma_{\|\alpha}^{\lambda c}+\Gamma_{\|\alpha}^{\lambda}\Phi_{\|}^{\lambda c}\ \ \Gamma_{43\alpha}^{\lambda 0}=\Psi_{\varepsilon}^{\lambda}(\Gamma_{\|\alpha}^{\lambda c}+\Gamma_{\|\alpha}^{\lambda}\Phi_{\|}^{\lambda c})
\end{aligned}
\tag{82}
$$

Here $\triangle_3$ denotes the 3×3 identity matrix.

Finally, for any FCSR, LTR and RTR cases, we have all the information needed to obtain the zeroth-order approximation of the asymptotically universal shell model with the following energy functional:

$$
2\Pi=(\mathcal{E}^c)^T A^{0\mathrm{eff}}(\mathcal{E}^c)+2(\mathcal{E}^c)^T A_{\alpha}^{01\mathrm{eff}}(\mathcal{E}_{;\alpha}^c)+(\mathcal{E}_{;\alpha}^c)^T B_{\alpha\beta}^{11\mathrm{eff}}(\mathcal{E}_{;\beta}^c) \tag{83}
$$

where

$$
\begin{aligned}
&A^{0\mathrm{eff}}=(\Gamma^{\lambda})^T A^{0\lambda}(\Gamma^{\lambda})+2(\Gamma^{\lambda})^T A^{0\lambda}(\Gamma_R^{\lambda 0})+(\Gamma_R^{\lambda 0})^T A^{0\lambda}(\Gamma_R^{\lambda 0})+A^{0c}\\
&A_{\alpha}^{01\mathrm{eff}}=(\Gamma^{\lambda})^T A^{0\lambda}(\Gamma_{\alpha}^{\lambda 0})+(\Gamma_R^{\lambda 0})^T A^{0\lambda}(\Gamma_{\alpha}^{\lambda 0})\\
&B_{\alpha\beta}^{11\mathrm{eff}}=(\Gamma_{\alpha}^{\lambda 0})^T A^{0\lambda}(\Gamma_{\beta}^{\lambda 0})
\end{aligned}
\tag{84}
$$

3.2 PA(11EE)

An energy functional of 2D laminated shell model derived by the VAM found in Yu and Hodges [28] asymptotically correct up to the order of h/R, it is unnecessary to calculate the refined warping functions with respect to h/R. However, as a validation to demonstrate the capability and accuracy of the present approach, the cases of numerical examples $l\sim R$ should also be included. Therefore, in the present approach denoting by 11EE, we calculated the refined warping function with respect to h/R as

well as h/l (See Sect. 2.2.3).

The energy functional storing in the composite sandwich shell, asymptotically correct up to the second order, can be simply obtained by utilizing Eq. (53) for two skin-layers and one core-layer, resulting in

$$\begin{aligned}2\Pi = &(\mathcal{E}^{\lambda})^{T}(A^{0\lambda}+A_{R1}^{0\lambda}+A_{R2}^{0\lambda})(\mathcal{E}^{\lambda})+2(\mathcal{E}^{c})^{T}[A_{\alpha}^{01\lambda}(\mathcal{E}_{;\alpha}^{\lambda})+A_{R\alpha}^{01\lambda}(\mathcal{E}_{;\alpha}^{\lambda})+A_{\alpha\beta}^{02\lambda}(\mathcal{E}_{;\alpha\beta}^{\lambda})]\\ &+(\mathcal{E}^{c})^{T}(A^{0c}+A_{R1}^{0c}+A_{R2}^{0c})(\mathcal{E}^{c})+2(\mathcal{E}^{c})^{T}[A_{\alpha}^{01c}(\mathcal{E}_{;\alpha}^{c})+A_{R\alpha}^{01c}(\mathcal{E}_{;\alpha}^{c})+A_{\alpha\beta}^{02c}(\mathcal{E}_{;c}^{\lambda})]\\ &+(\mathcal{E}_{;\alpha}^{\lambda})^{T}A_{\alpha\beta}^{11\lambda}(\mathcal{E}_{;\beta}^{\lambda})+(\mathcal{E}_{;\alpha}^{c})^{T}A_{\alpha\beta}^{11c}(\mathcal{E}_{;\beta}^{c})\end{aligned} \tag{85}$$

In the same way, as in Sect. 3.1., we can then derive the following kinematic identities of the generalized LK strain and transverse motion measures of two skin-layers in terms of the corresponding ones of the core-layer,

$$\begin{aligned}\varepsilon^{\lambda} = &\varepsilon^{c}+\Gamma_{\kappa}^{\lambda c}\kappa^{c}+\Gamma_{\|\alpha}^{\lambda c}\varphi_{\|;\alpha}^{c}+\Gamma_{\perp\alpha\beta}^{\lambda c}\varphi_{3;\alpha\beta}^{c}+\Gamma_{\|\alpha}^{\lambda}\varphi_{\|;\alpha}^{\lambda}+\Gamma_{\perp R}^{\lambda c}\varphi_{3}^{c}+\Gamma_{\perp R}^{\lambda}\varphi_{3}^{\lambda}\\ &+\Gamma_{\|R\alpha}^{\lambda c}\varphi_{\|;\alpha}^{c}+\Gamma_{R}^{\lambda c}(\varepsilon^{c}+\Gamma_{\kappa}^{\lambda c}\kappa^{c}+\Gamma_{\perp R}^{\lambda c}\varphi_{3}^{c}+\Gamma_{\perp R}^{\lambda}\varphi_{3}^{\lambda})+\Gamma_{\|R\alpha}^{\lambda}(\Gamma_{\|\alpha}^{\lambda c}\varphi_{\|;\alpha}^{c}+\Gamma_{\|\alpha}^{\lambda}\varphi_{\|;\alpha}^{\lambda})\end{aligned} \tag{86}$$

where

$$\begin{aligned}&\Gamma_{\perp\alpha\beta}^{\lambda c}=-\frac{h^{\lambda}}{2}\frac{h^{c}}{2}I_{\alpha}e_{\beta} \quad \Gamma_{\|R\alpha}^{\lambda c}=\frac{h^{\lambda}}{2}\frac{h^{c}}{2}I_{\alpha}e_{R}^{c}\\ &\Gamma_{R}^{\lambda c}=-\delta^{\lambda}\frac{h^{c}}{2}\left[1+\frac{h^{\lambda}}{h^{c}}\right]I_{Re}^{c} \quad \Gamma_{\|R\alpha}^{\lambda}=-\frac{h^{c}}{2}\left[1+\frac{h^{\lambda}}{h^{c}}\right]I_{R\alpha}^{c}\end{aligned} \tag{87}$$

From Eq. (86) with Eqs. (74) and (75), we obtain $\varphi_{\|}^{\lambda}$ and φ_{3}^{λ} in terms of $\varphi_{\|}^{c}$, φ_{3}^{c}, $\mathcal{E}^{\lambda}$ and $\mathcal{E}^{c}$

$$
\begin{aligned}
\varphi_{\|}^{\lambda} &= \Phi_{\|}^{\lambda c}\varphi_{\|}^{c} + \Phi_{\varepsilon\alpha}^{\lambda c}\varepsilon_{;\alpha}^{c} + \Phi_{\kappa\alpha}^{\lambda c}\kappa_{;\alpha}^{c} + \Phi_{\perp\alpha}^{\lambda c}\varphi_{3;\alpha}^{c} + \Phi_{\varepsilon\alpha}^{\lambda}\varepsilon_{;\alpha}^{\lambda} + \Phi_{\perp\alpha}^{\lambda}\varphi_{3;\alpha}^{\lambda} \\
&\quad + \Phi_{\|R}^{\lambda c}\varphi_{\|}^{c} + \Phi_{\|RR}^{\lambda c}\varphi_{\|}^{c} + \Phi_{\perp R\alpha}^{\lambda c}\varphi_{3;\alpha}^{c} + \Phi_{\|R}^{\lambda}\varphi_{\|}^{\lambda} + \Phi_{\|RR}^{\lambda}\varphi_{\|}^{\lambda} + \Phi_{\perp R\alpha}^{\lambda}\varphi_{3;\alpha}^{\lambda} \\
\varphi_{3}^{\lambda} &= \Psi_{\varepsilon}^{\lambda c}\varepsilon^{c} + \Psi_{\perp}^{\lambda c}\varphi_{3}^{c} + \Psi_{\|\alpha}^{\lambda c}\varphi_{\|;\alpha}^{c} + \Psi_{\varepsilon}^{\lambda}\varepsilon^{\lambda} + \Psi_{\|\alpha}^{\lambda}\varphi_{\|;\alpha}^{\lambda} + \Psi_{\varepsilon R}^{\lambda c}\varepsilon^{c} + \Psi_{\kappa R}^{\lambda c}\kappa^{c} \\
&\quad + \Psi_{\perp R}^{\lambda c}\varphi_{3}^{c} + \Psi_{\perp RR}^{\lambda c}\varphi_{3}^{c} + \Psi_{\|R\alpha}^{\lambda c}\varphi_{\|;\alpha}^{c} + \Psi_{\varepsilon R}^{\lambda}\varepsilon^{\lambda} + \Psi_{\perp R}^{\lambda}\varphi_{3}^{\lambda} + \Psi_{\perp RR}^{\lambda}\varphi_{3}^{\lambda} + \Psi_{\|R\alpha}^{\lambda}\varphi_{\|;\alpha}^{\lambda}
\end{aligned}
\tag{88}
$$

where

$$
\begin{aligned}
&\Phi_{\varepsilon\alpha}^{\lambda c} = -\delta^{\lambda}\frac{h^{c}}{2}(D_{s}^{\lambda})^{-1}I_{\alpha}^{T}D_{e}^{c} \quad \Phi_{\kappa\alpha}^{\lambda c} = -\frac{(h^{c})^{2}}{12}\left\{(D_{s}^{\lambda})^{-1}(D_{s}^{c})D_{\|\alpha}^{c} - \left(\frac{h^{\lambda}}{h^{c}}\right)^{2}D_{\|\alpha}^{\lambda}\right\} \\
&\Phi_{\perp\alpha}^{\lambda c} = -\delta^{\lambda}\frac{h^{c}}{2}(D_{s}^{\lambda})^{-1}D_{s}^{c}(D_{s\alpha}^{c} - e_{\alpha}) \quad \Phi_{\varepsilon\alpha}^{\lambda} = -\delta^{\lambda}\frac{h^{\lambda}}{2}(D_{s}^{\lambda})^{-1}I_{\alpha}^{T}D_{e}^{\lambda} \\
&\Phi_{\perp\alpha}^{\lambda} = -\delta^{\lambda}\frac{h^{\lambda}}{2}(D_{s\alpha}^{\lambda} - e_{\alpha}) \quad \Phi_{\|R}^{\lambda c} = -\delta^{\lambda}\frac{h^{c}}{2}(D_{s}^{\lambda})^{-1}D_{s}^{c}(D_{R\varphi}^{c} + e_{R}^{c}) \\
&\Phi_{\|RR}^{\lambda c} = \left(\frac{h^{c}}{2}\right)^{2}(D_{s}^{\lambda})^{-1}D_{s}^{c}e_{R}^{c}e_{R}^{c} \quad \Phi_{\perp R\alpha}^{\lambda c} = -\left(\frac{h^{c}}{2}\right)^{2}(D_{s}^{\lambda})^{-1}D_{s}^{c}e_{R}^{c}e_{\alpha} \\
&\Phi_{\|R}^{\lambda} = -\delta^{\lambda}\frac{h^{\lambda}}{2}(D_{R\varphi}^{\lambda} + e_{R}^{\lambda}) \quad \Phi_{\|RR}^{\lambda} = -\left(\frac{h^{\lambda}}{2}\right)^{2}e_{R}^{\lambda}e_{R}^{\lambda} \\
&\Phi_{\perp R\alpha}^{\lambda} = \left(\frac{h^{\lambda}}{2}\right)^{2}e_{R}^{\lambda}e_{\alpha} \quad \Psi_{\|\alpha}^{\lambda c} = -\delta^{\lambda}\frac{h^{c}}{2}(D_{t}^{\lambda})^{-1}D_{t}^{c}[D_{t\alpha}^{c} - (D_{\perp}^{c})^{T}I_{\alpha}] \\
&\Psi_{\|\alpha}^{\lambda} = -\delta^{\lambda}\frac{h^{\lambda}}{2}[D_{t\alpha}^{\lambda} - (D_{\perp}^{\lambda})^{T}I_{\alpha}] \quad \Psi_{\varepsilon R}^{\lambda c} = \delta^{\lambda}\frac{h^{c}}{2}(D_{t}^{\lambda})^{-1}D_{t}^{c}[D_{R\varepsilon}^{c} - (D_{\perp}^{c})^{T}I_{Re}^{c}] \\
&\Psi_{\kappa R}^{\lambda c} = \frac{(h^{c})^{2}}{12}(D_{t}^{\lambda})^{-1}D_{t}^{c}(D_{R\kappa}^{c} - 3(D_{\perp}^{c})^{T}I_{Re}^{c}) - \frac{(h^{\lambda})^{2}}{12}(D_{R\kappa}^{\lambda} - 3(D_{\perp}^{\lambda})^{T}I_{Re}^{\lambda}) \\
&\Psi_{\perp R}^{\lambda c} = -\delta^{\lambda}\frac{h^{c}}{2}(D_{t}^{\lambda})^{-1}D_{t}^{c}(k_{11}^{c} + k_{22}^{c} - (D_{\perp}^{c})^{T}I_{R}^{c}) \\
&\Psi_{\perp RR}^{\lambda c} = -\left(\frac{h^{c}}{2}\right)^{2}(D_{t}^{\lambda})^{-1}D_{t}^{c}(D_{\perp}^{c})^{T}I_{Re}^{c}I_{R}^{c} \quad \Psi_{\|R\alpha}^{\lambda c} = -\left(\frac{h^{c}}{2}\right)^{2}(D_{t}^{\lambda})^{-1}D_{t}^{c}(D_{\perp}^{c})^{T}I_{\alpha}e_{R\alpha}^{c} \\
&\Psi_{\varepsilon R}^{\lambda} = \delta^{\lambda}\frac{h^{\lambda}}{2}(D_{R\varepsilon}^{\lambda} - (D_{\perp}^{\lambda})^{T}I_{Re}^{\lambda}) \quad \Psi_{\perp R}^{\lambda} = -\delta^{\lambda}\frac{h^{\lambda}}{2}(k_{11}^{\lambda} + k_{22}^{\lambda} - (D_{\perp}^{\lambda})^{T}I_{R}^{\lambda}) \\
&\Psi_{\perp RR}^{\lambda} = \left(\frac{h^{\lambda}}{2}\right)^{2}(D_{\perp}^{\lambda})^{T}I_{Re}^{\lambda}I_{R}^{\lambda} \quad \Psi_{\|R\alpha}^{\lambda} = \left(\frac{h^{\lambda}}{2}\right)^{2}(D_{\perp}^{\lambda})^{T}I_{\alpha}e_{R\alpha}^{\lambda}
\end{aligned}
\tag{89}
$$

By using Eq. (86) and (88), the kinematic identities of the generalized

LK strain and transverse motion measures of two skin-layers for PA(11EE) can be derived in terms of the corresponding ones and their partial derivatives of the core-layer through the first-order approximation. viz.,

$$\mathcal{E}^{\lambda} = (\Gamma^{\lambda} + \Gamma^{\lambda}_{R} + \Gamma^{\lambda}_{RR})\mathcal{E}^{c} + (\Gamma^{\lambda}_{\alpha} + \Gamma^{\lambda}_{R\alpha})\mathcal{E}^{c}_{;\alpha} + \Gamma^{\lambda}_{\alpha\beta}\mathcal{E}^{c}_{;\alpha\beta} \tag{90}$$

Here the associated operators used in Eq. (90) are also defined as

$$\begin{aligned}
\Gamma^{\lambda}_{\alpha} &= \begin{bmatrix} 0 & 0 & \Gamma^{\lambda}_{13\alpha} & 0 \\ 0 & 0 & 0 & 0 \\ \Gamma^{\lambda}_{31\alpha} & \Gamma^{\lambda}_{32\alpha} & 0 & \Gamma^{\lambda}_{34\alpha} \\ 0 & 0 & \Gamma^{\lambda}_{43\alpha} & 0 \end{bmatrix} \qquad \Gamma^{\lambda}_{\alpha\beta} = \begin{bmatrix} 0 & 0 & 0 & \Gamma^{\lambda}_{14\alpha\beta} \\ 0 & 0 & 0 & \Gamma^{\lambda}_{24\alpha\beta} \\ 0 & 0 & \Gamma^{\lambda}_{33\alpha\beta} & 0 \\ 0 & 0 & 0 & \Gamma^{\lambda}_{44\alpha\beta} \end{bmatrix} \\
\Gamma^{\lambda}_{R} &= \begin{bmatrix} \Gamma^{\lambda}_{11R} & \Gamma^{\lambda}_{12R} & 0 & \Gamma^{\lambda}_{14R} \\ 0 & \Gamma^{\lambda}_{22R} & 0 & 0 \\ 0 & 0 & \Gamma^{\lambda}_{33R} & 0 \\ \Gamma^{\lambda}_{41R} & \Gamma^{\lambda}_{42R} & 0 & \Gamma^{\lambda}_{44R} \end{bmatrix} \qquad \Gamma^{\lambda}_{RR} = \begin{bmatrix} 0 & 0 & 0 & \Gamma^{\lambda}_{14RR} \\ 0 & 0 & 0 & 0 \\ 0 & 0 & \Gamma^{\lambda}_{33RR} & 0 \\ 0 & 0 & \Gamma^{\lambda}_{43RR} & 0 \end{bmatrix} \\
\Gamma^{\lambda}_{R\alpha} &= \begin{bmatrix} 0 & 0 & \Gamma^{\lambda}_{13R\alpha} & 0 \\ 0 & 0 & \Gamma^{\lambda}_{23R\alpha} & 0 \\ 0 & 0 & 0 & \Gamma^{\lambda}_{34R\alpha} \\ 0 & 0 & \Gamma^{\lambda}_{43R\alpha} & 0 \end{bmatrix}
\end{aligned} \tag{91}$$

with

$$\begin{aligned}
&\Gamma^{\lambda}_{31\alpha} = \Phi^{\lambda c}_{\varepsilon\alpha} + \Phi^{\lambda}_{\varepsilon\alpha} + \Phi^{\lambda}_{\perp\alpha}(\Psi^{\lambda c}_{\varepsilon} + \Psi^{\lambda}_{\varepsilon}) \quad \Gamma^{\lambda}_{32\alpha} = \Phi^{\lambda c}_{\kappa\alpha} + (\Phi^{\lambda}_{\varepsilon\alpha} + \Phi^{\lambda}_{\perp\alpha}\Psi^{\lambda}_{\varepsilon})\Gamma^{\lambda c}_{\kappa} \\
&\Gamma^{\lambda}_{34\alpha} = \Phi^{\lambda c}_{\perp\alpha} + \Phi^{\lambda c}_{\perp\alpha}\Psi^{\lambda c}_{\perp} \quad \Gamma^{\lambda}_{43\alpha} = \Psi^{\lambda c}_{\|\alpha} + \Psi^{\lambda}_{\varepsilon}(\Gamma^{\lambda c}_{\|\alpha} + \Gamma^{\lambda}_{\|\alpha}\Phi^{\lambda c}_{\|}) + \Psi^{\lambda}_{\|\alpha}\Phi^{\lambda c}_{\|} \\
&\Gamma^{\lambda}_{14\alpha\beta} = \Gamma^{\lambda c}_{\perp\alpha\beta} + \Gamma^{\lambda}_{\|\alpha}(\Phi^{\lambda c}_{\perp\beta} + \Phi^{\lambda}_{\perp\beta}\Psi^{\lambda c}_{\perp}) \quad \Gamma^{\lambda}_{24\alpha\beta} = -\delta^{\lambda}\frac{h^{c}}{2}I_{\alpha}e_{\beta} \\
&\Gamma^{\lambda}_{33\alpha\beta} = \Phi^{\lambda}_{\varepsilon\alpha}(\Gamma^{\lambda c}_{\|\beta} + \Gamma^{\lambda}_{\|\beta}\Phi^{\lambda c}_{\|}) + \Phi^{\lambda}_{\perp\alpha}[\Psi^{\lambda c}_{\|\beta} + \Psi^{\lambda}_{\varepsilon}\Gamma^{\lambda c}_{\|\beta} + (\Psi^{\lambda}_{\varepsilon}\Gamma^{\lambda}_{\|\beta} + \Psi^{\lambda}_{\|\beta})\Phi^{\lambda c}_{\|}] \\
&\Gamma^{\lambda}_{44\alpha\beta} = \Psi^{\lambda}_{\varepsilon}\Gamma^{\lambda c}_{\perp\alpha\beta} + (\Psi^{\lambda}_{\varepsilon}\Gamma^{\lambda}_{\|\alpha} + \Psi^{\lambda}_{\|\alpha})(\Phi^{\lambda c}_{\perp\beta} + \Phi^{\lambda}_{\perp\beta}\Psi^{\lambda c}_{\perp}) \\
&\Gamma^{\lambda}_{11R} = \Gamma^{\lambda c}_{R} + \Gamma^{\lambda}_{\perp R}(\Psi^{\lambda c}_{\varepsilon} + \Psi^{\lambda}_{\varepsilon}) \quad \Gamma^{\lambda}_{12R} = (\Gamma^{\lambda c}_{R} + \Gamma^{\lambda}_{\perp R}\Psi^{\lambda}_{\varepsilon})\Gamma^{\lambda c}_{\kappa} \quad \Gamma^{\lambda}_{22R} = \Gamma^{\lambda c}_{R} \\
&\Gamma^{\lambda}_{33R} = \Phi^{\lambda c}_{\|R} + \Phi^{\lambda}_{\|R}\Phi^{\lambda c}_{\|} \quad \Gamma^{\lambda}_{41R} = \Psi^{\lambda}_{\varepsilon}\Gamma^{\lambda c}_{R} + \Psi^{\lambda c}_{\varepsilon R} + \Psi^{\lambda}_{\varepsilon R} + (\Psi^{\lambda}_{\varepsilon}\Gamma^{\lambda}_{\perp R} + \Psi^{\lambda}_{\perp R})(\Psi^{\lambda c}_{\varepsilon} + \Psi^{\lambda}_{\varepsilon})
\end{aligned}$$

$$
\begin{aligned}
\Gamma^{\lambda}_{42R} &= (\Psi^{\lambda}_{\varepsilon}\Gamma^{\lambda c}_{R}+\Psi^{\lambda}_{\varepsilon R})\Gamma^{\lambda c}_{\kappa}+\Psi^{\lambda c}_{\kappa R}+(\Psi^{\lambda}_{\varepsilon}\Gamma^{\lambda}_{\perp R}+\Psi^{\lambda}_{\perp R})\Psi^{\lambda}_{\varepsilon}\Gamma^{\lambda c}_{\kappa}\\
\Gamma^{\lambda}_{44R} &= \Psi^{\lambda}_{\varepsilon}\Gamma^{\lambda c}_{\perp R}+\Psi^{\lambda c}_{\perp R}+(\Psi^{\lambda}_{\varepsilon}\Gamma^{\lambda}_{\perp R}+\Psi^{\lambda}_{\perp R})\Psi^{\lambda c}_{\perp}\\
\Gamma^{\lambda}_{14RR} &= \Gamma^{\lambda c}_{R}(\Gamma^{\lambda c}_{\perp R}+\Gamma^{\lambda}_{\perp R}\Psi^{\lambda c}_{\perp})+\Gamma^{\lambda}_{\perp R}(\Psi^{\lambda}_{\varepsilon}\Gamma^{\lambda c}_{\perp R}+\Psi^{\lambda c}_{\perp R})(1+\Psi^{\lambda c}_{\perp})\\
\Gamma^{\lambda}_{33RR} &= \Phi^{\lambda c}_{\parallel RR}+\Phi^{\lambda}_{\parallel R}(\Phi^{\lambda c}_{\parallel R}+\Phi^{\lambda}_{\parallel R}\Phi^{\lambda c}_{\parallel})+\Phi^{\lambda}_{\parallel RR}\Phi^{\lambda c}_{\parallel}\\
\Gamma^{\lambda}_{43RR} &= (\Psi^{\lambda}_{\varepsilon}\Gamma^{\lambda c}_{R}+\Psi^{\lambda}_{\varepsilon R})(\Gamma^{\lambda c}_{\perp R}+\Gamma^{\lambda}_{\perp R}\Psi^{\lambda c}_{\perp})+\Psi^{\lambda c}_{\perp RR}+\Psi^{\lambda}_{\perp RR}\Psi^{\lambda c}_{\perp}\\
&\quad+(\Psi^{\lambda}_{\varepsilon}\Gamma^{\lambda}_{\perp R}+\Psi^{\lambda}_{\perp R})(\Psi^{\lambda}_{\varepsilon}\Gamma^{\lambda c}_{\perp R}+\Psi^{\lambda c}_{\perp R})(1+\Psi^{\lambda c}_{\perp})\\
\Gamma^{\lambda}_{13R\alpha} &= \Gamma^{\lambda}_{\parallel\alpha}(\Phi^{\lambda c}_{\parallel R}+\Phi^{\lambda}_{\parallel R}\Phi^{\lambda c}_{\parallel})+\Gamma^{\lambda c}_{\parallel R\alpha}+(\Gamma^{\lambda}_{\parallel R\alpha}+\Gamma^{\lambda}_{\perp R}\Psi^{\lambda}_{\varepsilon})(\Gamma^{\lambda c}_{\parallel\alpha}+\Gamma^{\lambda}_{\parallel\alpha}\Phi^{\lambda c}_{\parallel})\\
&\quad+\Gamma^{\lambda}_{\perp R}(\Psi^{\lambda c}_{\parallel\alpha}+\Psi^{\lambda}_{\parallel\alpha}\Phi^{\lambda c}_{\parallel})\\
\Gamma^{\lambda}_{23R\alpha} &= \delta^{\lambda}\frac{h^{c}}{2}I_{\alpha}e^{c}_{R}\\
\Gamma^{\lambda}_{34R\alpha} &= (\Phi^{\lambda}_{\varepsilon\alpha}+\Phi^{\lambda}_{\perp\alpha}\Psi^{\lambda}_{\varepsilon})(\Gamma^{\lambda c}_{\perp R}+\Gamma^{\lambda}_{\perp R}\Psi^{\lambda c}_{\perp})+\Phi^{\lambda}_{\perp\alpha}(\Psi^{\lambda c}_{\perp R}+\Psi^{\lambda}_{\perp R}\Psi^{\lambda c}_{\perp})\\
&\quad+\Phi^{\lambda c}_{\perp R\alpha}+\Phi^{\lambda}_{\perp R\alpha}\Psi^{\lambda c}_{\perp}+\Phi^{\lambda}_{\parallel R}(\Phi^{\lambda c}_{\perp\alpha}+\Phi^{\lambda}_{\perp\alpha}\Psi^{\lambda c}_{\perp})\\
\Gamma^{\lambda}_{43R\alpha} &= (\Psi^{\lambda}_{\varepsilon}\Gamma^{\lambda}_{\parallel\alpha}+\Psi^{\lambda}_{\parallel\alpha})(\Phi^{\lambda c}_{\parallel R}+\Phi^{\lambda}_{\parallel R}\Phi^{\lambda c}_{\parallel})+\Psi^{\lambda}_{\varepsilon}\Gamma^{\lambda c}_{\parallel R\alpha}+\Psi^{\lambda c}_{\parallel R\alpha}+\Psi^{\lambda}_{\parallel R\alpha}\Phi^{\lambda c}_{\parallel}\\
&\quad+(\Psi^{\lambda}_{\varepsilon}\Gamma^{\lambda}_{\parallel R\alpha}+\Psi^{\lambda}_{\varepsilon R})(\Gamma^{\lambda c}_{\parallel\alpha}+\Gamma^{\lambda}_{\parallel\alpha}\Phi^{\lambda c}_{\parallel})\\
&\quad+(\Psi^{\lambda}_{\varepsilon}\Gamma^{\lambda}_{\perp R}+\Psi^{\lambda}_{\perp R})[\Psi^{\lambda c}_{\parallel\alpha}+\Psi^{\lambda}_{\varepsilon}\Gamma^{\lambda c}_{\parallel\alpha}+(\Psi^{\lambda}_{\varepsilon}\Gamma^{\lambda}_{\parallel\alpha}+\Psi^{\lambda}_{\parallel\alpha})\Phi^{\lambda c}_{\parallel}]
\end{aligned}
\tag{92}
$$

Finally, we have all the information needed to obtain the universal asymptotic model with the following energy functional asymptotically correct up to the order of $\mu(h/l)^2\hat{\varepsilon}^2$ and $\mu(h/R)^2\hat{\varepsilon}^2$

$$
\begin{aligned}
2\Pi &= (\mathcal{E}^{c})^{T}A^{0\mathrm{eff}}(\mathcal{E}^{c})+2(\mathcal{E}^{c})^{T}\Big[A^{01\mathrm{eff}}_{\alpha}(\mathcal{E}^{c}_{;\alpha})+A^{02\mathrm{eff}}_{\alpha\beta}(\mathcal{E}^{c}_{;\alpha\beta})+A^{03\mathrm{eff}}_{\alpha\beta\gamma}(\mathcal{E}^{c}_{;\alpha\beta\gamma})\Big]\\
&+2(\mathcal{E}^{c})^{T}A^{04\mathrm{eff}}_{\alpha\beta\gamma\delta}(\mathcal{E}^{c}_{;\alpha\beta\gamma\delta})+(\mathcal{E}^{c}_{;\alpha})^{T}B^{11\mathrm{eff}}_{\alpha\beta}(\mathcal{E}^{c}_{;\beta})+2(\mathcal{E}^{c}_{;\alpha})^{T}B^{12\mathrm{eff}}_{\alpha\beta\gamma}(\mathcal{E}^{c}_{;\beta\gamma})\\
&+2(\mathcal{E}^{c}_{;\alpha})^{T}B^{13\mathrm{eff}}_{\alpha\beta\gamma\delta}(\mathcal{E}^{c}_{;\beta\gamma\delta})+(\mathcal{E}^{c}_{;\alpha\beta})^{T}G^{22\mathrm{eff}}_{\alpha\beta\gamma\delta}(\mathcal{E}^{c}_{;\gamma\delta})
\end{aligned}
\tag{93}
$$

where

$$
\begin{aligned}
A^{0\mathrm{eff}} &= (\Gamma^{\lambda}+\Gamma^{\lambda}_{R}+\Gamma^{\lambda}_{RR})^{T}A^{0\lambda}(\Gamma^{\lambda}+\Gamma^{\lambda}_{R}+\Gamma^{\lambda}_{RR})+(\Gamma^{\lambda}+\Gamma^{\lambda}_{R})^{T}A^{0\lambda}_{R1}(\Gamma^{\lambda}+\Gamma^{\lambda}_{R}+2\Gamma^{\lambda}_{RR})\\
&\quad+(\Gamma^{\lambda})^{T}A^{0\lambda}_{R2}(\Gamma^{\lambda}+2\Gamma^{\lambda}_{R}+2\Gamma^{\lambda}_{RR})+(\Gamma^{\lambda}_{R})^{T}A^{0\lambda}_{R2}(\Gamma^{\lambda}_{R})+A^{0c}+A^{0c}_{R1}+A^{0c}_{R2}
\end{aligned}
$$

$$
\begin{aligned}
A_{\alpha}^{01\mathrm{eff}} &= (\Gamma^{\lambda}+\Gamma_{R}^{\lambda}+\Gamma_{RR}^{\lambda})^{T}A^{0\lambda}(\Gamma_{\alpha}^{\lambda}+\Gamma_{R\alpha}^{\lambda})+(\Gamma^{\lambda}+\Gamma_{R}^{\lambda})^{T}A_{R1}^{0\lambda}(\Gamma_{\alpha}^{\lambda}+\Gamma_{R\alpha}^{\lambda})+A_{R\alpha}^{01c}\\
&+(\Gamma_{RR}^{\lambda})^{T}A_{R1}^{0\lambda}(\Gamma_{\alpha}^{\lambda})+(\Gamma^{\lambda})A_{R2}^{0\lambda}(\Gamma_{\alpha}^{\lambda}+\Gamma_{R\alpha}^{\lambda})+(\Gamma_{R}^{\lambda})^{T}A_{\alpha}^{01\lambda}(\Gamma^{\lambda}+\Gamma_{R}^{\lambda}+\Gamma_{RR}^{\lambda})\\
&+(\Gamma^{\lambda})^{T}(A_{\alpha}^{01\lambda}+A_{R\alpha}^{01\lambda})(\Gamma^{\lambda}+\Gamma_{R}^{\lambda}+\Gamma_{RR}^{\lambda})+(\Gamma_{R}^{\lambda})^{T}A_{\alpha}^{01\lambda}(\Gamma^{\lambda}+\Gamma_{R}^{\lambda}+\Gamma_{RR}^{\lambda})\\
&+(\Gamma_{R}^{\lambda})^{T}A_{R\alpha}^{01\lambda}(\Gamma^{\lambda}+\Gamma_{R}^{\lambda})+(\Gamma_{RR}^{\lambda})^{T}A_{\alpha}^{01\lambda}(\Gamma^{\lambda}+\Gamma_{R}^{\lambda})+(\Gamma_{RR}^{\lambda})^{T}A_{R\alpha}^{01\lambda}(\Gamma^{\lambda})+A_{\alpha}^{01c}\\
A_{\alpha\beta}^{02\mathrm{eff}} &= (\Gamma^{\lambda}+\Gamma_{R}^{\lambda}+\Gamma_{RR}^{\lambda})^{T}A^{0\lambda}(\Gamma_{\alpha\beta}^{\lambda})+(\Gamma^{\lambda}+\Gamma_{R}^{\lambda})^{T}A_{R1}^{0\lambda}(\Gamma_{\alpha\beta}^{\lambda})+(\Gamma^{\lambda})^{T}A_{R2}^{0\lambda}(\Gamma_{\alpha\beta}^{\lambda})\\
&+(\Gamma^{\lambda})^{T}(A_{\alpha}^{01\lambda}+A_{R\alpha}^{01\lambda})(\Gamma_{\beta}^{\lambda}+\Gamma_{R\beta}^{\lambda})+(\Gamma^{\lambda})^{T}A_{\alpha\beta}^{02\lambda}(\Gamma^{\lambda}+\Gamma_{R}^{\lambda}+\Gamma_{RR}^{\lambda})\\
&+(\Gamma_{R}^{\lambda})^{T}A_{\alpha}^{01\lambda}(\Gamma_{\beta}^{\lambda}+\Gamma_{R\beta}^{\lambda})+(\Gamma_{R}^{\lambda})^{T}A_{R\alpha}^{01\lambda}(\Gamma_{\beta}^{\lambda})+(\Gamma_{R}^{\lambda})^{T}A_{\alpha\beta}^{02\lambda}(\Gamma^{\lambda}+\Gamma_{R}^{\lambda})\\
&+(\Gamma_{RR}^{\lambda})^{T}A_{\alpha\beta}^{02\lambda}(\Gamma^{\lambda})+A_{\alpha\beta}^{02c}\\
A_{\alpha\beta\gamma}^{03\mathrm{eff}} &= (\Gamma^{\lambda})^{T}(A_{\alpha}^{01\lambda}+A_{R\alpha}^{01\lambda})(\Gamma_{\beta\gamma}^{\lambda})+(\Gamma^{\lambda})^{T}A_{\alpha\beta}^{02\lambda}(\Gamma_{\gamma}^{\lambda}+\Gamma_{R\gamma}^{\lambda})\\
&+(\Gamma_{R}^{\lambda})^{T}A_{\alpha}^{01\lambda}(\Gamma_{\beta\gamma}^{\lambda})+(\Gamma_{R}^{\lambda})^{T}A_{\alpha\beta}^{02\lambda}(\Gamma_{\gamma}^{\lambda})\\
A_{\alpha\beta\gamma\delta}^{04\mathrm{eff}} &= (\Gamma^{\lambda})^{T}A_{\alpha\beta}^{02\lambda}(\Gamma_{\gamma\delta}^{\lambda})\\
B_{\alpha\beta}^{11\mathrm{eff}} &= (\Gamma_{\alpha}^{\lambda}+\Gamma_{R\alpha}^{\lambda})A^{0\lambda}(\Gamma_{\beta}^{\lambda}+\Gamma_{R\beta}^{\lambda})+(\Gamma_{\alpha}^{\lambda})^{T}A_{R1}^{0\lambda}(\Gamma_{\beta}^{\lambda}+\Gamma_{R\beta}^{\lambda})+(\Gamma_{R\alpha}^{\lambda})^{T}A_{R1}^{0\lambda}(\Gamma_{\beta}^{\lambda})\\
&+(\Gamma_{\alpha}^{\lambda})^{T}A_{R2}^{0\lambda}(\Gamma_{\beta}^{\lambda})+2(\Gamma_{\alpha}^{\lambda})^{T}A_{\beta}^{01\lambda}(\Gamma^{\lambda}+\Gamma_{R}^{\lambda}+\Gamma_{RR}^{\lambda})+2(\Gamma_{\alpha}^{\lambda})^{T}A_{R\beta}^{01\lambda}(\Gamma^{\lambda}+\Gamma_{R}^{\lambda})\\
&+2(\Gamma_{R\alpha}^{\lambda})^{T}A_{\beta}^{01\lambda}(\Gamma^{\lambda}+\Gamma_{R}^{\lambda})+2(\Gamma_{R\alpha}^{\lambda})^{T}A_{R\beta}^{01\lambda}(\Gamma^{\lambda})\\
&+(\Gamma^{\lambda}+\Gamma_{R}^{\lambda}+\Gamma_{RR}^{\lambda})^{T}A_{\alpha\beta}^{11\lambda}(\Gamma^{\lambda}+\Gamma_{R}^{\lambda}+\Gamma_{RR}^{\lambda})+A_{\alpha\beta}^{11c}\\
B_{\alpha\beta\gamma}^{12\mathrm{eff}} &= (\Gamma_{\alpha}^{\lambda}+\Gamma_{R\alpha}^{\lambda})^{T}A^{0\lambda}(\Gamma_{\beta\gamma}^{\lambda})+(\Gamma_{\alpha}^{\lambda})^{T}A_{R1}^{0\lambda}(\Gamma_{\beta\gamma}^{\lambda})+(\Gamma_{\alpha}^{\lambda})^{T}A_{\beta}^{01\lambda}(\Gamma_{\gamma}^{\lambda}+\Gamma_{R\gamma}^{\lambda})\\
&+(\Gamma_{\alpha}^{\lambda})^{T}A_{R\beta}^{01\lambda}(\Gamma_{\gamma}^{\lambda})+(\Gamma_{\alpha}^{\lambda})^{T}A_{\beta\gamma}^{02\lambda}(\Gamma^{\lambda}+\Gamma_{R}^{\lambda})+(\Gamma_{R\alpha}^{\lambda})^{T}A_{\beta}^{01\lambda}(\Gamma_{\gamma}^{\lambda})+(\Gamma_{R\alpha}^{\lambda})^{T}A_{\beta\gamma}^{02\lambda}(\Gamma^{\lambda})\\
&+(\Gamma^{\lambda}+\Gamma_{R}^{\lambda})^{T}(A_{\alpha}^{01\lambda})^{T}(\Gamma_{\beta\gamma}^{\lambda})+(\Gamma^{\lambda})^{T}(A_{R\alpha}^{01\lambda})^{T}(\Gamma_{\beta\gamma}^{\lambda})\\
&+(\Gamma^{\lambda}+\Gamma_{R}^{\lambda}+\Gamma_{RR}^{\lambda})^{T}A_{\alpha\beta}^{11\lambda}(\Gamma_{\beta}^{\lambda}+\Gamma_{R\gamma}^{\lambda})\\
B_{\alpha\beta\gamma\delta}^{13\mathrm{eff}} &= (\Gamma_{\alpha}^{\lambda})^{T}A_{\beta}^{01\lambda}(\Gamma_{\gamma\delta}^{\lambda})+(\Gamma_{\alpha}^{\lambda})^{T}A_{\beta\gamma}^{02\lambda}(\Gamma_{\delta}^{\lambda})+(\Gamma^{\lambda}+\Gamma_{R}^{\lambda}+\Gamma_{RR}^{\lambda})^{T}A_{\alpha\beta}^{11\lambda}(\Gamma_{\gamma\delta}^{\lambda})\\
G_{\alpha\beta\gamma\delta}^{22\mathrm{eff}} &= (\Gamma_{\alpha\beta}^{\lambda})^{T}A^{0\lambda}(\Gamma_{\gamma\delta}^{\lambda})+2(\Gamma_{\alpha\beta}^{\lambda})^{T}A_{\gamma}^{01\lambda}(\Gamma_{\delta}^{\lambda})+2(\Gamma_{\alpha\beta}^{\lambda})^{T}A_{\gamma\delta}^{02\lambda}(\Gamma^{\lambda})\\
&+(\Gamma_{\beta}^{\lambda}+\Gamma_{R\beta}^{\lambda})^{T}A_{\alpha\gamma}^{11\lambda}(\Gamma_{\delta}^{\lambda}+\Gamma_{R\delta}^{\lambda})
\end{aligned}
\tag{94}
$$

3.3 PA(22CS)

An energy functional of the approximation theory denoting by 22CS is similar to the energy functional derived by the VAM found in Yu and Hodges [28]. Therefore, the energy functional storing in the composite sandwich shell, asymptotically correct up to the second order, can be simply

obtained by utilizing Eq. (57) for two skin-layers and one core-layer, resulting in

$$\begin{aligned}2\Pi = &(\mathcal{E}^{\lambda})^{T}(A^{0\lambda}+A_{R1}^{0\lambda})(\mathcal{E}^{\lambda})+2(\mathcal{E}^{c})^{T}[A_{\alpha}^{01\lambda}(\mathcal{E}_{;\alpha}^{\lambda})+A_{\alpha\beta}^{02\lambda}(\mathcal{E}_{;\alpha\beta}^{\lambda})]+(\mathcal{E}_{;\alpha}^{\lambda})^{T}A_{\alpha\beta}^{11\lambda}(\mathcal{E}_{;\beta}^{\lambda})\\ &+(\mathcal{E}^{c})^{T}(A^{0c}+A_{R1}^{0c})(\mathcal{E}^{c})+2(\mathcal{E}^{c})^{T}[A_{\alpha}^{01c}(\mathcal{E}_{;\alpha}^{c})+A_{\alpha\beta}^{02c}(\mathcal{E}_{;c}^{\lambda})]+(\mathcal{E}_{;\alpha}^{c})^{T}A_{\alpha\beta}^{11c}(\mathcal{E}_{;\beta}^{c})\end{aligned} \tag{95}$$

In the same way, as in Sect. 3.1., we can then derive the following kinematic identities of the generalized LK strain and transverse motion measures of two skin-layers in terms of the corresponding ones of the core-layer,

$$\varepsilon^{\lambda}=\varepsilon^{c}+\Gamma_{\kappa}^{\lambda c}\kappa^{c}+\Gamma_{\|\alpha}^{\lambda c}\varphi_{\|;\alpha}^{c}+\Gamma_{\perp\alpha\beta}^{\lambda c}\varphi_{3;\alpha\beta}^{c}+\Gamma_{\|\alpha}^{\lambda}\varphi_{\|;\alpha}^{\lambda}+\Gamma_{\perp R}^{\lambda c}\varphi_{3}^{c}+\Gamma_{\perp R}^{\lambda}\varphi_{3}^{\lambda} \tag{96}$$

From Eq. (86) with Eqs. (74) and (75), we obtain $\varphi_{\|}^{\lambda}$ and φ_{3}^{λ} in terms of $\varphi_{\|}^{c}$, φ_{3}^{c}, $\mathcal{E}^{\lambda}$ and $\mathcal{E}^{c}$

$$\begin{aligned}\varphi_{\|}^{\lambda}=&\Phi_{\|}^{\lambda c}\varphi_{\|}^{c}+\Phi_{\varepsilon\alpha}^{\lambda c}\varepsilon_{;\alpha}^{c}+\Phi_{\kappa\alpha}^{\lambda c}\kappa_{;\alpha}^{c}+\Phi_{\perp\alpha}^{\lambda c}\varphi_{3;\alpha}^{c}+\Phi_{\varepsilon\alpha}^{\lambda}\varepsilon_{;\alpha}^{\lambda}+\Phi_{\perp\alpha}^{\lambda}\varphi_{3;\alpha}^{\lambda}\\ &+\Phi_{\|R}^{\lambda c*}\varphi_{\|}^{c}+\Phi_{\|R}^{\lambda *}\varphi_{\|}^{\lambda}\\ \varphi_{3}^{\lambda}=&\Psi_{\varepsilon}^{\lambda c}\varepsilon^{c}+\Psi_{\perp}^{\lambda c}\varphi_{3}^{c}+\Psi_{\|\alpha}^{\lambda c}\varphi_{\|;\alpha}^{c}+\Psi_{\varepsilon}^{\lambda}\varepsilon^{\lambda}+\Psi_{\|\alpha}^{\lambda}\varphi_{\|;\alpha}^{\lambda}\\ &+\Psi_{\perp R}^{\lambda c*}\varphi_{3}^{c}+\Psi_{\perp R}^{\lambda *}\varphi_{3}^{\lambda}\end{aligned} \tag{97}$$

with

$$\begin{aligned}\Phi_{\|R}^{\lambda c*}=&-\delta^{\lambda}\frac{h^{c}}{2}(D_{s}^{\lambda})^{-1}D_{s}^{c}e_{R}^{c} \quad \Phi_{\|R}^{\lambda *}=-\delta^{\lambda}\frac{h^{\lambda}}{2}e_{R}^{\lambda}\\ \Psi_{\perp R}^{\lambda c*}=&\delta^{\lambda}\frac{h^{c}}{2}(D_{t}^{\lambda})^{-1}D_{t}^{c}(D_{\perp}^{c})^{T}I_{R}^{c} \quad \Psi_{\perp R}^{\lambda}=\delta^{\lambda}\frac{h^{\lambda}}{2}(D_{\perp}^{\lambda})^{T}I_{R}^{\lambda}\end{aligned} \tag{98}$$

By using Eq. (96) and (97), the kinematic identities of the generalized LK strain and transverse motion measures of two skin-layers for PA(22CS) can

be derived in terms of the corresponding ones and their partial derivatives of the core-layer through the first-order approximation. viz.,

$$\mathcal{E}^{\lambda} = (\Gamma^{\lambda} + \Gamma_R^{\lambda^*})\mathcal{E}^c + (\Gamma_\alpha^{\lambda})\mathcal{E}_{;\alpha}^c + \Gamma_{\alpha\beta}^{\lambda}\mathcal{E}_{;\alpha\beta}^c \tag{99}$$

Here the associated operators used in Eq. (99) are also defined as

$$\Gamma_R^{\lambda} = \begin{bmatrix} 0\,0 & 0 & \Gamma_{14R}^{\lambda} \\ 0\,0 & 0 & 0 \\ 0\,0 & \Gamma_{33R}^{\lambda^*} & 0 \\ 0\,0 & 0 & \Gamma_{44R}^{\lambda^*} \end{bmatrix} \text{ with } \begin{aligned} \Gamma_{33R}^{\lambda^*} &= \Phi_{\|R}^{\lambda c^*} + \Phi_{\|R}^{\lambda^*}\Phi_{\|}^{\lambda c} \\ \Gamma_{44R}^{\lambda^*} &= \Psi_{\varepsilon}^{\lambda}\Gamma_{\perp R}^{\lambda c} + \Psi_{\perp R}^{\lambda c^*} + (\Psi_{\varepsilon}^{\lambda}\Gamma_{\perp R}^{\lambda} + \Psi_{\perp R}^{\lambda^*})\Psi_{\perp}^{\lambda c} \end{aligned} \tag{100}$$

Finally, we have all the information needed to obtain the universal asymptotic model with the following energy functional asymptotically correct up to the order of $\mu(h/l)^2\hat{\varepsilon}^2$ and $\mu(h/R)\hat{\varepsilon}^2$

$$\begin{aligned} 2\Pi = {} & (\mathcal{E}^c)^T A^{0\text{eff}}(\mathcal{E}^c) + 2(\mathcal{E}^c)^T\left[A_\alpha^{01\text{eff}}(\mathcal{E}_{;\alpha}^c) + A_{\alpha\beta}^{02\text{eff}}(\mathcal{E}_{;\alpha\beta}^c) + A_{\alpha\beta\gamma}^{03\text{eff}}(\mathcal{E}_{;\alpha\beta\gamma}^c)\right] \\ & + 2(\mathcal{E}^c)^T A_{\alpha\beta\gamma\delta}^{04\text{eff}}(\mathcal{E}_{;\alpha\beta\gamma\delta}^c) + (\mathcal{E}_{;\alpha}^c)^T B_{\alpha\beta}^{11\text{eff}}(\mathcal{E}_{;\beta}^c) + 2(\mathcal{E}_{;\alpha}^c)^T B_{\alpha\beta\gamma}^{12\text{eff}}(\mathcal{E}_{;\beta\gamma}^c) \\ & + 2(\mathcal{E}_{;\alpha}^c)^T B_{\alpha\beta\gamma\delta}^{13\text{eff}}(\mathcal{E}_{;\beta\gamma\delta}^c) + (\mathcal{E}_{;\alpha\beta}^c)^T G_{\alpha\beta\gamma\delta}^{22\text{eff}}(\mathcal{E}_{;\gamma\delta}^c) \end{aligned} \tag{101}$$

where

$$\begin{aligned} A^{0\text{eff}} &= (\Gamma^{\lambda} + \Gamma_R^{\lambda^*})^T A^{0\lambda}(\Gamma^{\lambda} + \Gamma_R^{\lambda^*}) + (\Gamma^{\lambda})^T A_{R1}^{0\lambda}(\Gamma^{\lambda} + 2\Gamma_R^{\lambda^*}) + A^{0c} + A_{R1}^{0c} \\ A_\alpha^{01\text{eff}} &= (\Gamma^{\lambda} + \Gamma_R^{\lambda^*})^T A^{0\lambda}(\Gamma_\alpha^{\lambda}) + (\Gamma^{\lambda})^T A_{R1}^{0\lambda}(\Gamma_\alpha^{\lambda}) \\ &\quad + (\Gamma^{\lambda})^T(A_\alpha^{01\lambda})(\Gamma^{\lambda} + \Gamma_R^{\lambda^*}) + (\Gamma_R^{\lambda^*})^T A_\alpha^{01\lambda}(\Gamma^{\lambda}) + A_\alpha^{01c} \\ A_{\alpha\beta}^{02\text{eff}} &= (\Gamma^{\lambda} + \Gamma_R^{\lambda^*})^T A^{0\lambda}(\Gamma_{\alpha\beta}^{\lambda}) + (\Gamma^{\lambda})^T A_{R1}^{0\lambda}(\Gamma_{\alpha\beta}^{\lambda}) \\ &\quad + (\Gamma^{\lambda})^T(A_\alpha^{01\lambda})(\Gamma_\beta^{\lambda}) + (\Gamma^{\lambda})^T A_{\alpha\beta}^{02\lambda}(\Gamma^{\lambda} + \Gamma_R^{\lambda^*}) \\ &\quad + (\Gamma_R^{\lambda^*})^T A_\alpha^{01\lambda}(\Gamma_\beta^{\lambda}) + (\Gamma_R^{\lambda^*})^T A_{\alpha\beta}^{02\lambda}(\Gamma^{\lambda}) + A_{\alpha\beta}^{02c} \\ A_{\alpha\beta\gamma}^{03\text{eff}} &= (\Gamma^{\lambda})^T(A_\alpha^{01\lambda})(\Gamma_{\beta\gamma}^{\lambda}) + (\Gamma^{\lambda})^T A_{\alpha\beta}^{02\lambda}(\Gamma_\gamma^{\lambda}) \\ A_{\alpha\beta\gamma\delta}^{04\text{eff}} &= (\Gamma^{\lambda})^T A_{\alpha\beta}^{02\lambda}(\Gamma_{\gamma\delta}^{\lambda}) \end{aligned}$$

$$
\begin{aligned}
B^{11\mathrm{eff}}_{\alpha\beta} &= (\Gamma^{\lambda}_{\alpha})A^{0\lambda}(\Gamma^{\lambda}_{\beta}) + (\Gamma^{\lambda}_{\alpha})^{T}A^{0\lambda}_{R1}(\Gamma^{\lambda}_{\beta}) + 2(\Gamma^{\lambda}_{\alpha})^{T}A^{01\lambda}_{\beta}(\Gamma^{\lambda} + \Gamma^{\lambda^{*}}_{R}) \\
&\quad + (\Gamma^{\lambda})^{T}A^{11\lambda}_{\alpha\beta}(\Gamma^{\lambda} + 2\Gamma^{\lambda^{*}}_{R}) + A^{11c}_{\alpha\beta} \\
B^{12\mathrm{eff}}_{\alpha\beta\gamma} &= (\Gamma^{\lambda}_{\alpha})^{T}A^{0\lambda}(\Gamma^{\lambda}_{\beta\gamma}) + (\Gamma^{\lambda}_{\alpha})^{T}A^{01\lambda}_{\beta}(\Gamma^{\lambda}_{\gamma}) + (\Gamma^{\lambda}_{\alpha})^{T}A^{02\lambda}_{\beta\gamma}(\Gamma^{\lambda}) \\
&\quad + (\Gamma^{\lambda})^{T}(A^{01\lambda}_{\alpha})^{T}(\Gamma^{\lambda}_{\beta\gamma}) + (\Gamma^{\lambda})^{T}A^{11\lambda}_{\alpha\beta}(\Gamma^{\lambda}_{\beta}) \\
B^{13\mathrm{eff}}_{\alpha\beta\gamma\delta} &= (\Gamma^{\lambda}_{\alpha})^{T}A^{01\lambda}_{\beta}(\Gamma^{\lambda}_{\gamma\delta}) + (\Gamma^{\lambda}_{\alpha})^{T}A^{02\lambda}_{\beta\gamma}(\Gamma^{\lambda}_{\delta}) + (\Gamma^{\lambda})^{T}A^{11\lambda}_{\alpha\beta}(\Gamma^{\lambda}_{\gamma\delta}) \\
G^{22\mathrm{eff}}_{\alpha\beta\gamma\delta} &= (\Gamma^{\lambda}_{\alpha\beta})^{T}A^{0\lambda}(\Gamma^{\lambda}_{\gamma\delta}) + 2(\Gamma^{\lambda}_{\alpha\beta})^{T}A^{01\lambda}_{\gamma}(\Gamma^{\lambda}_{\delta}) + 2(\Gamma^{\lambda}_{\alpha\beta})^{T}A^{02\lambda}_{\gamma\delta}(\Gamma^{\lambda}) \\
&\quad + (\Gamma^{\lambda}_{\beta})^{T}A^{11\lambda}_{\alpha\gamma}(\Gamma^{\lambda}_{\delta})
\end{aligned}
\tag{102}
$$

4. Recovery relations from 2D to 3D

Now one can use the stiffness coefficients as input for the 2D shell theory to accurately calculate the 2D displacement field, generalized strains and stress resultants of the composite sandwich shells. However, in many engineering applications this is not sufficient. Recovery relations, (i.e., expressions for 3D displacement, strain, and stress fields in terms of 2D shell variables, their partial derivatives and x_3) are necessary ingredients for such theories. Indeed, one of the ways fidelity of the sandwich shell model can be evaluated is how well it predicts the 3D fields for the original 3D structure. Hence, comparison of results obtained for 3D field variables from the recovery relations versus those from a fully 3D model should be a significant part of validation for any composite sandwich shell theory.

4.1 Second-order approximation (22CS)

Before deriving 3D recovery relations from the 2D shell model (22CS), let us recall that the universal asymptotic model that has been constructed only ensures a good fit with the asymptotically correct 3D strain fields (thus the 3D stress fields) and interlaminar 3D displacement/transverse stress continuity conditions through the first order in h/l and h/R, while the energy functional is approximated to the second order in h/l. Thus, in order

to obtain asymptotically correct recovery relations that are valid to the same order as the energy formulation, the VAM iteration need to be applied one more time. Using a procedure similar to that of the first-order approximation from the ESL perspective, the 3D warping function of the second order in h/l can be simply expressed as

$$y_{\|} = \bar{v}_{\|} + z_{\|} \text{ and } y_3 = \bar{y}_3 + v_3 + z_3 \tag{103}$$

Substituting Eq. (103) back into Eq. (28) then into (37) and by considering the warping constraint in Eq. (21), one obtains the following warping functions: for $z_{\|}$

$$z_{\|} = -\frac{1}{6}\left[x_3^2 - \left(\frac{h}{2}\right)^2\right][(D_{\|\alpha} + D_{s\alpha}D_{\perp}^T)I_\beta - D_{s\alpha}D_{t\beta}](x_3\varphi_{\|;\alpha\beta}) \tag{104}$$

And for z_3

$$\begin{aligned} z_3 = {} & \frac{1}{6}\left[x_3^2 - \left(\frac{h}{2}\right)^2\right]((D_{t\alpha}D_s^{-1}I_\beta^T D_e)(x_3\varepsilon_{;\alpha\beta}) \\ & + \frac{1}{4}\left\{\left[x_3^2 - \left(\frac{h}{2}\right)^2\right]D_{t\alpha}D_{\|\beta} + \left[x_3^2 - 5\left(\frac{h}{2}\right)^2\right]D_t^{-1}e_\alpha^T D_s e_\beta D_\perp^T\right\}(\kappa_{;\alpha\beta}) \\ & + (D_{t\alpha}D_{s\beta} - D_t^{-1}e_\alpha^T D_s e_\beta)(x_3\varphi_{3;\alpha\beta})) \end{aligned} \tag{105}$$

From the LW perspective, let us now consider the interlaminar displacement and transverse stress continuity conditions up to the second order. In a manner similar to the procedure used to obtain the kinematic identities of the generalized LK strain and transverse motion measures for the first-order approximation, one can obtain the following kinematic

identities of the generalized LK strain and transverse motion measures of two skin-layers in terms of the corresponding ones and their partial derivatives of the core-layer for the second-order approximation. viz.,

$$\mathcal{E}^{\lambda} = (\Gamma^{\lambda} + \overline{\Gamma}^{\lambda^*}_{R})\mathcal{E}^{c} + (\Gamma^{\lambda}_{\alpha} + \overline{\Gamma}^{\lambda^*}_{R\alpha})\mathcal{E}^{c}_{;\alpha} + \overline{\Gamma}^{\lambda}_{\alpha\beta}\mathcal{E}^{c}_{;\alpha\beta} + \overline{\Gamma}^{\lambda}_{\alpha\beta\gamma}\mathcal{E}^{c}_{;\alpha\beta\gamma} \tag{106}$$

Here the associated operators used in Eq. (106) are also defined as

$$\begin{aligned}
\overline{\Gamma}^{\lambda^*}_{R} &= \begin{bmatrix} \Gamma^{\lambda}_{11R} & \Gamma^{\lambda}_{12R} & 0 & \Gamma^{\lambda}_{14R} \\ 0 & \Gamma^{\lambda}_{22R} & 0 & 0 \\ 0 & 0 & \Gamma^{\lambda^*}_{33R} & 0 \\ \Gamma^{\lambda^*}_{41R} & \Gamma^{\lambda^*}_{42R} & 0 & \Gamma^{\lambda^*}_{44R} \end{bmatrix} \quad \Gamma^{\lambda^*}_{R\alpha} = \begin{bmatrix} 0 & 0 & \Gamma^{\lambda^*}_{13R\alpha} & 0 \\ 0 & 0 & \Gamma^{\lambda^*}_{23R\alpha} & 0 \\ 0 & 0 & 0 & \Gamma^{\lambda^*}_{34R\alpha} \\ 0 & 0 & \Gamma^{\lambda^*}_{43R\alpha} & 0 \end{bmatrix} \\
\overline{\Gamma}^{\lambda}_{\alpha\beta} &= \begin{bmatrix} \overline{\Gamma}^{\lambda}_{11\alpha\beta} & \overline{\Gamma}^{\lambda}_{12\alpha\beta} & 0 & \overline{\Gamma}^{\lambda}_{14\alpha\beta} \\ 0 & 0 & 0 & \overline{\Gamma}^{\lambda}_{24\alpha\beta} \\ 0 & 0 & \overline{\Gamma}^{\lambda}_{33\alpha\beta} & 0 \\ \overline{\Gamma}^{\lambda}_{41\alpha\beta} & \overline{\Gamma}^{\lambda}_{42\alpha\beta} & 0 & \overline{\Gamma}^{\lambda}_{44\alpha\beta} \end{bmatrix} \quad \overline{\Gamma}^{\lambda}_{\alpha\beta\gamma} = \begin{bmatrix} 0 & 0 & \overline{\Gamma}^{\lambda}_{13\alpha\beta\gamma} & 0 \\ 0 & 0 & 0 & 0 \\ 0 & 0 & 0 & \overline{\Gamma}^{\lambda}_{34\alpha\beta\gamma} \\ 0 & 0 & \overline{\Gamma}^{\lambda}_{43\alpha\beta\gamma} & 0 \end{bmatrix}
\end{aligned} \tag{107}$$

with

$$\begin{aligned}
&\Gamma^{\lambda^*}_{41R} = \Psi^{\lambda}_{\varepsilon}\Gamma^{\lambda c}_{R} + \Psi^{\lambda^*}_{\varepsilon R} + (\Psi^{\lambda}_{\varepsilon}\Gamma^{\lambda}_{\perp R} + \Psi^{\lambda^*}_{\perp R})(\Psi^{\lambda c}_{\varepsilon} + \Psi^{\lambda}_{\varepsilon}) \\
&\Gamma^{\lambda^*}_{42R} = (\Psi^{\lambda}_{\varepsilon}\Gamma^{\lambda c}_{R} + \Psi^{\lambda^*}_{\varepsilon R})\Gamma^{\lambda c}_{\kappa} + \Psi^{\lambda c^*}_{\kappa R} + (\Psi^{\lambda}_{\varepsilon}\Gamma^{\lambda}_{\perp R} + \Psi^{\lambda}_{\perp R})\Psi^{\lambda}_{\varepsilon}\Gamma^{\lambda c}_{\kappa} \\
&\Gamma^{\lambda^*}_{13R\alpha} = \Gamma^{\lambda}_{\|\alpha}(\Phi^{\lambda c^*}_{\|R} + \Phi^{\lambda^*}_{\|R}\Phi^{\lambda c}_{\|}) + \Gamma^{\lambda c}_{\|R\alpha} + (\Gamma^{\lambda}_{\|R\alpha} + \Gamma^{\lambda}_{\perp R}\Psi^{\lambda}_{\varepsilon})(\Gamma^{\lambda c}_{\|\alpha} + \Gamma^{\lambda}_{\|\alpha}\Phi^{\lambda c}_{\|}) \\
&\qquad + \Gamma^{\lambda}_{\perp R}(\Psi^{\lambda c}_{\|\alpha} + \Psi^{\lambda}_{\|\alpha}\Phi^{\lambda c}_{\|}) \\
&\Gamma^{\lambda^*}_{34R\alpha} = (\Phi^{\lambda}_{\varepsilon\alpha} + \Phi^{\lambda}_{\perp\alpha}\Psi^{\lambda}_{\varepsilon})(\Gamma^{\lambda c}_{\perp R} + \Gamma^{\lambda}_{\perp R}\Psi^{\lambda c}_{\perp}) + \Phi^{\lambda}_{\perp\alpha}(\Psi^{\lambda c^*}_{\perp R} + \Psi^{\lambda^*}_{\perp R}\Psi^{\lambda c}_{\perp}) \\
&+ \Phi^{\lambda c}_{\perp R\alpha} + \Phi^{\lambda}_{\perp R\alpha}\Psi^{\lambda c}_{\perp} + \Phi^{\lambda^*}_{\|R}(\Phi^{\lambda c}_{\perp\alpha} + \Phi^{\lambda}_{\perp\alpha}\Psi^{\lambda c}_{\perp}) \\
&\Gamma^{\lambda^*}_{43R\alpha} = (\Psi^{\lambda}_{\varepsilon}\Gamma^{\lambda}_{\|\alpha} + \Psi^{\lambda}_{\|\alpha})(\Phi^{\lambda c^*}_{\|R} + \Phi^{\lambda^*}_{\|R}\Phi^{\lambda c}_{\|}) + \Psi^{\lambda}_{\varepsilon}\Gamma^{\lambda c}_{\|R\alpha} + (\Psi^{\lambda}_{\varepsilon}\Gamma^{\lambda}_{\|R\alpha} + \Psi^{\lambda^*}_{\varepsilon R})(\Gamma^{\lambda c}_{\|\alpha} + \Gamma^{\lambda}_{\|\alpha}\Phi^{\lambda c}_{\|}) \\
&+ \Psi^{\lambda c}_{\|R\alpha} + \Psi^{\lambda}_{\|R\alpha}\Phi^{\lambda c}_{\|} + (\Psi^{\lambda}_{\varepsilon}\Gamma^{\lambda}_{\perp R} + \Psi^{\lambda^*}_{\perp R})[\Psi^{\lambda c}_{\|\alpha} + \Psi^{\lambda}_{\varepsilon}\Gamma^{\lambda c}_{\|\alpha} + (\Psi^{\lambda}_{\varepsilon}\Gamma^{\lambda}_{\|\alpha} + \Psi^{\lambda}_{\|\alpha})\Phi^{\lambda c}_{\|}] \\
&\overline{\Gamma}^{\lambda}_{11\alpha\beta} = \Gamma^{\lambda}_{\|\alpha}[\Phi^{\lambda c}_{\varepsilon\beta} + \Phi^{\lambda}_{\varepsilon\beta} + \Phi^{\lambda}_{\perp\beta}(\Psi^{\lambda c}_{\varepsilon} + \Psi^{\lambda}_{\varepsilon})] \\
&\overline{\Gamma}^{\lambda}_{12\alpha\beta} = \Gamma^{\lambda}_{\|\alpha}[\Phi^{\lambda c}_{\kappa\beta} + (\Phi^{\lambda}_{\varepsilon\beta} + \Phi^{\lambda}_{\perp\beta}\Psi^{\lambda}_{\varepsilon})\Gamma^{\lambda c}_{\kappa}]
\end{aligned}$$

$$
\begin{aligned}
\overline{\Gamma}^{\lambda}_{33\alpha\beta} &= \Phi^{\lambda c}_{\|\alpha\beta} + (\Phi^{\lambda}_{\varepsilon\alpha} + \Phi^{\lambda}_{\perp\alpha}\Psi^{\lambda}_{\varepsilon})(\Gamma^{\lambda c}_{\|\beta} + \Gamma^{\lambda}_{\|\beta}\Phi^{\lambda c}_{\|}) + \Phi^{\lambda}_{\perp\alpha}\Psi^{\lambda c}_{\|\beta} + (\Phi^{\lambda}_{\perp\alpha} + \Psi^{\lambda}_{\|\beta} + \Phi^{\lambda}_{\|\alpha\beta})\Phi^{\lambda c}_{\|} \\
\overline{\Gamma}^{\lambda}_{41\alpha\beta} &= \Psi^{\lambda c}_{\varepsilon\alpha\beta} + (\Psi^{\lambda}_{\varepsilon}\Gamma^{\lambda}_{\|\alpha} + \Psi^{\lambda}_{\|\alpha})[\Phi^{\lambda c}_{\varepsilon\beta} + \Phi^{\lambda}_{\varepsilon\beta} + \Phi^{\lambda}_{\perp\beta}(\Psi^{\lambda c}_{\varepsilon} + \Psi^{\lambda}_{\varepsilon})] \\
&\quad + \Psi^{\lambda}_{\perp\alpha\beta}(\Psi^{\lambda c}_{\varepsilon} + \Psi^{\lambda}_{\varepsilon}) + \Psi^{\lambda}_{\varepsilon\alpha\beta} \\
\overline{\Gamma}^{\lambda}_{42\alpha\beta} &= \Psi^{\lambda c}_{\kappa\alpha\beta} + (\Psi^{\lambda}_{\varepsilon}\Gamma^{\lambda}_{\|\alpha} + \Psi^{\lambda}_{\|\alpha})[\Phi^{\lambda c}_{\kappa\beta} + (\Phi^{\lambda}_{\varepsilon\beta} + \Phi^{\lambda}_{\perp\beta}\Psi^{\lambda}_{\varepsilon})\Gamma^{\lambda c}_{\kappa}] + (\Psi^{\lambda}_{\perp\alpha\beta}\Psi^{\lambda}_{\varepsilon} + \Psi^{\lambda}_{\varepsilon\alpha\beta})\Gamma^{\lambda c}_{\kappa} \\
\overline{\Gamma}^{\lambda}_{44\alpha\beta} &= \Psi^{\lambda c}_{\perp\alpha\beta} + \Psi^{\lambda}_{\varepsilon}\Gamma^{\lambda c}_{\perp\alpha\beta} + (\Psi^{\lambda}_{\varepsilon}\Gamma^{\lambda}_{\|\alpha} + \Psi^{\lambda}_{\|\alpha})(\Phi^{\lambda c}_{\perp\beta} + \Phi^{\lambda}_{\perp\beta}\Psi^{\lambda c}_{\perp}) + \Psi^{\lambda}_{\perp\alpha\beta}\Psi^{\lambda c}_{\perp} \\
\overline{\Gamma}^{\lambda}_{13\alpha\beta\gamma} &= \Gamma^{\lambda}_{\|\alpha}[\Phi^{\lambda c}_{\|\beta\gamma} + (\Phi^{\lambda}_{\varepsilon} + \Phi^{\lambda}_{\perp\beta}\Psi^{\lambda}_{\varepsilon})(\Gamma^{\lambda c}_{\|\gamma} + \Gamma^{\lambda}_{\|\gamma}\Phi^{\lambda c}_{\|}) + \Phi^{\lambda}_{\perp\beta}\Psi^{\lambda c}_{\|\gamma}] \\
&\quad + \Gamma^{\lambda}_{\|\alpha}(\Phi^{\lambda}_{\perp\beta}\Psi^{\lambda}_{\|\gamma} + \Phi^{\lambda}_{\|\beta\gamma})\Phi^{\lambda c}_{\|} \\
\overline{\Gamma}^{\lambda}_{34\alpha\beta\gamma} &= \Phi^{\lambda c}_{\perp\alpha\beta\gamma} + (\Phi^{\lambda}_{\varepsilon\alpha} + \Phi^{\lambda}_{\perp\alpha}\Psi^{\lambda c}_{\varepsilon})\Gamma^{\lambda c}_{\perp\beta\gamma} + [(\Phi^{\lambda}_{\varepsilon\alpha} + \Phi^{\lambda}_{\perp\alpha}\Psi^{\lambda}_{\varepsilon})\Gamma^{\lambda}_{\|\beta} \\
&\quad + \Phi^{\lambda}_{\perp\alpha}\Psi^{\lambda}_{\|\beta} + \Phi^{\lambda}_{\|\alpha\beta}](\Phi^{\lambda c}_{\perp\alpha} + \Phi^{\lambda}_{\perp\alpha}\Psi^{\lambda c}_{\perp}) + \Phi^{\lambda}_{\perp\alpha}(\Psi^{\lambda c}_{\perp\beta\gamma} + \Psi^{\lambda}_{\perp\beta\gamma}\Psi^{\lambda c}_{\perp}) \\
\overline{\Gamma}^{\lambda}_{43\alpha\beta\gamma} &= (\Psi^{\lambda}_{\varepsilon}\Gamma^{\lambda}_{\|\alpha} + \Psi^{\lambda}_{\|\alpha})[\Phi^{\lambda c}_{\|\beta\gamma} + (\Phi^{\lambda}_{\varepsilon\beta} + \Phi^{\lambda}_{\perp\beta}\Psi^{\lambda}_{\varepsilon})(\Gamma^{\lambda c}_{\|\gamma} + \Gamma^{\lambda}_{\|\gamma}\Phi^{\lambda c}_{\|}) + \Phi^{\lambda}_{\perp\beta}\Phi^{\lambda c}_{\|\gamma} \\
&\quad + (\Phi^{\lambda}_{\perp\beta}\Psi^{\lambda}_{\|\gamma} + \Phi^{\lambda}_{\|\beta\gamma})\Phi^{\lambda c}_{\|}] + \Psi^{\lambda}_{\perp\alpha\beta}\Psi^{\lambda c}_{\|\gamma} + (\Psi^{\lambda}_{\perp\alpha\beta}\Psi^{\lambda}_{\varepsilon} + \Psi^{\lambda}_{\varepsilon\alpha\beta})(\Gamma^{\lambda c}_{\|\gamma} + \Gamma^{\lambda}_{\|\gamma}\Phi^{\lambda c}_{\|}) \\
&\quad + \Psi^{\lambda}_{\perp\alpha\beta}\Psi^{\lambda}_{\|\gamma}\Phi^{\lambda c}_{\|}
\end{aligned}
\tag{108}
$$

with

$$
\begin{aligned}
&\Psi^{\lambda c*}_{\varepsilon R} = -\delta^{\lambda}\frac{h^c}{2}(D^{\lambda}_t)^{-1}D^c_t(D^c_{\perp})^T I^c_{Re} \\
&\Psi^{\lambda c*}_{\kappa R} = -\left(\frac{h^c}{2}\right)^2(D^{\lambda}_t)^{-1}D^c_t(D^c_{\perp})^T I^c_{Re} + \left(\frac{h^{\lambda}}{2}\right)^2(D^{\lambda}_{\perp})^T I^{\lambda}_{Re} \\
&\Psi^{\lambda *}_{\varepsilon R} = -\delta^{\lambda}\frac{h^{\lambda}}{2}(D^{\lambda}_{\perp})^T I^{\lambda}_{Re} \qquad \Phi^{\lambda c}_{\|\alpha\beta} = -\delta^{\lambda}\frac{(h^e)^2}{12}[(D^c_{\|\alpha} + D^c_{s\alpha}(D^c_{\perp})^T)I_{\beta} - D^c_{s\alpha}D^c_{t\beta}] \\
&\Phi^{\lambda c}_{\perp\alpha\beta\gamma} = -\delta^{\lambda}\frac{h^c(h^{\lambda})^2}{24}D^{\lambda}_{\|\alpha}I_{\beta}e_{\gamma} \qquad \Phi^{\lambda}_{\|\alpha\beta} = \delta^{\lambda}\frac{(h^{\lambda})^2}{12}[(D^{\lambda}_{\|\alpha} + D^{\lambda}_{s\alpha}(D^{\lambda}_{\perp})^T)I_{\beta} - D^{\lambda}_{s\alpha}D^{\lambda}_{t\beta}] \\
&\Psi^{\lambda c}_{\varepsilon\alpha\beta} = \delta^{\lambda}\frac{(h^c)^2}{12}(D^{\lambda}_t)^{-1}D^c_t D^c_{t\alpha}(D^c_s)^{-1}I^T_{\beta}D^c_e \\
&\Psi^{\lambda c}_{\kappa\alpha\beta} = -\delta^{\lambda}\frac{(h^c)^3}{24}(D^{\lambda}_t)^{-1}e_{\alpha}\left[D^c_s e_{\beta}(D^c_{\perp})^T + \left(\frac{h^{\lambda}}{h^c}\right)^3 D^{\lambda}_s e_{\beta}(D^{\lambda}_{\perp})^T\right] \\
&\Psi^{\lambda}_{\perp\alpha\beta} = \delta^{\lambda}\frac{(h^{\lambda})^2}{12}[D^{\lambda}_{t\alpha}D^{\lambda}_{s\beta} - (D^{\lambda}_t)^{-1}e^T_{\alpha}D^{\lambda}_s e_{\beta}] \\
&\Psi^{\lambda}_{\varepsilon\alpha\beta} = -\delta^{\lambda}\frac{(h^{\lambda})^2}{12}D^{\lambda}_{t\alpha}(D^{\lambda}_s)^{-1}I^T_{\beta}D^{\lambda}_e
\end{aligned}
\tag{109}
$$

4.2 3D Refined Recovery Relations (22CS)

By subtracting Eq. (1) from Eq. (22) for one layer of the composite sandwich shell, 3D displacement fields can be first recovered with Eqs. (44), (56), (109) and (105) through the second-order as:

$$\begin{aligned} U_\alpha &= u_\alpha + x_3\hat{C}_{3\alpha} + \hat{C}_{\alpha i}(x_3\varphi_i) + \hat{C}_{3\alpha}y_3 + \hat{C}_{\alpha\beta}v_\beta + \hat{C}_{3\alpha}v_3 + \hat{C}_{\alpha\beta}z_\beta + \hat{C}_{3\alpha}z_3 \\ U_3 &= u_3 + x_3(\hat{C}_{33}-1) + \hat{C}_{3i}(x_3\varphi_i) + \hat{C}_{33}y_3 + \hat{C}_{3\alpha}v_\alpha + \hat{C}_{33}v_3 + \hat{C}_{3\alpha}z_\alpha + \hat{C}_{33}z_3 \end{aligned} \tag{110}$$

where U_i are 3D displacement measures in the $\boldsymbol{b}_i$ basis, u_i are the 2D displacements in the $\boldsymbol{b}_i$ basis, and $\hat{C}_{ij}$ is the direction-cosine matrix relating B_i and $\boldsymbol{b}_i$, given in Eq. (13). In addition, to recover the 3D displacement fields for the composite sandwich shell, the following continuity conditions are established from Eqs. (62), (74) and (75): for the top skin-layer and the core-layer,

$$\begin{aligned} u_\alpha^t &= u_\alpha^c - \frac{h^t}{2}\hat{C}_{\beta\alpha}^c\hat{C}_{3\beta}^t + \frac{h^c}{2}\left[1+\frac{h^t}{h^c}\right]\hat{C}_{3\alpha}^c + \hat{C}_{\alpha i}^c\left(\frac{h^c}{2}\varphi_i^c + \frac{h^t}{2}\varphi_i^t\right) \\ u_3^t &= u_3^c - \frac{h^t}{2}\hat{C}_{\alpha 3}^c\hat{C}_{3\alpha}^t + \frac{h^c}{2}\left[1+\frac{h^t}{h^c}\right](\hat{C}_{33}^c-1) + \hat{C}_{3i}^c\left(\frac{h^c}{2}\varphi_i^c + \frac{h^t}{2}\varphi_i^t\right) \end{aligned} \tag{111}$$

and for the bottom skin-layer and the core-layer,

$$\begin{aligned} u_\alpha^b &= u_\alpha^c + \frac{h^b}{2}\hat{C}_{\beta\alpha}^c\hat{C}_{3\beta}^b - \frac{h^c}{2}\left[1+\frac{h^b}{h^c}\right]\hat{C}_{3\alpha}^c - \hat{C}_{\alpha i}^c\left(\frac{h^c}{2}\varphi_i^c + \frac{h^b}{2}\varphi_i^b\right) \\ u_3^b &= u_3^c + \frac{h^b}{2}\hat{C}_{\alpha 3}^c\hat{C}_{3\alpha}^b - \frac{h^c}{2}\left[1+\frac{h^b}{h^c}\right](\hat{C}_{33}^c-1) - \hat{C}_{3i}^c\left(\frac{h^c}{2}\varphi_i^c + \frac{h^b}{2}\varphi_i^b\right) \end{aligned} \tag{112}$$

From Eq. (25) through the second order, one can also recover the 3D

strain fields for the individually layer of the composite sandwich shell as

$$\begin{aligned}
\Gamma_e &= \varepsilon + x_3\kappa + I_\alpha(x_3\varphi_{\|;\alpha} + v_{\|;\alpha}) + I_R(x_3\varphi_3 + y_3) - x_3 I_{Re}(\varepsilon + x_3\kappa) \\
2\Gamma_s &= \varphi_\| + v_\|' + z_\|' + e_\alpha(x_3\varphi_{3;\alpha} + y_{3;\alpha} + v_{3;\alpha}) - e_R(x_3\varphi_\|) \\
\Gamma_t &= \varphi_3 + y_3' + v_3' + z_3'
\end{aligned} \tag{113}$$

Finally, the 3D stress fields can be also recovered in a straightforward manner using the original 3D constitutive relations:

$$\begin{aligned}
\sigma_e &= D_e\Gamma_e + D_{et}\Gamma_t \\
\sigma_s &= D_s(2\Gamma_s) \\
\sigma_t &= D_{et}^T\Gamma_e + D_t\Gamma_t
\end{aligned} \tag{114}$$

Finally, one obtains the 3D strain/stress fields for the composite sandwich shell (22CS) by introducing Eq. (106) into Eqs. (113) and (114).

4.3 3D Recovery relations with stress recovery (00EE&11EE)

By subtracting Eq. (1) from Eq. (22) for one layer of the composite sandwich shell, 3D displacement fields can be first recovered with Eqs. (44) and (56) as:

$$\begin{aligned}
U_\alpha &= u_\alpha + x_3\hat{C}_{3\alpha} + \hat{C}_{\alpha i}(x_3\varphi_i) + \hat{C}_{3\alpha}y_3 + \underline{\hat{C}_{\alpha\beta}v_\beta + \hat{C}_{3\alpha}v_3} \\
U_3 &= u_3 + x_3(\hat{C}_{33} - 1) + \hat{C}_{3i}(x_3\varphi_i) + \hat{C}_{33}y_3 + \underline{\hat{C}_{3\alpha}v_\alpha + \hat{C}_{33}v_3}
\end{aligned} \tag{115}$$

The underlined terms are additive higher-order term which will affect only 11EE approach and can be simply dropped for 00EE approach. To recover the 3D displacement fields for the composite sandwich shell, the following continuity conditions are established from Eqs. (62), (74) and (75): for the top skin-layer and the core-layer,

$$
\begin{aligned}
u_\alpha^t &= u_\alpha^c - \frac{h^t}{2}\hat{C}_{\beta\alpha}^c\hat{C}_{3\beta}^t + \frac{h^c}{2}\left[1+\frac{h^t}{h^c}\right]\hat{C}_{3\alpha}^c + \hat{C}_{\alpha i}^c\left(\frac{h^c}{2}\varphi_i^c + \frac{h^t}{2}\varphi_i^t\right) \\
u_3^t &= u_3^c - \frac{h^t}{2}\hat{C}_{\alpha 3}^c\hat{C}_{3\alpha}^t + \frac{h^c}{2}\left[1+\frac{h^t}{h^c}\right](\hat{C}_{33}^c - 1) + \hat{C}_{3i}^c\left(\frac{h^c}{2}\varphi_i^c + \frac{h^t}{2}\varphi_i^t\right)
\end{aligned}
\tag{116}
$$

and for the bottom skin-layer and the core-layer,

$$
\begin{aligned}
u_\alpha^b &= u_\alpha^c + \frac{h^b}{2}\hat{C}_{\beta\alpha}^c\hat{C}_{3\beta}^b - \frac{h^c}{2}\left[1+\frac{h^b}{h^c}\right]\hat{C}_{3\alpha}^c - \hat{C}_{\alpha i}^c\left(\frac{h^c}{2}\varphi_i^c + \frac{h^b}{2}\varphi_i^b\right) \\
u_3^b &= u_3^c + \frac{h^b}{2}\hat{C}_{\alpha 3}^c\hat{C}_{3\alpha}^b - \frac{h^c}{2}\left[1+\frac{h^b}{h^c}\right](\hat{C}_{33}^c - 1) - \hat{C}_{3i}^c\left(\frac{h^c}{2}\varphi_i^c + \frac{h^b}{2}\varphi_i^b\right)
\end{aligned}
\tag{117}
$$

From Eq. (25) through the second-order, one can also recover the 3D strain fields for the individually layer of the composite sandwich shell as

$$
\begin{aligned}
\Gamma_e &= \varepsilon + x_3\kappa + \underline{I_\alpha(x_3\varphi_{\|;\alpha} + v_{\|;\alpha}) - I_{Re}x_3(\varepsilon + x_3\kappa) + I_{RRe}x_3^2(\varepsilon + x_3\kappa) - I_\alpha e_{R\alpha}x_3^2\varphi_{\|;\alpha}} \\
&\quad \underline{+ I_R(x_3\varphi_3 + y_3 + v_3) - I_{Re}I_R(x_3^2\varphi_3 + y_3) + x_3^2 I_{RRw}\varepsilon} \\
2\Gamma_s &= \varphi_\| + \underline{v_\|' + e_\alpha(x_3\varphi_{3;\alpha} + y_{3;\alpha} + v_{3;\alpha}) - e_R\{x_3\varphi_\| + v_\|\}} \\
&\quad \underline{- e_R\{e_\alpha(x_3^2\varphi_{3;\alpha} + x_3 y_{3;\alpha}) - e_R x_3^2\varphi_\|\}} \\
\Gamma_t &= \varphi_3 + \underline{y_3' + v_3'}
\end{aligned}
\tag{118}
$$

Finally, for the present approaches(00EE, 11EE), the 3D transverse stress fields can be alternatively recovered from integration of the equilibrium equations of the 3D elasticity through the shell thickness, similar to the approaches found in Tornabene and Brischetto [19] and Sayyad and Naik [20]. The following elasticity equilibrium equation neglecting the body forces is first used to derive the expression for the 3D transverse shear and normal stress fields

$$\begin{aligned}\sigma_{13} &= \overline{R}_1(-\overline{\sigma}_{13} + C_1)\\ \sigma_{23} &= \overline{R}_2(-\overline{\sigma}_{23} + C_2)\\ \sigma_{33} &= \overline{R}_3(-\overline{\sigma}_{33} + C_3)\end{aligned} \tag{119}$$

with

$$\begin{aligned}\overline{\sigma}_{13} &= -\int\left(\frac{R_1}{\overline{R}_3}\sigma_{11;1} + R_2(R_1+x_3)^2\sigma_{12;2}\right)dx_3\\ \overline{\sigma}_{23} &= -\int\left(\frac{R_2}{\overline{R}_3}\sigma_{22;2} + R_1(R_2+x_3)^2\sigma_{12;1}\right)dx_3\\ \overline{\sigma}_{33} &= -\int\left((R_2+x_3)(R_1\sigma_{13;1} - \sigma_{11}) + (R_1+x_3)(R_2\sigma_{23;2} - \sigma_{22})\right)dx_3\end{aligned}$$

$$\overline{R}_1 = \frac{1}{(R_1+x_3)^2(R_2+x_3)}\quad \overline{R}_2 = \frac{1}{(R_1+x_3)(R_2+x_3)^2}\quad \overline{R}_3 = \frac{1}{(R_1+x_3)(R_2+x_3)} \tag{120}$$

Where R_α representing mean radius of curvature evaluated in x_α directions. Here, to estimate C_i above, the associated boundary conditions at the top and bottom faces of the shell are also provided such as

$$\begin{aligned}\sigma_{\alpha 3}\big|_{x_3 = h/2} &= \tau_\alpha \qquad \sigma_{\alpha 3}\big|_{x_3 = -h/2} = -\beta_\alpha\\ \sigma_{33}\big|_{x_3 = h/2} &= \tau_3 \qquad \sigma_{33}\big|_{x_3 = -h/2} = -\beta_3\end{aligned} \tag{121}$$

In a manner similar to obtain the 3D displacement and strain/stress fields for the composite sandwich shell, imposing Eqs. (119) and (121) into Eqs. (63) we obtain the following transverse shear and normal stresses fields:

$$\begin{aligned}\sigma_{i3}^{t} &= \overline{R}_i^{t}(-\overline{\sigma}_{13}^{t} + C_i^{t}) \\ \sigma_{i3}^{c} &= \overline{R}_i^{c}(-\overline{\sigma}_{13}^{c} + C_i^{c}) \\ \sigma_{i3}^{b} &= \overline{R}_i^{b}(-\overline{\sigma}_{13}^{b} + C_i^{b})\end{aligned} \tag{122}$$

where

$$\begin{aligned}C_i^{t} &= \frac{\overline{R}_i^{c-}\overline{R}_i^{b-}(-\overline{\alpha}_i + \overline{\gamma}_i) - \overline{R}_i^{c+}\overline{R}_i^{b-}(-\overline{\beta}_i + \overline{\gamma}_i) - \overline{R}_i^{c+}\overline{R}_i^{b+}(\overline{\alpha}_i + \overline{\beta}_i + 2\beta_i - 2\tau_i)}{2\Delta_i} \\ C_i^{c} &= \frac{\overline{R}_i^{t+}\overline{R}_i^{b+}(\overline{\alpha}_i - \overline{\gamma}_i) - \overline{R}_i^{t-}\overline{R}_i^{b-}(-\overline{\beta}_i + \overline{\gamma}_i) - \overline{R}_i^{t-}\overline{R}_i^{b+}(\overline{\alpha}_i + \overline{\beta}_i + 2\beta_i - 2\tau_i)}{2\Delta_i} \\ C_i^{b} &= \frac{\overline{R}_i^{t+}\overline{R}_i^{c-}(\overline{\alpha}_i - \overline{\gamma}_i) + \overline{R}_i^{t+}\overline{R}_i^{c+}(-\overline{\beta}_i + \overline{\gamma}_i) - \overline{R}_i^{t+}\overline{R}_i^{c-}(\overline{\alpha}_i + \overline{\beta}_i + 2\beta_i - 2\tau_i)}{2\Delta_i}\end{aligned} \tag{123}$$

with $\overline{\alpha}_i = (\overline{\sigma}_{i3}^{t})^{\pm} - (\overline{\sigma}_{i3}^{c})^{\mp} - (\overline{\sigma}_{i3}^{b})^{\mp}$, $\overline{\beta}_i = (\overline{\sigma}_{i3}^{t})^{\mp} + (\overline{\sigma}_{i3}^{c})^{\mp} + (\overline{\sigma}_{13}^{b})^{\pm}$, $\overline{\gamma}_i = (\overline{\sigma}_{i3}^{t})^{\mp} + (\overline{\sigma}_{i3}^{c})^{\pm} - (\overline{\sigma}_{13}^{b})^{\mp}$, $\Delta_i = \overline{R}_i^{t+}\overline{R}_i^{c+}\overline{R}_i^{b+} + \overline{R}_i^{t-}\overline{R}_i^{c-}\overline{R}_i^{b-}$, $(\bullet)^{\pm} = (\bullet)^{+} + (\bullet)^{-}$ and $(\bullet)^{\mp} = (\bullet)^{+} - (\bullet)^{-}$.

5. Validation Examples

As a preliminary validation to demonstrate the capability and accuracy of the present approach, a set of numerical examples will be performed for various FCSR, LTR and RTR cases. Although a plate is just a special case of a shell and the plate model should be able to be reduced from the shell model given in this paper by specifying the initial curvatures to be zero, we study plate examples as well as shell examples, to validate the capability and accuracy for various LTR and RTR cases separately. In particular, for sandwich structures (plates and shells) in which each layer is made of an isotropic or composite material, a geometrically linear, static analysis is carried out to compare analytical results generated in this study with 3D exact solutions available in the literature. Together with 3D exact solutions provided by Pagano [4] and Brischetto [5], several types of associated plate/shell theories will be compared with the present approach in all tables and graphics to be presented in this section,

EDN: Nth-order ESL- and displacement-based theory

EDZN: Nth-order ESL- and displacement-based theory including Murakami's Zig-Zag function

LDN: Nth-order LW- and displacement-based theory

EMCN: Nth-order ESL- and displacement-based mixed theory

EMZCN: Nth-order EDZ- and displacement-based mixed theory

LMN: Nth-order LD- and displacement-based mixed theory

VAPAS: Second-orderESL-andstrain-basedtheory

It is noteworthy to point out that the present approach used 6 DOFs for its zeroth-order (PA(00EE)) and second-order (PA(11EE) and PA(22CS)) approximations. Here, from Demasi [31], ED types are indicated as a sort of Advanced Higher-order Shear Deformation Theories (AHSDT), and EDZ is named as Advanced Higher-order Shear Deformation Theories with Zig-Zag effects included (AHSDTZ). In addition, LD theories are indicated as Advanced Layer-wise Theories (ALWT), and from Yu [13, 14], VAPAS denotes the second-order approximation of Variational Asymptotic Plate and Shell Analysis (VAPAS) and has the same potential energy functional of the 2D generalized Reissner-like model. And the character M included in the types means mixed models based on Reissner's mixed variational theorem. In this section, the six proposed examples are taken to be simply supported along all four edges and are subjected to the following harmonic transverse normal loads at the top of the whole structure

$$\tau_\alpha = \beta_i = 0 \quad \tau_3 = p_0 \sin\left(\frac{m\pi}{L_1}x_1\right)\sin\left(\frac{n\pi}{L_2}x_2\right) \tag{124}$$

where p_0 is the amplitude of transverse applied pressure, m and n are the half-wave numbers. And L_α representing length evaluated in x_α directions. Moreover, for the purpose of presenting the results graphically, the three kinds of non-dimensional quantities are adopted in the following forms:

$$\begin{aligned} &\overline{U}_\alpha = U_\alpha \frac{E^\lambda}{p_0 h (L/h)^3} \quad \overline{U}_3 = U_3 \frac{100E^\lambda}{p_0 h (L/h)^4} \quad \overline{x}_3 = \frac{x_3}{h} \\ &\overline{\sigma}_{\alpha\beta} = \frac{\sigma_{\alpha\beta}}{p_0 (L/h)^2} \quad \overline{\sigma}_{\alpha 3} = \frac{\sigma_{\alpha 3}}{p_0 (L/h)} \quad \overline{\sigma}_{33} = \frac{\sigma_{33}}{p_0} \end{aligned} \tag{124}$$

,

$$\overline{U}_\alpha = U_\alpha \frac{E^c}{p_0 h (L/h)^3} \quad \overline{U}_3 = U_3 \frac{100E^c}{p_0 h (L/h)^4} \quad \overline{x}_3 = \frac{x_3}{h}$$
$$\overline{\sigma}_{\alpha\beta} = \sigma_{\alpha\beta} \quad \overline{\sigma}_{\alpha 3} = \sigma_{\alpha 3} \quad \overline{\sigma}_{33} = \sigma_{33} \tag{126}$$

and

$$\overline{U}_i = U_i \frac{10E^\lambda}{p_0 h (R/h)^4} \quad \overline{x}_3 = \frac{x_3}{h}$$
$$\overline{\sigma}_{\alpha\beta} = \frac{\sigma_{\alpha\beta}}{p_0 (R/h)^2} \quad \overline{\sigma}_{\alpha 3} = \frac{\sigma_{\alpha 3}}{p_0 (R/h)} \quad \overline{\sigma}_{33} = \frac{\sigma_{33}}{p_0} \tag{127}$$

As the relative error Err%, number in parentheses on the right of results calculated from different plate and shell theories are also defined as follows:

$$Err\% = \frac{Result\ from\ the\ theory\ -\ 3D\ exact\ solution}{3D\ exact\ solution} \times 100 \tag{128}$$

This section is organized as follows: in Sect.5.1., we investigate the effect of the order transition of 2D generalized transverse motion measures due to mismatch of material constants between constituent materials in developing a universal model. Referring to the published literature, one can easily observe that several benchmarks with various FCSRs, LTRs and RTRs have been critically performed to assess the capability and accuracy of different higher-order sandwich plate/shell theories. Therefore, in Sect.5.2. and Sect.5.3., for the purpose of a detailed comparison with 3D exact solutions found in Pagano [4] and Brischetto [5], let us especially consider bending problems of composite sandwich plates/shells suggested by Pagano [4], Carrera and Demasi [6], Carrera and Brischetto [7,9], Demasi and Yu [8].

5.1 Effect of different orders of 2D generalized transverse motion measures into two universal theories

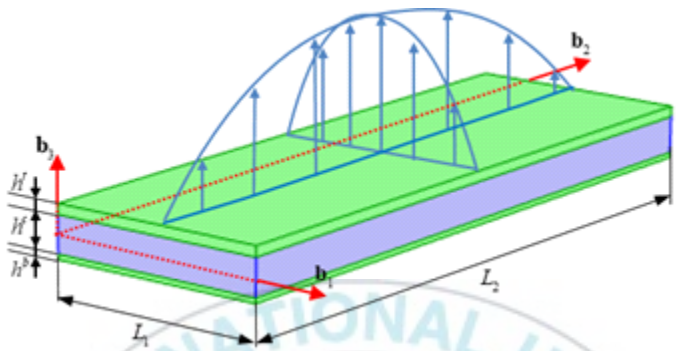

Fig. 3 Antisymmetric sandwich plate configuration of the bending problem

As depicted in Fig. 3 from Demasi and Yu [8], an antisymmetric rectangular sandwich plate made of isotropic materials is considered with width $L_2 = 3L_1$ and the total thickness $h = h^t + h^b + h^c$ along x_3 direction. In particular, each thickness of top and bottom skin-layers has $h^t = 0.1h$ and $h^b = 0.2h$, while the core-layer has $h^c = 0.7h$. It is also a thick $(L_1/h = 4)$ with three FCSR cases $(1.25E^t/E^c = E^b/E^c = \{10^1, 10^3, 10^5\})$. As far as Poisson's ratio is concerned, the same values are used as $\nu^t = \nu^b = \nu^c = 0.34$.

To present the results graphically, we used the normalization scheme of Eq. (125). Together with the exact 3D solution found in Brischetto [6], the through-thickness distributions of $\overline{U}_3(L_1/2, L_2/2, \overline{x}_3)$, $\overline{\sigma}_{11}(L_1/2, L_2/2, \overline{x}_3)$, $\overline{\sigma}_{13}(0, L_2/2, \overline{x}_3)$, $\overline{\sigma}_{33}(L_1/2, L_2/2, \overline{x}_3)$ are predicted by two different refined universal theories: in developing a refined universal model, we take the

present approach with $\varphi_i \sim (l/h)\hat{\varepsilon}$ (PA(22CS)) and the present approach with $\varphi_i \sim \hat{\varepsilon}$ (PA(22CSO)).

Here it is noted that a somewhat different asymptotic approach for composite sandwich plates was independently introduced by Rao et al. [32]. Rather than following Berdichevsky's works, an analytical framework similar to that used by Yu [13, 14] was used. It involves adopting a deformed plate triad, $\mathbf{B}_i$, that takes into account transverse shear deformations and assuming the order associated with the transverse shear strains to be $\hat{\varepsilon}$ throughout the development. Although we cannot make a direct comparison with their asymptotic models, PA(22CSO) will be alternatively used and examined because of following the same order analysis used by Rao et al. [32] when the corresponding asymptotically correct energy functional up through the second order has been constructed.

First, let us take the isotropic and thick sandwich plate with not hard-skin (FCSR=10^1). From the plotted results in Fig. 6, one can observe that results obtained from PA(22CS) and PA(22CSO) are almost identical to 3D exact solutions because the effect of transverse shear deformation is not significant for this case.

Next, other sandwich plates with different FCSRs are investigated to demonstrate the dominant effect of the order transition of φ_i in developing a refined universal model for thick composite sandwich plates. From the plots in Figs. 7 and 8 for hard-skin (FCSR=10^3) and very hard-skin (FCSR=10^5), respectively, one can easily observe that the difference

dramatically increases with increasing FCSR. Unlike results calculated by PA(22CSO), those from PA(22CS) for both hard-skin and very hard-skin cases has all excellent agreement with 3D exact solutions because as pointed out by Berdichevsky's papers, the 2D generalized transverse motion measures are chosen to be of the order of $l\hat{\varepsilon}/h$ when the thick sandwich plate with the hard-skin FCSR is investigated as the worst scenario case. Therefore, this clearly proves that to model the sandwich plates confidently and obtain accurate results over a wide range of FCSRs, it is very important to capture the order transition of 2D generalized transverse motion measures caused by mismatch of material properties between constituent materials as the essential consideration when the refined universal theory is asymptotically constructed.

5.2 Bending analysis of composite sandwich plates/shells related to different values of LTR and RTR for a fixed FCSR

In section 5.2.1., as depicted in Fig. 4, a symmetric square sandwich plate is considered with identical width $L = L_\alpha$ along x_α and total thickness h. And both skin layers have equal thickness $h^t = h^b = 0.1h$ and the core layer thickness is $h^c = 0.8h$, where the total thickness of the plate is $h = 10mm$. In addition, the material properties of both skin layers are $E_L = 172{,}375MPa$,$E_T = 6{,}895MPa$, $G_{LT} = 3{,}516MPa$, $G_{TT} = 1{,}379MPa$ and $\nu_{LT} = \nu_{TT} = 0.25$,

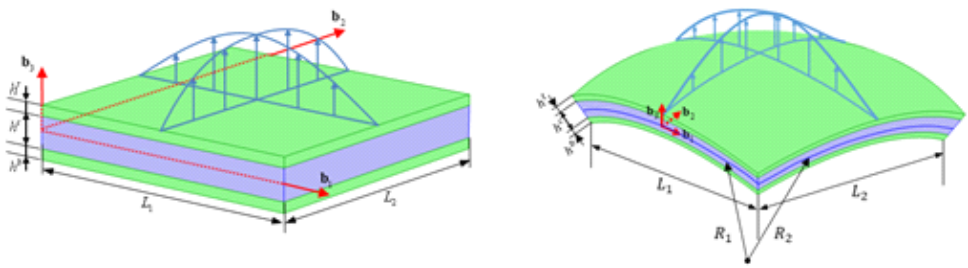

Fig. 4 Symmetric sandwich plate and spherical sandwich shell configuration of the bending problem

where the two subs-cripts L and T signify the parallel and transverse directions to the fibers, respectively. On the other hand, the core material is transversely isotropic with respect to x_3 and has $E_{11} = E_{22} = 275.8MPa$, $E_{33} = 3{,}477.5MPa$, $G_{11} = G_{22} = 413.7MPa$, $G_{33} = 1{,}103.2GPa$ and $\nu_{31} = \nu_{32} = \nu_{12} = 0.25$. Thus, the FCSR is $E_I/E_{11} = 625$, which represents the not hard-skin case. The pressure is sinusoidally distributed over the top surface ($m = n = 1$). The corresponding boundary conditions for the sandwich plate are the same as those used in the previous section. In section 5.2.2., a spherical sandwich shell is considered with same properties of the symmetric square sandwich plate and, in addition, geometric data for shell $R = R_\alpha$ representing mean radius of curvature evaluated in x_α directions. And the results have been proposed in Sect. 5.2. in terms of non-dimensional form of Eq. (125).

5.2.1 Symmetric sandwich plate proposed by Pagano [4] and Carrera and Demasi [6]

Firstly, to assess the accuracy of the present approach for moderately thick and thick plates, the symmetric sandwich plate proposed by Pagano [4] and Carrera and Demasi [6] are carried out and compared with the 3D exact solution obtained from Pagano [4] for a fixed FCSR and various LTRs. The different values of LTR that are used are {2,4,10}, where LTR=2 represents a very thick sandwich plate, LTR=4 a thick one and LTR=10 a moderately thick one. Here to present the results graphically we used the same normalization scheme as one introduced by the previous subsection.

In Tables 1-3, results obtained from the present approaches have been compared with ones from 3D elasticity theory (3D Exact) and various ESL- and LW-plate theories for moderately to very thick cases; the percentage relative error is also placed in parenthesis. As shown in Table 1 for maximum transverse deflection and 2 for maximum in-plane normal stress, respectively, the our refined approach has very similar predictions as LD2 and LD3 for all LTR cases. However, from the table, one can easily determine that our refined approach is generally better than PA(00EE) and VAPAS for thick to very thick plates because our refined approach is the universal theory based on the asymptotically correct energy functional, taking into account the higher-order mechanical deformations of sandwich structures.

Moreover, from the Table 3 for maximum transverse shear stress, it is possible to see that the present approach(22CS) has an accuracy comparable or superior to all other higher-order theories listed in the table for all LTR cases, except the only one case of EDZ3 for the LTR=2. However, from the results in Tables 1 and 2, the present approach(22CS) presents a great compromise between accuracy and efficiency because the present approaches requires only 6 DOFs for predicting mechanical characteristics of composite sandwich plates with various LTRs.

For the purpose of confirming the above results graphically, the transverse displacement and transverse stress distributions of the thick sandwich plate are predicted by three different approaches (3D Exact, PA(00EE), VAPAS) and plotted versus the normalized thickness coordinates in Fig. 9, where Fig. 9(a) depicts the transverse displacement distribution $\overline{U}_3$, Fig. 9(b) the in-plane normal stress distribution $\overline{\sigma}_{11}$ and Fig. 9(c) and (d) the transverse shear/normal stress distributions $\overline{\sigma}_{13}$ and $\overline{\sigma}_{33}$, respectively. Unlike results obtained from the present approaches, those from VAPAS differ from the 3D exact solutions for the transverse displacement and shear stress, although PA(00EE) agrees well for the transverse shear stress. Therefore, one can easily observe that PA(22CS) has excellent agreement with the 3D exact solution (Pagano [4]) for all displacement and stress components investigated in the thick case.

5.2.2 Bending analysis of sandwich spherical shells

The sandwich spherical shell is considered to assess the accuracy of the present approaches and compared with the 3D exact solution obtained from Brischetto [5] for a fixed FCSR and various RTRs. The different values of RTR that are used are {10, 100}. Here to present the results graphically we used the same normalization scheme as one introduced by the previous subsection.

Together with the exact 3D solution found in Brischetto [5], the through-thickness distributions of $\overline{U}_3, \overline{\sigma}_{11}, \overline{\sigma}_{13}, \overline{\sigma}_{33}$ are predicted mainly by two different refined universal theories: in developing a refined universal model, we take the approach with $l \sim R$ (PA(11EE)) and the approach with $l \sim \sqrt{hR}$ (PA(22CS)).

To investigate the effect of the order of the curvature radius of the reference surface specifically, all parameters are fixed except for RTR. In Fig. 10 and 11 show the through-the-thickness distributions of $\overline{U}_3, \overline{\sigma}_{11}, \overline{\sigma}_{13}$ passing through the centroid of the shell and $\overline{\sigma}_{13}$ passing through the point $(0, L/2, \overline{x}_3)$. In Fig. 10(d) and 11(d), different shell theories are markedly distinguished, observing that PA(00EE) and PA(11EE) with a stress recovery in which equilibrium equations are integrated along the thickness direction as an extra post processing step describe the transverse normal stress more accurately than PA(22CS) and VAPAS with a refined recovery relations in which second-order warpings are included additionally. And Fig. 10(a)-(c)

for $l \sim \sqrt{hR}$, one can observe that results obtained from PA(11EE) and PA(22CS) are almost identical to 3D exact solutions. From the Fig. 11(a) and (b) for $l \sim R$, both approach PA(11EE) and PA(22CS) have similar error rates, however, in the Fig. 11(c), the trend of the solutions of PA(11EE) is similar with 3D exact solutions, unlike results calculated by PA(22CS). Therefore, to obtain accurate results over a wide range of RTRs, the order $l \sim R$ is better than the order $l \sim \sqrt{hR}$ when the refined universal theory is asymptotically constructed.

5.3 Bending analysis of composite sandwich plates/shells related to different values of LTR, RTR and FCSR

In order to explore how the various values of LTR, RTR and FCSR can affect the response of sandwich plates/shells, the sandwich plate problems conducted by Carrera and Brischetto [7], Demasi and Yu [8], and the sandwich shell problems conducted by Carrera and Brischetto [9] will be considered. The plate problem is similar to the geometric configuration used in the Sect.5.1. And, a curved shell panel denoted as Ren shell and a cylindrical shell well-known as Varadan-Baskar shell will be considered, respectively; see Fig.5. And, in this section 5.3., a metallic material of two top skin-layers is $E = 73GPa$, $G = 27.239GPa$ and $\nu = 0.34$, while a Nomex material of the core-layer is transversely isotropic with respect to x_3 and is $E_L = E_T = 0.01MPa$, $E_z = 75.85MPa, G = 22.5MPa$ and $\nu = 0.01$. Stiffer skins and softer cores have been obtained by multiplying the Nomex

material properties by various factors. Thus, three different cases of $FCSR_L$= E^t/E_L^c and $FCSR_z$= E^t/E_z^c were analyzed; this range of $FCSR_L$ is $7.3\times\{10^4,10^6,10^8\}$ and this range of $FCSR_z$ is $9.624\times\{10^0,10^2,10^4\}$.

5.3.1 Symmetric sandwich plate proposed by Carrera and Brischetto [7] and Demasi and Yu [8]

To assess the accuracy of the present approaches for various FCSRs and LTRs, the plate case consists of the validation problems conducted by Carrera and Brischetto [7] and Demasi and Yu [8]. Similar to the geometric configuration used in Sect. 5.1., different values of the thickness parameter are treated; this range of LTRs is {2,4,10}. Both skin-layers have equal thickness $h^t = h^b = 0.1h$ and the core layer has $h^c = 0.8h$, respectively. Moreover, for the purpose of presenting the results graphically, as another kind of non-dimensional quantities Eq. (126) is adopted.

Table 4 compares different higher-order approaches with 3D exact solutions found in Brischetto [5]. Maximum transverse displacements in correspondence to the middle surface are given for different values of the LTR and FCSR ($FCSR_L$ and $FCSR_z$). From the table, one can observe that our refined approaches has excellent agreement with the 3D exact solution for all FCSR and LTR case investigated but results obtained from VAPAS are highly inaccurate for all sandwich plates with very hard and extremely hard FCSRs in any LTRs investigated. This can be indirectly explained that LW-based plate theories are required to predict accurate maximum transverse

displacements for the sandwich plate problems in high FCSR and small LTR cases.

Next, significant stress comparisons with 3D exact solutions for different plate theories are given in Table 5 for maximum in-plane normal stress and 6 for maximum transverse shear stress. As shown in these table, similar observations to those made earlier can be made. Therefore, for 3D stress predictions of composite sandwich plates, the present approach (22CS) has a very good accuracy, generally better than all other theories listed in the tables. Moreover, from Table 6, it seems that PA(11EE) cannot describe accurately the distributions of transverse shear stress for high value FCSR and thick plate due to PA(11EE) results of transverse shear stress with unsatisfied accuracy.

To confirm the above results graphically, Figs. 12-14 show the through-the-thickness distributions of 3D displacement and stress distributions of the thick sandwich plates with three different FCSR cases: (a) hard skin FCSR ($FCSR_L = 7.3 \times 10^4$ and $FCSR_z = 9.624$), (b) very hard skin FCSR ($FCSR_L = 7.3 \times 10^6$ and $FCSR_z = 9.624 \times 10^2$), (c) extremely hard skin FCSR ($FCSR_L = 7.3 \times 10^8$ and $FCSR_z = 9.624 \times 10^4$), where Figs. 12(a), 13(a) and 14(a) depicts the transverse displacement distributions $\overline{U}_3$, and Figs. 12(b), 13(b) and 14(b) the in-plane stress distributions $\overline{\sigma}_{11}$, Figs. 12(c), 13(c) and 14(c) the transverse shear stress distributions $\overline{\sigma}_{13}$ and Figs. 12(d), 13(d) and 14(d) the transverse normal stresses $\overline{\sigma}_{33}$, respectively.

In the first FCSR case, one can easily observe that our refined

approaches have excellent agreement with 3D exact solutions for all displacement and stress components investigated, even though PA(00EE) and VAPAS differ slightly from the 3D exact solution for the transverse shear stress. Moreover, for thick plates with the very and extremely hard skin FCSR case one can easily observe that the results obtained from PA(22CS), PA(11EE) and PA(00EE) still agree excellent, but VAPAS is not meaningful with those from 3D exact solutions. However, from the plots for thick plates with extremely hard skin (largest values of FCSR), VAPAS results were not presented because they are not meaningful. In particular, the transverse displacement distribution for PA(00EE) on Fig. 14(a) shows that the difference dramatically increases with increasing FCSR in the thick case, while PA(22CS) and PA(11EE) have excellent agreement with the 3D exact solution over the whole plate thickness. Moreover, from Fig. 14(c), our refined approaches demonstrate the unsymmetric distribution of the transverse shear stress $\bar{\sigma}_{13}$ throughout the plate thickness in the thick and extremely hard skin FCSR case, while such asymmetry of $\bar{\sigma}_{13}$ cannot be described by PA(00EE). On the other hand, similar to Shah and Batra [18], the transverse normal stress obtained from the 3D constitutive relation for PA(22CS) on Fig. 14(d) does not accurately capture the boundary layer phenomenon near the top and the bottom surfaces of the composite sandwich plate. However, the refined approach PA(11EE) of PA(00EE), using integration of equilibrium equations of the 3D elasticity theory capture accurately, because PA(22CS) does not directly utilize the traction boundary conditions on top and bottom surfaces of the sandwich plate. As a result, PA(11EE) does not

have a satisfied accuracy of transverse shear stress passing through the point $(0, L/2, 0)$ compared to PA(22CS), but PA(11EE) has the strength to capture boundary layer effect well.

5.3.2 Single curved shells proposed by Carrera and Brischetto [9]

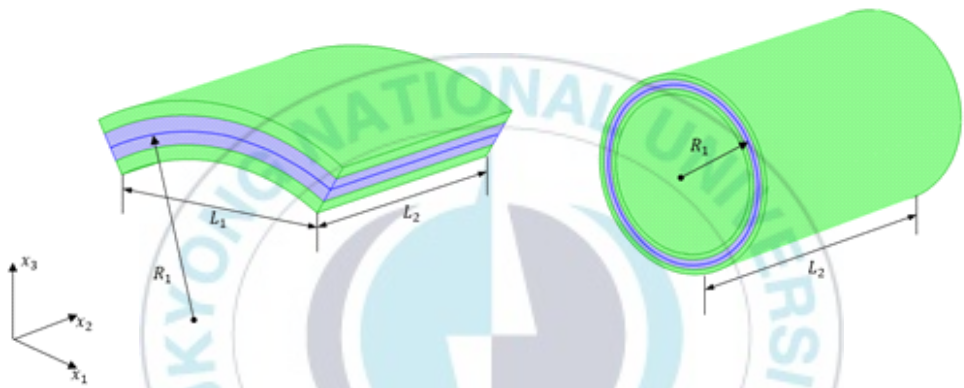

Fig. 5 Geometry of Ren(left) and Varadan and Baskar(right) shells

The first proposed problem of single curvature shells is a three-layered curved shell panel, as a Ren shell, undergoing cylindrical bending $(m=1, n=0)$. Details on the geometrical data of Ren shell are: $L_1 = \pi R_1/3$, $L_2 = 1$, $R_1 = 10$, $R_2 = \infty$. And as a second problem of single curvature shells, we investigate a three-layered composite cross-ply $(0^\circ/90^\circ/0^\circ)$ cylindrical shell which is called a Varadan-Baskar shell. Details on the geometrical data of Varadan-Baskar shell are: $L_1 = 2\pi R_1$, $L_2 = 40$, $R_1 = 10$, $R_2 = \infty$. $m=8, n=1$, pressure acts on the top surface. Both skin-layers

have equal thickness $h^t = h^b = 0.1h$ and the core layer has $h^c = 0.8h$, respectively. To assess the accuracy of the present approaches for various FCSRs and RTRs, the two problems consist of the validation problems conducted by Carrera and Brischetto [9]. To compare the present approaches with the results from the Carrera and Brischetto [5], Figs. 15-20 and Tables 7-12 show the through-the-thickness distributions of 3D displacement and stress distributions of the composite sandwich shells with three different FCSR cases. As we mentioned in the above, the case of hard skin FCSR, very hard skin FCSR and extremely hard skin FCSR will be used with different values of RTR; this range of RTRs is {4,10,100}. Moreover, for the purpose of presenting the results graphically, as another kind of non-dimensional quantities Eq. (127) is adopted.

Table 7 compares different higher-order mixed theories with 3D exact solutions for Ren shell. Maximum transverse displacement in correspondence to the middle surface are given for different values of the RTR and FCSR. From the table, the present approaches show better accuracy in thick and soft-core shell case compared ESL mixed theories and VAPAS. And LW mixed theories have relatively high accuracy compared other theories. In Table 10 maximum transverse displacement results for Varadan-Baskar shell are reported. As shown in Table 7, similar observations can be made. Moreover, from Tables 8 and 10 for maximum in-plane normal stress of Ren shell and Varadan-Baskar shell, respectively, PA(11EE) excellent agreement with the 3D exact solution for all FCSR and RTR case but ressults obtained from VAPAS are highly inaccurate as discussed in the

previous section. As mentioned in Sect. 5.3.1., maximum transverse normal stress results in Tables 9 and 12 show that PA(11EE) cannot describe accurately the distributions of transverse shear stress for high value FCSR and thick shell.

The results in Figs. 15 and 18 for the case of hard skin FCSR are similar to those in Fig. 11. Moreover, in Figs. 16 and 19 for very hard skin FCSR, PA(11EE) and PA(00EE) using integration of the equilibrium equations from the 3D elasticity theory capture boundary layer effect accurately, but PA(22CS), which takes second-order warpings into account additionally without integration of the equilibrium equations, cannot describe boundary layer effect accurately. And also VAPAS is not meaningful with those from 3D exact solutions. However, from the plots for thick shells with very hard and extremely hard skin, VAPAS results were not shown for the reason mentioned above. In particular, one can observe the strength of PA(11EE) dramatically in Figs. 17 and 20. For the case of extremely hard skin, to catch the boundary layer effect, the displacement-based theories have to expand the displacement field up to any desired degree and another theories, such as PA(22CS) and VAPAS, need to more unknown warpings. However, due to the complexity and computational cost, just adding the degree of freedom or unknown warpings should be avoided. Therefore, this difficulties can be partially supplemented by using integration of equilibrium equations as used in PA(11EE).

From all the above plate problem in this section, PA(22CS) and PA(11EE) present a great compromise between efficiency and accuracy for

predicting 3D displacement and stress components of composite sandwich plates for all cases considered for FCSR and LTR. However, in the case of extremely hard skin, PA(11EE) can capture boundary layer effect well, whereas PA(22CS) is not satisfied with transverse normal stress distributions. In addition, from the shell problems, PA(11EE) taken the order $l \sim R$ has a great tendency similar to 3D exact solutions even in the very extremely high skin and thick case, although high error rate is seen in the results of the transverse stress of the middle surface. Therefore, PA(11EE) with a stress recovery as an extra post processing step is capable of characterizing the boundary layer effect resulting from the mismatch in the material properties between constituent materials.

6. Conclusions

The construction of a universal asymptotic model is systematically implemented to estimate and predict compound mechanical behaviors of composite sandwich shells for various FCSR, LTR and RTR cases. Unlike the companion paper [1] for plates, a universal asymptotic shell model that the geometric parameter (h/R) should consider additionally has a great variety of possibilities for application of asymptotic methods. Therefore, we take the approach with $l \sim R$ (PA(11EE)) and the approach with $l \sim \sqrt{hR}$ (PA(22CS)) to compare the effect of the order of the curvature radius of the reference surface. When each layer of a sandwich structure can be modeled as an elastic shell and all constituent material constants of such shells are assumed to be of the same order, an equivalent 2D refined shell model is first derived in terms of the asymptotically correct energy functional taking account of transverse shear/normal deformation and incorporating the additional energy contributions. Unlike the previous derivation procedure from the ESL perspective, a new predominant order relative to FCSR for any LTR and RTR cases should be then taken into account during the refined derivation procedure from the LW perspective when the sandwich shell can be regarded as the assembly of three-layered structures with mismatched constituent material and geometric properties. With the help of the interlaminar displacement/transverse stress continuity conditions through the first-order approximation, the present approaches

derived the refined model for composite sandwich shells with various FCSRs, LTRs, and RTRs having an asymptotically correct energy functional in terms of the only core-layer's 2D generalized LK strain and transverse shear motion measures and their partial derivatives. At that time, the order of 2D generalized transverse motion measures can be transited into $(l/h)\hat{\varepsilon}$ due to mismatch of material properties between constituent materials in developing a universal model. Furthermore, to evaluate the accuracy and capability of the present approach (22CS) valid to the same order as the energy formulation, 3D refined recovery relations are directly established by introducing refined continuity conditions of interlaminar and transverse stresses into the 3D displacement/strain/stress fields for each layer without integrating the 3D elastic equilibrium over the thickness. In addition, in the present approaches (00EE, 11EE), 3D recovery relations are explicitly provided through conditions of interlaminar 3D displacement continuity and integrations of the 3D elastic equilibrium equations. Finally, together with critical comparisons of the present approaches versus 3D elasticity and different higher-order ESL- and LW-approaches, the capability and accuracy of the refined model introduced by the present approaches to predict the mechanical behavior of composite sandwich shells with various FCSRs, LTRs and RTRs has been illustrated using several examples available in the literature.

Table 1. Comparison of $\overline{U}_3(L/2, L/2, 0)$ from different plate theories

LTR	2	4	10
3D Exact	22.074	7.5845	2.1972
PA(11EE)	22.48 (1.85)	7.6711 (1.14)	2.2144 (0.78)
PA(22CS)	22.482 (1.85)	7.6711 (1.14)	2.2144 (0.78)
PA(00EE)	19.199 (13.02)	7.2128 (4.90)	2.1666 (1.39)
ED3	21.960 (0.52)	7.3560 (3.01)	2.1132 (3.82)
EDZ3	23.305 (5.58)	7.8710 (3.78)	2.2338 (1.67)
LD2	22.071 (0.01)	7.5931 (0.11)	2.2001 (0.13)
LD3	22.103 (0.13)	7.5948 (0.14)	2.2001 (0.13)
VAPAS	29.825 (35.11)	8.6399 (13.92)	2.2453 (2.19)

Table 2. Comparison of $\overline{\sigma}_{11}(L/2, L/2, h/2)$ from different plate theories

LTR	2	4	10
3D Exact	3.2812	1.5538	1.1511
PA(11EE)	3.6117 (10.07)	1.5837 (1.92)	1.1531 (0.17)
PA(22CS)	3.3906 (3.33)	1.6628 (7.02)	1.1745 (2.03)
PA(00EE)	2.7536 (16.08)	1.5114 (2.73)	1.1504 (0.06)
ED3	3.0752 (6.28)	NA	1.1452 (0.51)
EDZ3	3.1623 (3.62)	NA	1.1484 (0.23)
LD2	3.2259 (1.69)	NA	1.1322 (1.64)
LD3	3.2426 (1.18)	NA	1.1324 (1.62)
VAPAS	2.5066 (23.61)	1.6983 (9.30)	1.1781 (2.35)

Table 3. Comparison of $\overline{\sigma}_{13}(0, L/2, 0)$ from different plate theories

LTR	2	4	10
3D Exact	0.1845	0.2384	0.2995
PA(11EE)	0.2498 (35.39)	0.2617 (9.77)	0.3041 (1.54)
PA(22CS)	0.1878 (1.76)	0.2388 (0.16)	0.2993 (0.06)
PA(00EE)	0.1992 (7.95)	0.2422 (1.59)	0.3003 (0.25)
ED3	NA	NA	NA
EDZ3	0.1830 (0.82)	0.2375 (0.36)	0.2991 (0.15)
LD2	0.1783 (3.35)	0.2278 (4.44)	0.2802 (6.45)
LD3	0.1785 (3.25)	0.2278 (4.44)	0.2802 (6.45)
VAPAS	0.2642 (43.17)	0.2746 (15.19)	0.3064 (2.29)

Table 4. Comparison of $\overline{U}_3(L/2, L/2, 0)$ from different plate theories

LTR	2	4	10
	$FCSR_L = 7.3 \times 10^4$ and $FCSR_z = 9.624$		
3D Exact	45.6527	15.4839	7.0362
PA(11EE)	46.5644 (2.00)	15.59 (0.69)	7.0501 (0.20)
PA(22CS)	46.5644 (2.00)	15.59 (0.69)	7.0501 (0.20)
PA(00EE)	36.4298 (20.20)	14.4284 (6.82)	6.9350 (1.44)
ED3	NA	NA	NA
EDZ3	NA	NA	NA
LD2	45.6580 (0.01)	15.4824 (0.01)	7.0357 (0.01)
LD3	NA	NA	NA
VAPAS	45.6515 (0.00)	15.2521 (1.50)	6.9878 (0.69)
	$FCSR_L = 7.3 \times 10^6$ and $FCSR_z = 9.624 \times 10^2$		
3D Exact	1089.98	590.547	149.696
PA(11EE)	1090.06 (0.01)	590.516 (0.01)	149.695 (0.00)
PA(22CS)	1090.06 (0.01)	590.516 (0.01)	149.695 (0.00)
PA(00EE)	971.351 (10.88)	566.633 (4.05)	148.38 (0.88)
ED3	NA	100.85 (82.92)	22.059 (85.26)
EDZ3	NA	507.40 (14.08)	144.20 (3.67)
LD2	1089.20 (0.07)	590.45 (0.02)	149.70 (0.00)
LD3	NA	590.54 (0.00)	149.70 (0.00)
VAPAS	3962.61 (263.46)	971.591 (64.52)	159.08 (6.27)
	$FCSR_L = 7.3 \times 10^8$ and $FCSR_z = 9.624 \times 10^4$		
3D Exact	1469.77	1370.66	1260.32
PA(11EE)	1466.48 (0.22)	1370.47 (0.01)	1260.3 (0.00)
PA(22CS)	1466.48 (0.22)	1370.47 (0.01)	1260.3 (0.00)
PA(00EE)	1359.12 (7.53)	1343.6 (1.97)	1255.8 (0.35)
ED3	NA	111.42 (91.87)	24.045 (98.09)
EDZ3	NA	996.59 (27.29)	944.52 (25.06)
LD2	NA	1370.1 (0.04)	1260.2 (0.01)
LD3	NA	1370.6 (0.00)	1260.3 (0.00)
VAPAS	395540 (26811)	96589.7 (6947)	15352.8 (1118)

Table 5. Comparison of $\bar{\sigma}_{11}(L/2, L/2, h/2)$ from different plate theories

LTR	2	4	10
	$FCSR_L = 7.3 \times 10^4$ and $FCSR_z = 9.624$		
3D Exact	2.6161	7.7334	41.888
PA(11EE)	2.6628 (1.79)	7.7881 (0.71)	41.943 (0.13)
PA(22CS)	2.7199 (3.97)	7.8643 (1.69)	42.026 (0.33)
PA(00EE)	2.2747 (13.05)	7.2498 (6.25)	41.367 (1.24)
VAPAS	1.5986 (38.89)	7.4419 (3.77)	41.796 (0.22)
	$FCSR_L = 7.3 \times 10^6$ and $FCSR_z = 9.624 \times 10^2$		
3D Exact	-6.3489	67.955	144.538
PA(11EE)	-10.851 (70.91)	67.9765 (0.03)	144.592 (0.04)
PA(22CS)	-9.0864 (43.12)	67.8398 (0.17)	144.604 (0.05)
PA(00EE)	29.3525 (562.32)	71.1029 (4.63)	144.253 (0.20)
VAPAS	-67.5344 (963.71)	33.4484 (50.78)	95.367 (34.02)
	$FCSR_L = 7.3 \times 10^8$ and $FCSR_z = 9.624 \times 10^4$		
3D Exact	82.5078	408.17	859.639
PA(11EE)	80.5114 (2.42)	402.14 (1.48)	859.557 (0.01)
PA(22CS)	77.8032 (5.70)	398.24 (2.43)	859.208 (0.05)
PA(00EE)	40.5716 (50.83)	160.74 (60.62)	941.799 (9.56)
VAPAS	-6987.02 (8568.31)	2614.13 (540.45)	5336.1 (520.74)

Table 6. Comparison of $\bar{\sigma}_{13}(0, L/2, 0)$ from different plate theories

LTR	2	4	10
$FCSR_L = 7.3 \times 10^4$ and $FCSR_z = 9.624$			
3D Exact	0.3449	0.7102	1.7919
PA(11EE)	0.3541 (2.67)	0.7173 (1.00)	1.7950 (0.17)
PA(22CS)	0.3499 (1.45)	0.7120 (0.26)	1.7925 (0.03)
PA(00EE)	0.3895 (12.94)	0.7358 (3.61)	1.8026 (0.59)
ED3	NA	NA	NA
EDZ3	NA	NA	NA
LD2	NA	NA	NA
LD3	NA	NA	NA
VAPAS	0.3963 (14.91)	0.7367 (3.74)	1.8026 (0.60)
$FCSR_L = 7.3 \times 10^6$ and $FCSR_z = 9.624 \times 10^2$			
3D Exact	0.0913	0.4053	1.5740
PA(11EE)	0.0640 (29.90)	0.4006 (1.16)	1.5758 (0.11)
PA(22CS)	0.0911 (0.22)	0.4052 (0.02)	1.5738 (0.01)
PA(00EE)	0.1140 (24.87)	0.4273 (5.42)	1.5849 (0.70)
ED3	NA	0.6393 (57.74)	NA
EDZ3	NA	0.3499 (13.67)	NA
LD2	NA	0.4052 (0.02)	NA
LD3	NA	0.4053 (0.00)	NA
VAPAS	0.3887 (325.79)	0.7228 (78.34)	1.7688 (12.38)
$FCSR_L = 7.3 \times 10^8$ and $FCSR_z = 9.624 \times 10^4$			
3D Exact	0.0012	0.0095	0.1370
PA(11EE)	-0.0379 (3176.9)	-0.0103 (208.42)	0.1298 (5.26)
PA(22CS)	0.0012 (0.00)	0.0095 (0.00)	0.1370 (0.00)
PA(00EE)	0.0016 (29.55)	0.010 (7.37)	0.1387 (1.24)
ED3	NA	0.6328 (6561.05)	NA
EDZ3	NA	0.0069 (27.37)	NA
LD2	NA	0.0094 (1.05)	NA
LD3	NA	0.0094 (1.05)	NA
VAPAS	0.3887 (31434.7)	0.7227 (7507.37)	1.7684 (1190.8)

Table 7. Ren shell. Comparison of $\overline{U}_3(L_1/2, L_2/2, 0)$ from different shell theories

RTR	4	10	100
$FCSR_L = 7.3\times10^4$ and $FCSR_z = 9.624$			
3D Exact	6.8695	4.0202	3.4193
PA(11EE)	6.1837 (9.98)	3.8412 (4.45)	3.4025 (0.49)
PA(22CS)	6.2386 (9.18)	3.8482 (4.28)	3.4026 (0.49)
PA(00EE)	6.2183 (9.48)	3.8515 (4.20)	3.4026 (0.49)
EMC4	NA	NA	NA
EMZC3	NA	NA	NA
LM1	NA	NA	NA
LM2	NA	NA	NA
VAPAS	6.1458 (10.53)	3.4056 (15.29)	3.4025 (0.49)
$FCSR_L = 7.3\times10^6$ and $FCSR_z = 9.624\times10^2$			
3D Exact	234.88	47.587	3.8563
PA(11EE)	210.73 (10.28)	45.367 (4.67)	3.8372 (0.50)
PA(22CS)	213.60 (9.06)	45.388 (4.62)	3.8373 (0.49)
PA(00EE)	212.01 (9.74)	45.802 (3.75)	3.8448 (0.30)
EMC4	NA	9.2064 (80.65)	3.4718 (9.97)
EMZC3	NA	46.873 (1.50)	3.8577 (0.04)
LM1	233.41 (0.63)	NA	3.8562 (0.00)
LM2	234.88 (0.00)	NA	3.8562 (0.00)
VAPAS	270.19 (15.03)	45.977 (3.38)	3.8236 (0.86)
$FCSR_L = 7.3\times10^8$ and $FCSR_z = 9.624\times10^4$			
3D Exact	447.93	730.81	45.340
PA(11EE)	535.08 (19.46)	698.34 (4.44)	45.117 (0.49)
PA(22CS)	763.31 (70.41)	703.82 (3.69)	45.117 (0.49)
PA(00EE)	805.44 (79.81)	703.82 (4.17)	45.796 (1.01)
EMC4	NA	9.9477 (98.64)	3.4773 (92.33)
EMZC3	NA	557.33 (23.74)	44.644 (1.54)
LM1	530.79 (18.50)	NA	45.342 (0.00)
LM2	447.93 (0.00)	NA	45.342 (0.00)
VAPAS	26674 (5854.95)	4259.9 (482.90)	45.943 (1.33)

Table 8. Ren shell. Comparison of $\bar{\sigma}_{11}(L_1/2, L_2/2, h/2)$ from different shell theories

RTR	4	10	100
$FCSR_L = 7.3\times10^4$ and $FCSR_z = 9.624$			
3D Exact	1.6197	1.5516	1.5371
PA(11EE)	1.5753 (2.74)	1.5350 (1.07)	1.5352 (0.12)
PA(22CS)	1.2545 (22.55)	1.3987 (9.85)	1.5210 (1.05)
PA(00EE)	1.5085 (6.87)	1.4952 (3.63)	1.5309 (0.40)
VAPAS	1.0146 (37.36)	1.3701 (11.70)	1.5195 (1.15)
$FCSR_L = 7.3\times10^6$ and $FCSR_z = 9.624\times10^2$			
3D Exact	9.3821	3.2816	1.5560
PA(11EE)	8.2054 (12.54)	3.1742 (3.27)	1.5539 (0.13)
PA(22CS)	7.0058 (25.33)	2.9673 (9.58)	1.5397 (1.05)
PA(00EE)	10.468 (11.57)	3.2119 (2.12)	1.5501 (0.38)
VAPAS	-14.810 (257.85)	0.98742 (69.91)	1.5279 (1.81)
$FCSR_L = 7.3\times10^8$ and $FCSR_z = 9.624\times10^4$			
3D Exact	-23.147	29.986	3.3463
PA(11EE)	-22.665 (2.08)	28.519 (4.89)	3.3357 (0.32)
PA(22CS)	221.31 (1056.11)	26.959 (10.09)	3.3146 (0.95)
PA(00EE)	36.310 (256.87)	31.829 (6.15)	3.3772 (0.92)
VAPAS	-1597.3 (6800.68)	-37.274 (224.30)	2.3612 (29.44)

Table 9. Ren shell. Comparison of $\bar{\sigma}_{13}(0, L_2/2, 0)$ from different shell theories

RTR	4	10	100
$FCSR_L = 7.3\times10^4$ and $FCSR_z = 9.624$			
3D Exact	0.4593	0.4346	0.4170
PA(11EE)	0.4011 (12.67)	0.4129 (4.99)	0.4149 (0.50)
PA(22CS)	0.4136 (9.95)	0.4147 (4.58)	0.4150 (0.48)
PA(00EE)	0.3981 (13.32)	0.4122 (5.15)	0.4149 (0.50)
EMC4	NA	NA	NA
EMZC3	NA	NA	NA
LM1	NA	NA	NA
LM2	NA	NA	NA
VAPAS	0.4193 (8.71)	0.4157 (4.35)	0.4150 (0.48)
$FCSR_L = 7.3\times10^6$ and $FCSR_z = 9.624\times10^2$			
3D Exact	0.3380	0.4125	0.4168
PA(11EE)	0.2892 (14.44)	0.3917 (5.04)	0.4147 (0.50)
PA(22CS)	0.3102 (8.22)	0.3939 (4.51)	0.4147 (0.50)
PA(00EE)	0.2986 (11.66)	0.3913 (5.14)	0.4147 (0.50)
EMC4	NA	0.0679 (83.54)	0.0654 (84.31)
EMZC3	NA	0.4069 (1.36)	0.4169 (0.02)
LM1	NA	0.4131 (0.15)	0.4168 (0.00)
LM2	NA	0.4130 (0.12)	0.4168 (0.00)
VAPAS	0.4193 (24.05)	0.4157 (0.78)	0.4150 (0.43)
$FCSR_L = 7.3\times10^8$ and $FCSR_z = 9.624\times10^4$			
3D Exact	-0.0104	0.0655	0.3959
PA(11EE)	-0.1202 (1055.77)	0.0584 (10.84)	0.3940 (0.48)
PA(22CS)	0.0437 (520.19)	0.0634 (3.21)	0.3940 (0.48)
PA(00EE)	0.0115 (210.58)	0.0643 (1.83)	0.3936 (0.58)
EMC4	NA	7.7E-4 (98.82)	7.5E-4 (99.81)
EMZC3	NA	0.0464 (29.19)	0.2236 (43.52)
LM1	NA	0.0655 (0.00)	0.3960 (0.03)
LM2	NA	0.0655 (0.00)	0.3960 (0.03)
VAPAS	0.4193 (4131.73)	0.4157 (534.66)	0.4150 (4.82)

Table 10. Varadan-Baskar shell. Comparison of $\overline{U}_3(L_1/2, L_2/2, 0)$ from different shell theories

RTR	4	10	100
$FCSR_L = 7.3\times10^4$ and $FCSR_z = 9.624$			
3D Exact	2.5060	1.1557	0.7167
PA(11EE)	2.2515 (10.16)	1.1045 (4.43)	0.7132 (0.49)
PA(22CS)	2.2756 (9.19)	1.1081 (4.12)	0.7140 (0.38)
PA(00EE)	2.2321 (10.93)	1.1060 (4.30)	0.7140 (0.38)
VAPAS	2.2230 (11.29)	1.1005 (4.78)	0.7135 (0.45)
$FCSR_L = 7.3\times10^6$ and $FCSR_z = 9.624\times10^2$			
3D Exact	90.171	20.465	0.8539
PA(11EE)	81.178 (9.97)	19.513 (4.65)	0.8497 (0.49)
PA(22CS)	83.159 (7.78)	19.549 (4.48)	0.8506 (0.39)
PA(00EE)	81.184 (9.97)	19.539 (4.52)	0.8516 (0.27)
VAPAS	123.95 (37.46)	20.397 (0.33)	0.8451 (1.03)
$FCSR_L = 7.3\times10^8$ and $FCSR_z = 9.624\times10^4$			
3D Exact	378.97	134.26	3.0995
PA(11EE)	299.87 (20.87)	128.36 (4.39)	3.0842 (0.49)
PA(22CS)	197.51 (47.88)	129.59 (3.48)	3.0848 (0.47)
PA(00EE)	197.51 (48.17)	128.33 (4.42)	3.0865 (0.42)
VAPAS	1995.8 (426.64)	310.45 (131.23)	3.1064 (0.22)

Table 11. Varadan-Baskar shell. Comparison of $\bar{\sigma}_{11}(L_1/2, L_2/2, h/2)$ from different shell theories

RTR	4	10	100
$FCSR_L = 7.3\times10^4$ and $FCSR_z = 9.624$			
3D Exact	0.8476	0.7787	0.6218
PA(11EE)	0.8158 (3.75)	0.7702 (1.09)	0.6211 (0.11)
PA(22CS)	0.6620 (21.9)	0.7042 (9.57)	0.6161 (0.92)
PA(00EE)	0.7946 (6.25)	0.7504 (3.63)	0.6196 (0.35)
VAPAS	0.4542 (46.41)	0.6848 (12.06)	0.6152 (1.06)
$FCSR_L = 7.3\times10^6$ and $FCSR_z = 9.624\times10^2$			
3D Exact	6.3199	2.2280	0.6141
PA(11EE)	5.4643 (13.54)	2.1430 (3.82)	0.6133 (0.13)
PA(22CS)	4.6327 (26.70)	2.0226 (9.22)	0.6085 (0.91)
PA(00EE)	7.3512 (16.32)	2.2705 (1.91)	0.6118 (0.37)
VAPAS	-10.890 (272.31)	0.5653 (76.63)	0.6022 (1.94)
$FCSR_L = 7.3\times10^8$ and $FCSR_z = 9.624\times10^4$			
3D Exact	61.990	9.8685	0.4016
PA(11EE)	58.931 (4.93)	9.3234 (5.52)	0.4001 (0.37)
PA(22CS)	35.971 (41.97)	8.3698 (15.19)	0.3990 (0.65)
PA(00EE)	16.919 (72.71)	11.230 (13.80)	0.4014 (0.05)
VAPAS	5013.5 (7987.59)	340.13 (3346.62)	0.6186 (54.03)

Table 12. Varadan-Baskar shell. Comparison of $\bar{\sigma}_{13}(0, L_2/2, 0)$ from different shell theories

RTR	4	10	100
$FCSR_L = 7.3 \times 10^4$ and $FCSR_z = 9.624$			
3D Exact	0.3130	0.2961	0.2277
PA(11EE)	0.2735 (12.62)	0.2815 (4.93)	0.2266 (0.48)
PA(22CS)	0.2821 (9.87)	0.2828 (4.49)	0.2267 (0.44)
PA(00EE)	0.2712 (13.35)	0.2810 (5.10)	0.2267 (0.44)
VAPAS	0.2896 (7.48)	0.2838 (4.15)	0.2265 (0.53)
$FCSR_L = 7.3 \times 10^6$ and $FCSR_z = 9.624 \times 10^2$			
3D Exact	0.1803	0.2556	0.2182
PA(11EE)	0.1524 (15.47)	0.2435 (4.73)	0.2171 (0.50)
PA(22CS)	0.1676 (7.04)	0.2443 (4.42)	0.2172 (0.46)
PA(00EE)	0.1626 (9.82)	0.2428 (5.01)	0.2171 (0.50)
VAPAS	0.2743 (52.14)	0.2688 (5.16)	0.2177 (0.23)
$FCSR_L = 7.3 \times 10^8$ and $FCSR_z = 9.624 \times 10^4$			
3D Exact	0.0134	0.0153	0.0389
PA(11EE)	0.1228 (816.42)	0.0167 (9.15)	0.0388 (0.26)
PA(22CS)	0.0062 (53.73)	0.0148 (3.27)	0.0387 (0.51)
PA(00EE)	0.0039 (70.90)	0.0148 (8.50)	0.0386 (0.77)
VAPAS	0.0481 (258.96)	0.0432 (182.35)	0.0408 (4.88)

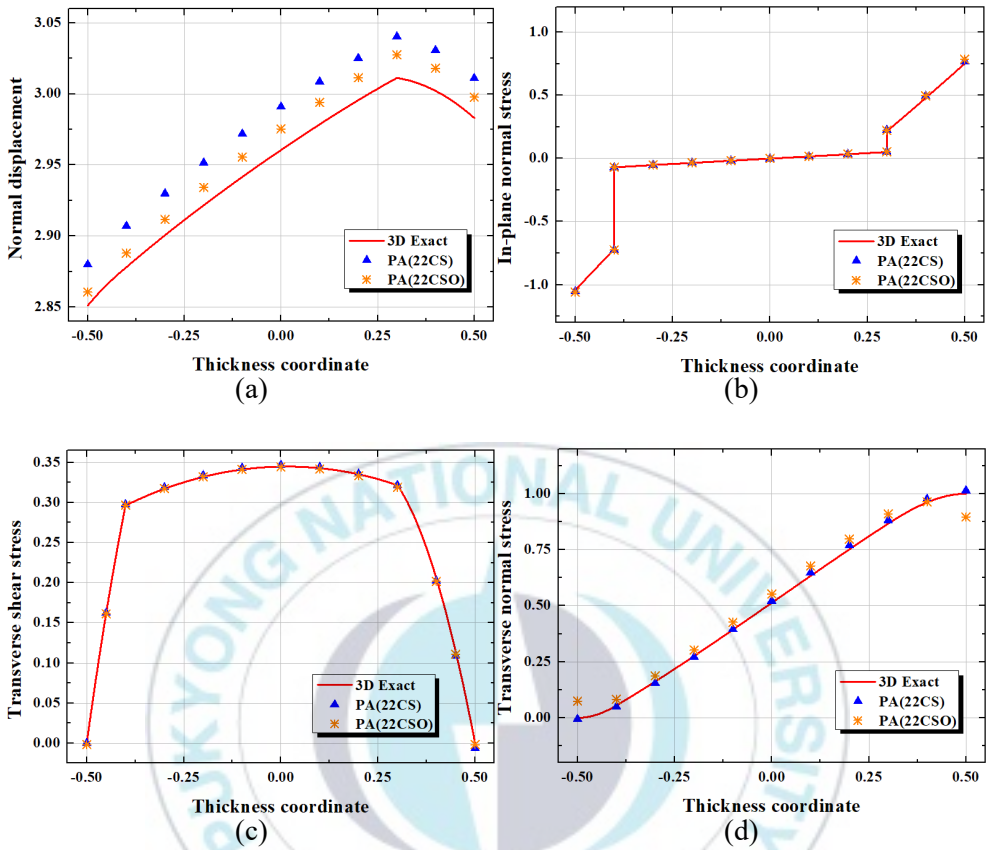

Fig. 6 Distribution of ($\overline{U}_3$(a), $\overline{\sigma}_{11}$(b), $\overline{\sigma}_{13}$(c), $\overline{\sigma}_{33}$(d)) vs. the through-thickness coordinate for FCSR=10^1

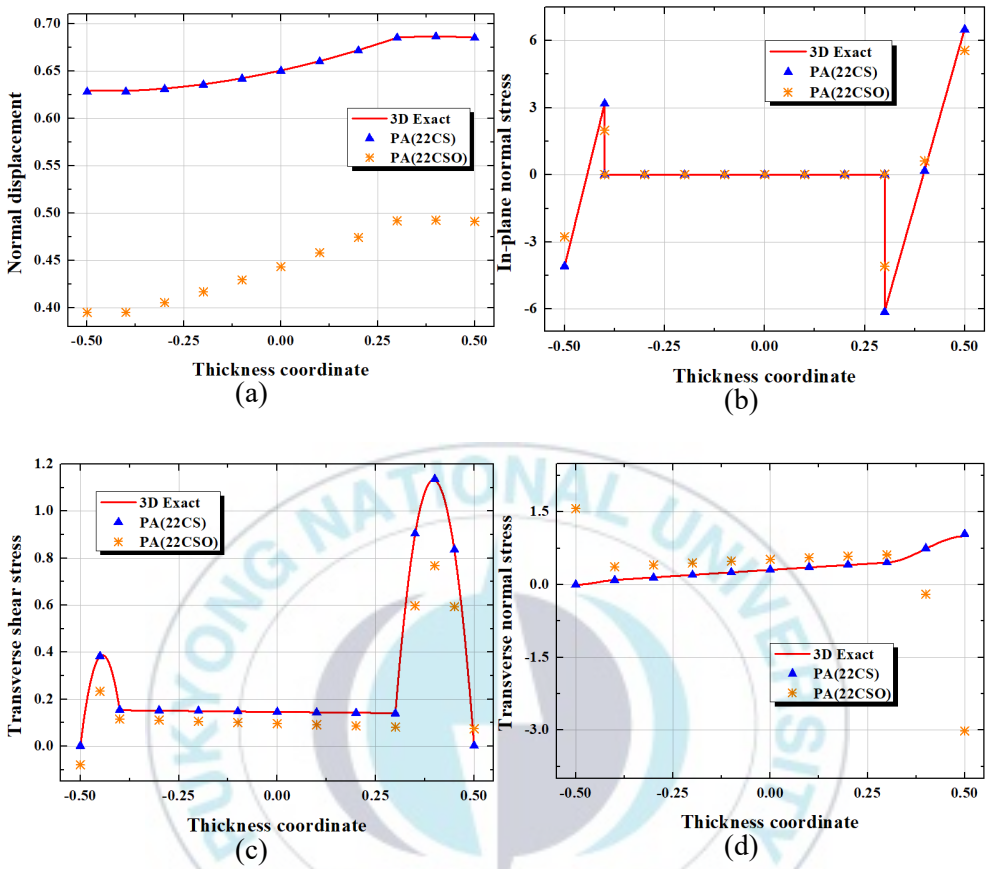

Fig. 7 Distribution of ($\overline{U}_3$(a), $\overline{\sigma}_{11}$(b), $\overline{\sigma}_{13}$(c), $\overline{\sigma}_{33}$(d)) vs. the through-thickness coordinate for FCSR=10^3

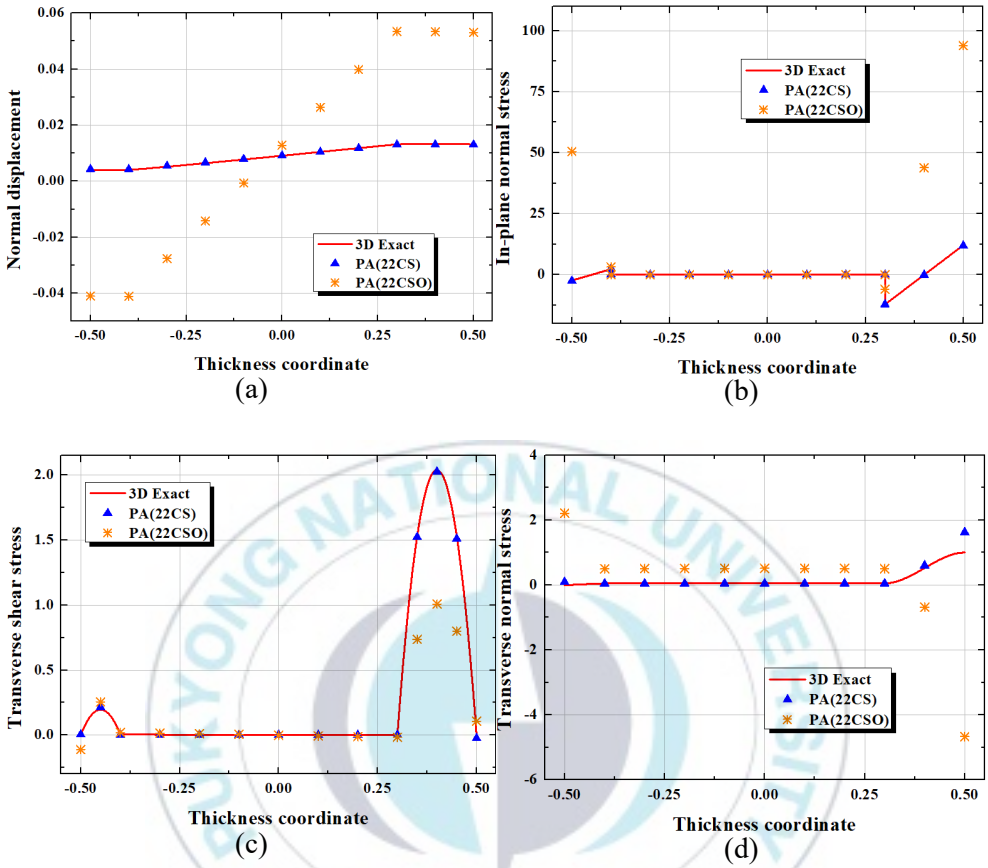

Fig. 8 Distribution of ($\overline{U}_3$(a), $\overline{\sigma}_{11}$(b), $\overline{\sigma}_{13}$(c), $\overline{\sigma}_{33}$(d)) vs. the through-thickness coordinate for FCSR=10^5

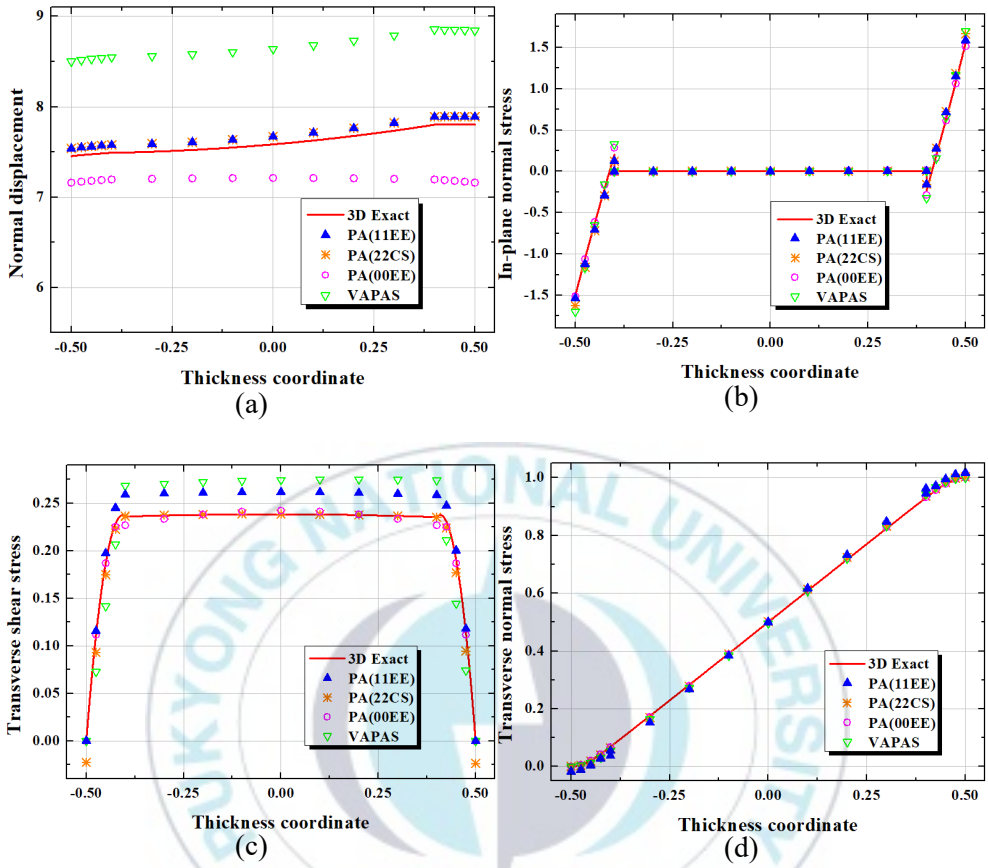

Fig. 9 Distribution of ($\overline{U}_3$(a), $\overline{\sigma}_{11}$(b), $\overline{\sigma}_{13}$(c), $\overline{\sigma}_{33}$(d)) vs. the through-thickness coordinate

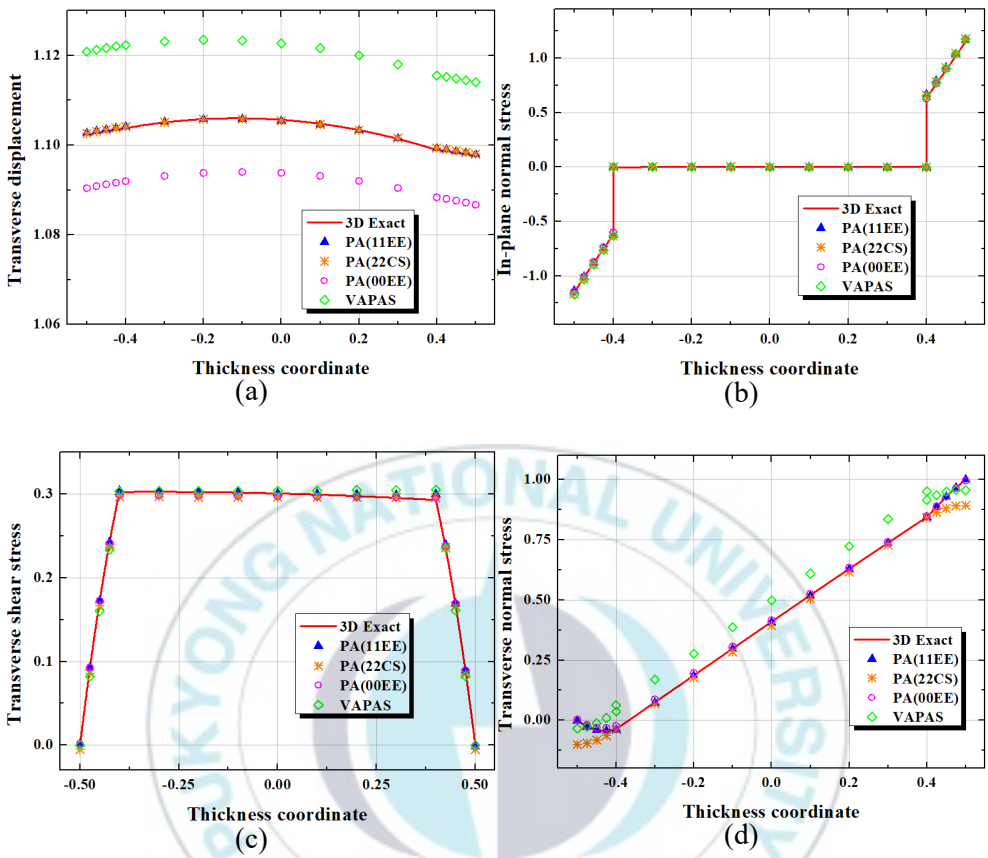

Fig. 10 Distribution of ($\overline{U}_3$(a), $\overline{\sigma}_{11}$(b), $\overline{\sigma}_{13}$(c), $\overline{\sigma}_{33}$(d)) vs. the through-thickness coordinate for $R/L=10$

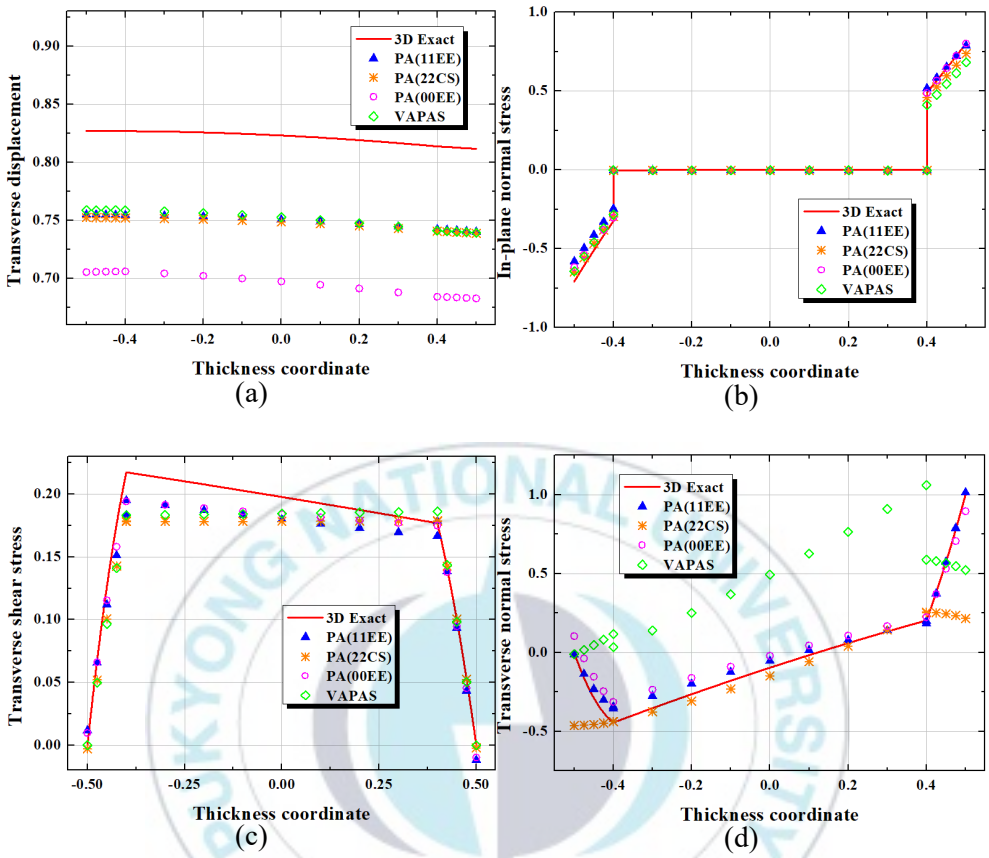

Fig. 11 Distribution of ($\overline{U}_3$(a), $\overline{\sigma}_{11}$(b), $\overline{\sigma}_{13}$(c), $\overline{\sigma}_{33}$(d)) vs. the through-thickness coordinate for $R/L=1$

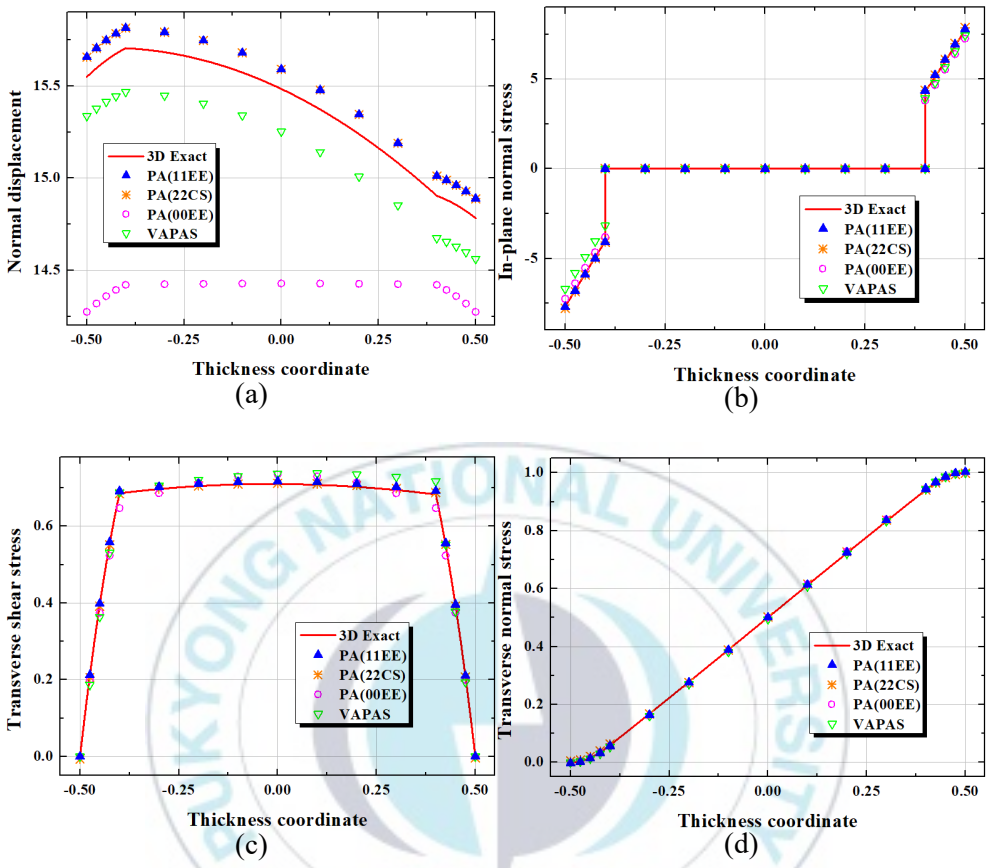

Fig. 12 Distribution of ($\overline{U}_3$(a), $\overline{\sigma}_{11}$(b), $\overline{\sigma}_{13}$(c), $\overline{\sigma}_{33}$(d)) vs. the through-thickness coordinate for $FCSR_L=7.3\times10^4$ and $FCSR_z=9.624$

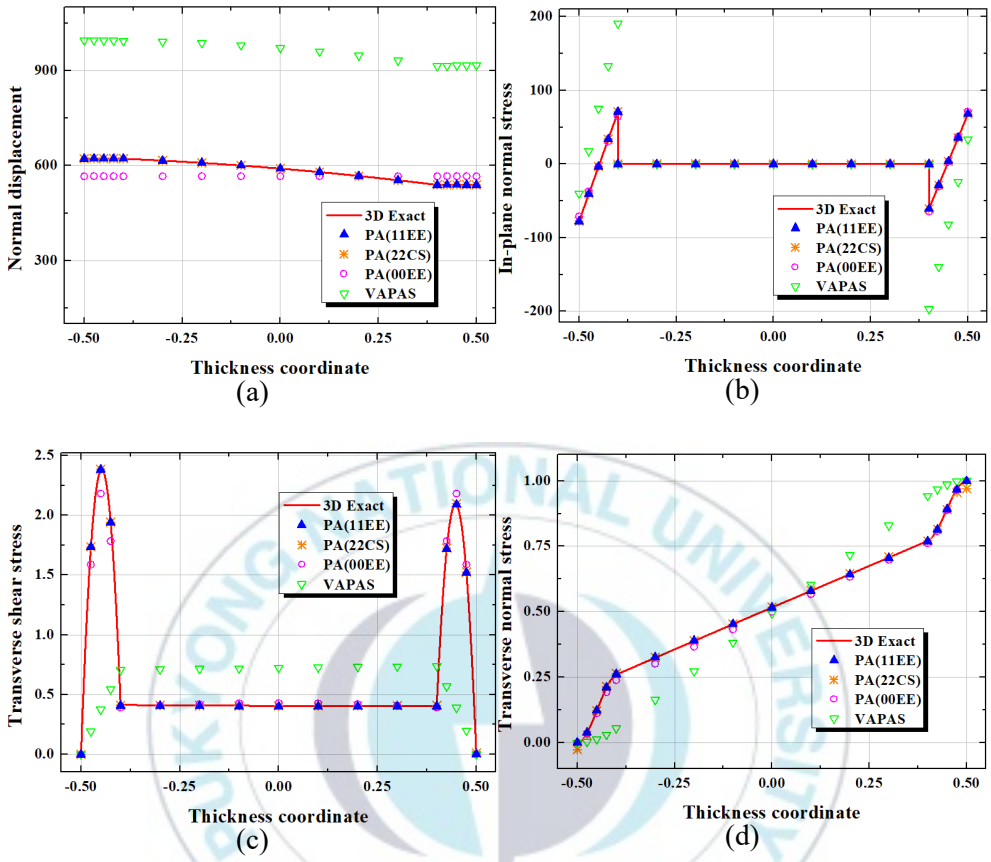

Fig. 13 Distribution of ($\overline{U}_3$(a), $\overline{\sigma}_{11}$(b), $\overline{\sigma}_{13}$(c), $\overline{\sigma}_{33}$(d)) vs. the through-thickness coordinate for $FCSR_L=7.3\times10^6$ and $FCSR_z=9.624\times10^2$

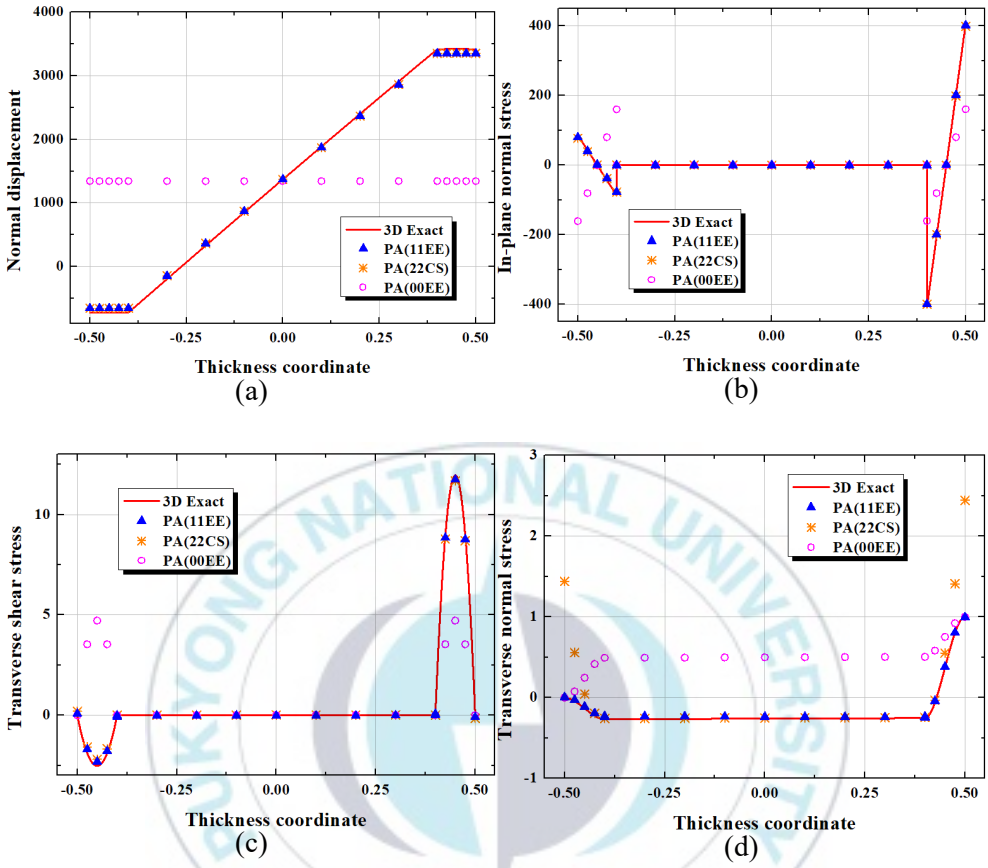

Fig. 14 Distribution of ($\overline{U}_3$(a), $\overline{\sigma}_{11}$(b), $\overline{\sigma}_{13}$(c), $\overline{\sigma}_{33}$(d)) vs. the through-thickness coordinate for $FCSR_L=7.3\times10^8$ and $FCSR_z=9.624\times10^4$

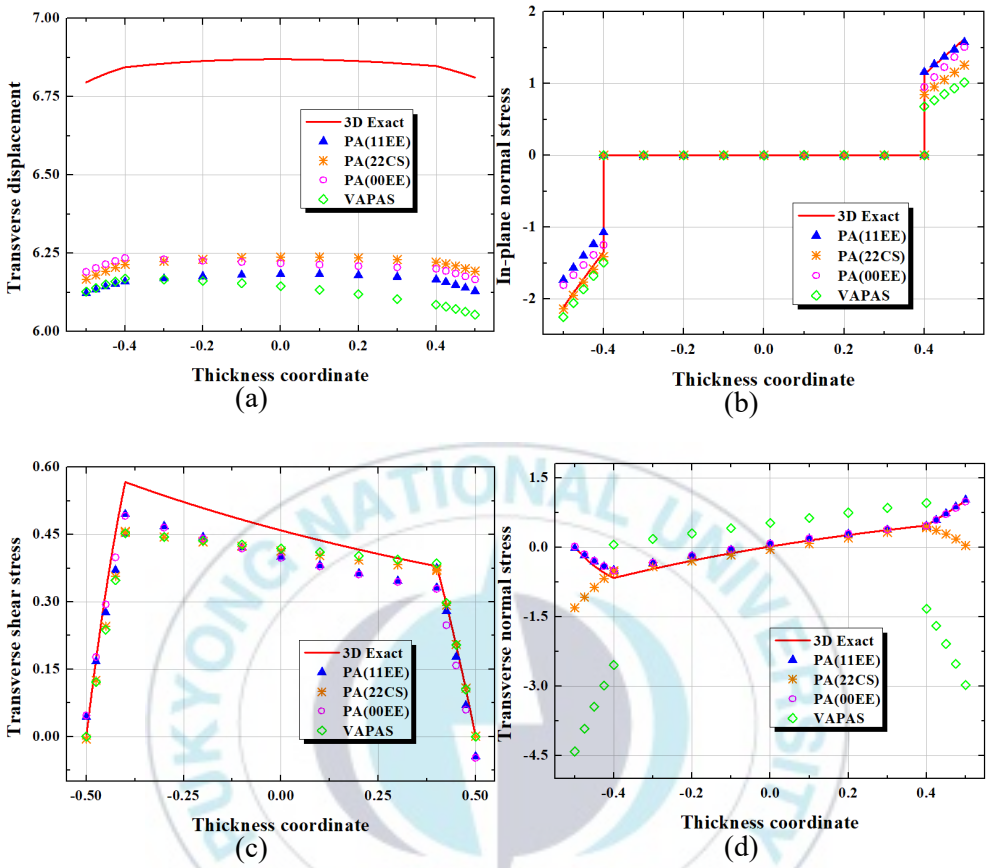

Fig. 15 Ren shell. Distribution of ($\overline{U}_3$(a), $\overline{\sigma}_{11}$(b), $\overline{\sigma}_{13}$(c), $\overline{\sigma}_{33}$(d)) vs. the through-thickness coordinate for $FCSR_L=7.3\times10^4$ and $FCSR_z=9.624$

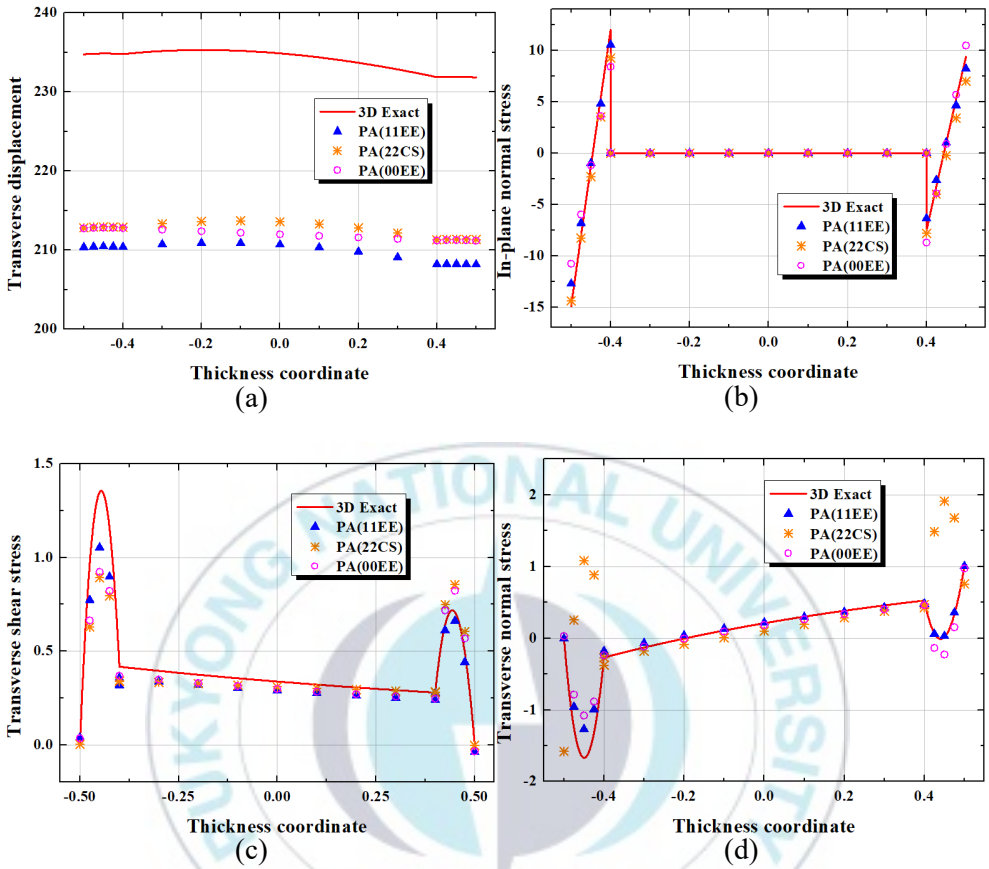

Fig. 16 Ren shell. Distribution of ($\overline{U}_3$(a), $\overline{\sigma}_{11}$(b), $\overline{\sigma}_{13}$(c), $\overline{\sigma}_{33}$(d)) vs. the through-thickness coordinate for $FCSR_L=7.3\times10^6$ and $FCSR_z=9.624\times10^2$

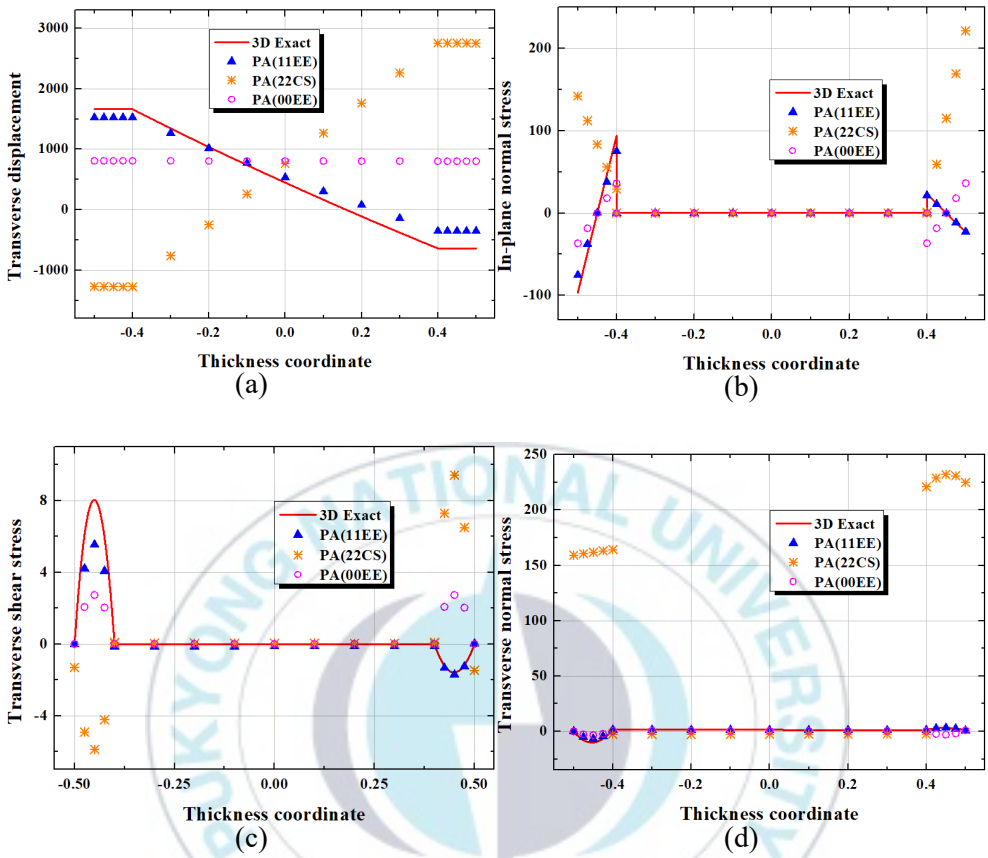

Fig. 17 Ren shell. Distribution of ($\overline{U}_3$(a), $\overline{\sigma}_{11}$(b), $\overline{\sigma}_{13}$(c), $\overline{\sigma}_{33}$(d)) vs. the through-thickness coordinate for $FCSR_L=7.3\times10^8$ and $FCSR_z=9.624\times10^4$

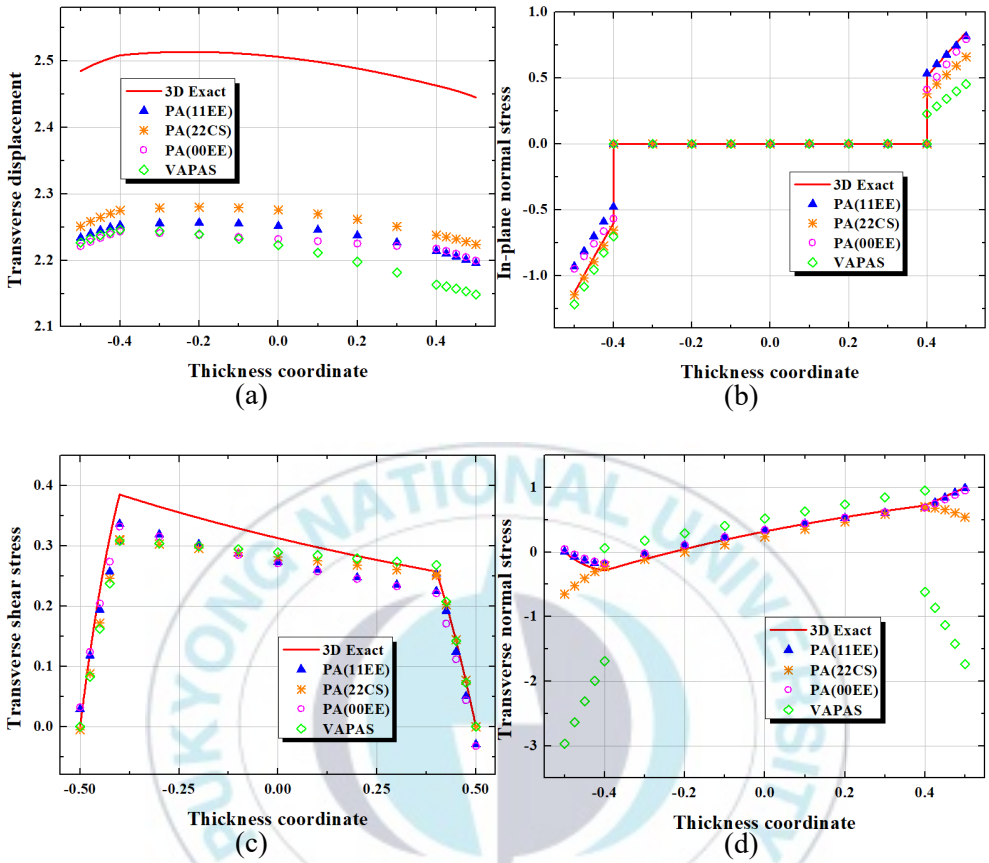

Fig. 18 Varadan-Baskar shell. Distribution of ($\overline{U}_3$(a), $\overline{\sigma}_{11}$(b), $\overline{\sigma}_{13}$(c), $\overline{\sigma}_{33}$(d)) vs. the through-thickness coordinate for $FCSR_L=7.3\times10^4$ and $FCSR_z=9.624$

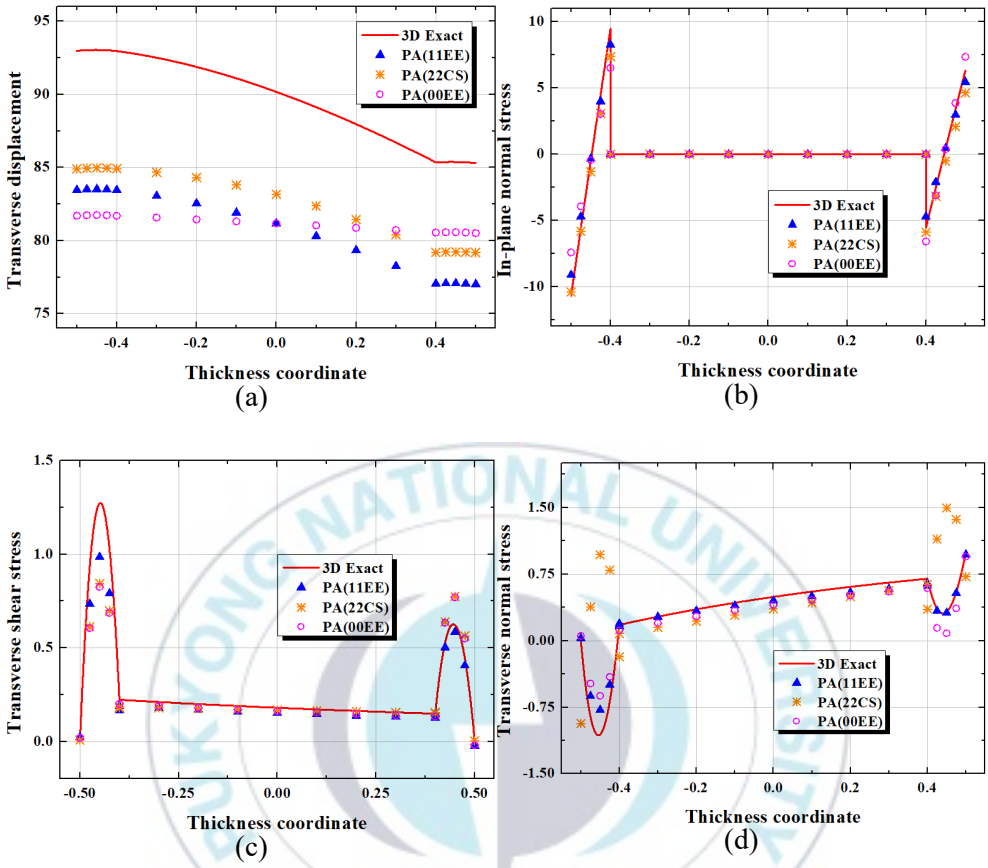

Fig. 19 Varadan-Baskar shell. Distribution of ($\overline{U}_3$(a), $\overline{\sigma}_{11}$(b), $\overline{\sigma}_{13}$(c), $\overline{\sigma}_{33}$(d)) vs. the through-thickness coordinate for $FCSR_L=7.3\times10^6$ and $FCSR_z=9.624\times10^2$

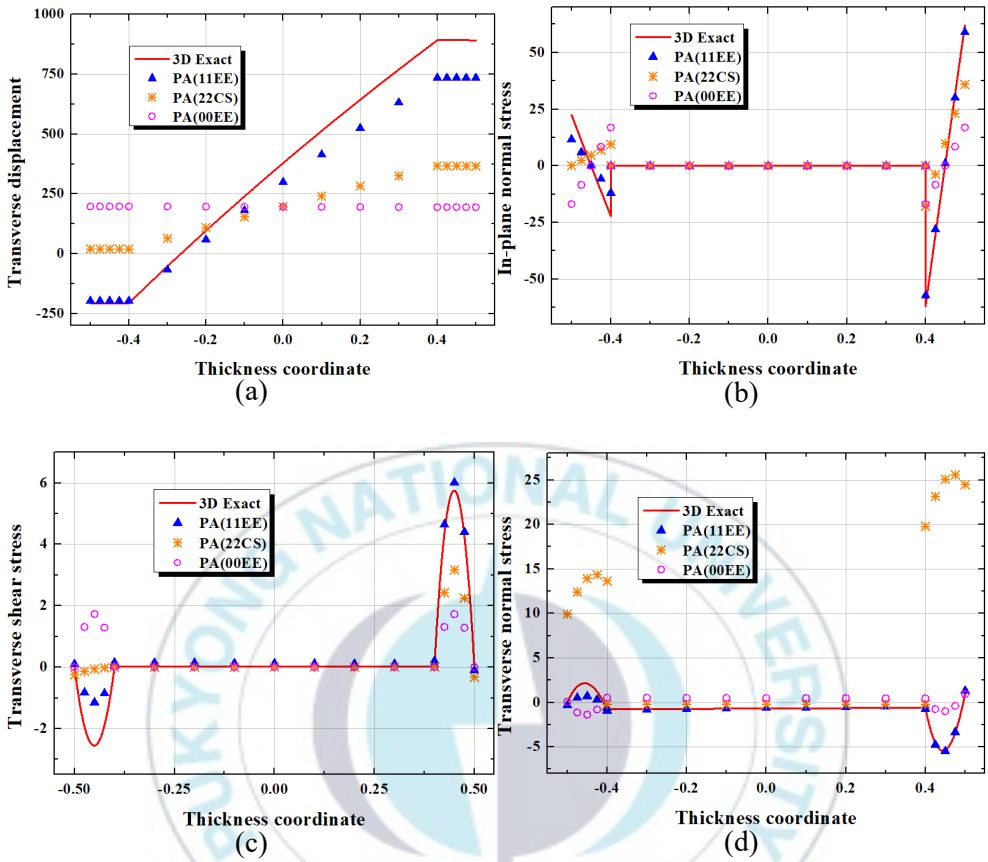

Fig. 20 Varadan-Baskar shell. Distribution of ($\overline{U}_3$(a), $\overline{\sigma}_{11}$(b), $\overline{\sigma}_{13}$(c), $\overline{\sigma}_{33}$(d)) vs. the through-thickness coordinate for $FCSR_L=7.3\times10^8$ and $FCSR_z=9.624\times10^4$

REFERENCES

[1] Sayyad, S., Ghugal, Y. M., "Bending, buckling and free vibration of laminated composite and sandwich beams: A critical review of literature," *Composite structures*, Vol. 171, 2017, pp. 486-504.

[2] Birman, V., Kardomateas, G. A., "Review of current trends in research and applications of sandwich structures," *Composite Part B: Engineering*, Vol. 142, 2018, pp. 221-240.

[3] Pagano, N. J., "Influence of shear coupling in cylindrical bending of anisotropic laminates," *Journal of composite materials*, Vol. 4, 1970, pp. 330-343.

[4] Pagano, N. J., "Exact solutions for rectangular bidirectional composites and sandwich plates," *Journal of composite materials*, Vol. 4, 1970, pp. 20-34.

[5] Brischetto, S., "Exact three-dimensional static analysis of single- and multi-layered plates and shells," *Composite Part B: Engineering*, Vol. 119, 2017, pp. 230-252.

[6] Carrera, E., Demasi, L., "Two benchmarks to assess two-dimensional theories of sandwich, composite plates," *AIAA Journal*, Vol. 41, 2003, pp. 1356-1362.

[7] Carrera, E., Brischetto, S., "A survey with numerical assessment of

classical and refined theories for the analysis of sandwich plates," *Applied Mechanics Reviews*, Vol. 62, 2009, pp. 1-17.

[8] Demasi, l., Yu, W., "Assess the accuracy of the variational asymptotic plate and shell analysis using the generalized unified formulation," Mechanics of Advanced Materials and Structures, Vol. 20, 2013, pp. 227-241.

[9] Carrera, E., Brischetto, S., "A comparison of various kinematic models for sandwich shell panels with soft core," *Journal of Composite Materials*, Vol. 43, 2009, pp. 2201-2221.

[10] Berdichevsky, V. L., "An asymptotic theory of sandwich plates," *International Journal of Engineering Science*, Vol. 48, 2010, pp. 383-404.

[11] Berdichevsky, V. L., "Nonlinear theory of hard-skin plates and shells," *International Journal of Engineering Science*, Vol. 48, 2010, pp. 357-369.

[12] Berdichevsky, V. L., "Variational-asymptotic method of constructing a theory of shells," *PMM*, Vol. 43, 1979, pp. 664-687

[13] Yu, W., *Variational asymptotic modeling of composite dimensionally reducible structures*, Ph.D. thesis, Aerospace Engineering, Georgia Institute of technology, 2002.

[14] Yu, W., "Mathematical construction of a reissner-mindline plate theory for composite laminates," *International Journal of Solids and*

Structures, Vol. 42, 2005, pp. 6680-6699.

[15] Lee, S., Lee, C.-Y., Hodges, D. H., "On the mechanics of composite sandwich plates with three-dimensional stress recovery," *International Journal of Engineering Science*, Vol. 157, 2020, 103406.

[16] Cho, M., Parmerter, R. R., "Efficient higher order composite plate theory for general lamination configuration", *AIAA Journal*, Vol. 31, 1993, pp. 1299-1306

[17] Ramalingeswara R., Ganesan N., "Interlaminar stresses in shells of revolution", *Mechanics of Composite Materials and Structures*, Vol. 3, 1996, pp. 321-339

[18] Shah P. H., Batra, R. C., "Through-thethickness stress distributions near edges of composite laminates using stress recovery scheme and third order shear and normal deformable theory", *Composite structures*, Vol. 131, 2015, pp. 397-413

[19] Tornabene, F., Brischetto, S., "3d capability of refined gdq models for the bending analysis of composite and sandwich plates, spherical and doubly-curved shells," *Thin-Walled Structures*, Vol. 129, 2018, pp. 94-124.

[20] Sayyad, A. S., Naik, N.S., "New displacement model for accurate prediction of transverse shear stresses in laminated and sandwich rectangular plates," *Journal of Aerospace Engineering*, Vol. 32, 2019, pp. 1-12.

[21] Hodges, D. H., Atilgan, A. R., Danielson, D. A., "A geometrically nonlinear theory of elastic plates," *Journal of Applied Mechanics*, Vol. 60, 1993, pp. 109-116.

[22] Danielson, D. A., *Vectors and Tensors in Engineering and Physics*, Pereus Books Publishing, Cambridge, Massachusetts, 2nd ed., 1997.

[23] Danielson, D. A., Hodges, D. H., "Nonlinear beam kinematics by decomposition of the rotation tensor," *Journal of Applied Mechanics*, Vol. 54, 1987, pp. 258-262.

[24] Yu, W., Hodges, D. H., Volovoi, V. V., "Asymptotic construction of reissner-like models for composite plates with accurate strain recovery," International Journal of Solids and Structures, Vol. 39, 2002, pp. 5185-5203.

[25] Yu, W., "Representative structural element: a new paradigm for multiscale structural modeling," *54th AIAA/ASME/ASCE/AHS/ASC Structures, Structural Dynamics, and Materials Conference*, 2013, p.1472

[26] Sutyrin, V. G., "Derivation of plate theory accounting asymptotically correct shear deformation," *Journal of Applied Mechanics*, Vol. 64, 1997, pp. 905-915.

[27] Berdichevsky, V. L., *Variational principles of continuum mechanics*, Springer, Berlin, 2009.

[28] Yu, W., Hodges, D. H., "Geometrically nonlinear shear deformation

theory for composite shells," *Journal of Applied Mechanics*, Vol. 71, 2004, pp.1-9.

[29] Lee, C.-Y., Hodges, D. H., "Hybrid energy transformation to generalized reissner-mindlin model for laminated composite shells," *International Journal of Engineering Science*, Vol. 122, 2018, pp. 30-55.

[30] Lee, C.-Y., "Generalized reissner-mindlin model for composite plates with no restrictions on constitutive materials," *AIAA Journal*, Vol. 57, 2019, pp. 1-12.

[31] Demasi, L., "An invariant model for any composite plate theory and fem applications: the generalized unified formulation," *50th AIAA/ASME/ASCE/AHS/ASC Structures, Structural Dynamics, and Materials Conference*, 2009, p. 2342.

[32] Rao, M. V. P., Harursampath, D., Renji, K., "Prediction of inter-laminar stresses in composite honeycomb sandwich panels under mechanical loading using variational asymptotic method", *Composite structures*, Vol. 94, 2012, pp. 2523-2537.